Technische Universität München

Fakultät für Medizin

Klinik für Herz- und Kreislauferkrankungen des Deutschen Herzzentrums München

Variants in *GUCY1A3* influencing coronary artery disease

Jana Wobst

Vollständiger Abdruck der von der Fakultät für Medizin der Technischen Universität München zur Erlangung des akademischen Grades eines

Doktors der Naturwissenschaften (Dr. rer. nat.)

genehmigten Dissertation.

Vorsitzende/r: Prof. Dr. Dr. Stefan Engelhardt

Prüfer der Dissertation:

1. Prof. Dr. Heribert Schunkert

2. Prof. Angelika Schnieke, Ph.D.

Die Dissertation wurde am 09.02.2017 bei der Fakultät für Medizin der Technischen Universität München eingereicht und durch die Fakultät für Medizin am 18.10.2017 angenommen.

Acknowledgement

First and foremost, I would like to express my appreciation and thanks to my first advisor Prof. Dr. Heribert Schunkert for the continuous support of my thesis and related research, for his motivation and immense knowledge. I would also like to thank Prof. Angelika Schnieke, Ph.D. for being my second advisor and for her insightful comments. I specially thank Dr. Thorsten Keßler. I could not have imagined a better mentor.

Table of Contents

List of Abbreviations

AAW	atherosclerotic arterial wall
ADP	adenosine diphosphate
ADP-RA	ADP-receptor antagonist
Ala	alanine
ANOVA	analysis of variance
APS	ammonium persulfate
Arg	arginine
AUC	area under the curve
BCA	bicinchoninic acid
BiFC	bimolecular fluorescence complementation
CAD	coronary artery disease
cAMP	cyclic adenosine-3',5'-monophosphate
cDNA	complementary DNA
CDS	coding sequence
cGMP	cyclic guanosine-3',5'-monophosphate
ChIP	chromatin immunoprecipitation
Co-IP	co-immunoprecipitation
cpm	counts per minute
Cys	cysteine
DBP	diastolic blood pressure
DNA	desoxyribonucleic acid
dNTP	desoxynucleoside triphosphate
E1	E-box 1
EMSA	electrophoretic mobility shift assay
ESP-EOMI	Exome Sequencing Project Early-Onset Myocardial Infarction
EYFP	enhanced yellow fluorescent protein
FRET	fluorescence resonance energy transfer
fs	frameshift
gDNA	genomic DNA
Glu	glutamic acid
Gly	glycine
GSNO	S-nitrosoglutathione
GUCY1A3	guanylyl cyclase 1 soluble subunit alpha

GWAS	genome-wide association studies
GYPA	glycophorin A
HEK	human embryonic kidney
HRP	horseradish peroxidase
IBMX	3-isobutyl-1-methylxanthin
Ile	isoleucine
IMA	internal mammary artery
IRAG	IP_3 receptor-associated cGMP kinase substrate
Iso	isoform
ITGB3	integrin subunit beta 3
LB	lysogeny broth
LD	linkage disequilibrium
Leu	leucine
Lys	lysine
Met	methionine
MI	myocardial infarction
MLCP	myosine light-chain phosphatase
mRNA	messenger RNA
NCBI	National Center for Biotechnology Information
NO	nitric oxide
PCR	polymerase chain reaction
Phe	phenylalanine
PPP	platelet poor plasma
PRP	platelet rich plasma
PTPRC	protein tyrosine receptor phosphatase C
qPCR	quantitative PCR
RNA	ribonucleic acid
ROS	reactive oxygen species
RPLP0	ribosomal protein lateral stalk subunit P0
SBP	systolic blood pressure
SEM	standard error mean
Ser	serine
sGC	soluble guanylyl cyclase
siRNA	silencer RNA
SMC	smooth muscle cell
SNP	sodium nitroprusside, single nucleotide polymorphism
STAGE	Stockholm Atherosclerosis Gene Expression

Thr	threonine
Tr	transcript variant
TR-FRET	time-resolved FRET
Tyr	tyrosine
UTR	untranslated region
Val	valine
VASP	vasodilator-stimulated phosphoprotein
VSMC	vascular smooth muscle cells
WB	whole blood
WT	wildtype
ZEB1	zinc finger E box-binding homeobox 1

List of Figures

List of Tables

Abstract

Coronary artery disease (CAD) and its main complication myocardial infarction (MI) are the leading causes of death in industrialised nations in both men and women. Besides traditional risk factors like lipid levels, diabetes and obesity, a positive familiy history plays an important role in the development of atherosclerosis and MI. Genome-wide association studies have pointed to the importance of nitric oxide (NO)/cyclic guanosine-3',5'-monophosphate (cGMP) signalling as two out of 56 loci genome-wide significantly associated with CAD are involved in this pathway. One of them tags the *NOS3* gene, encoding the endothelial nitric oxide synthase. The second locus contains the *GUCY1A3* gene, which codes for the α_1 subunit of the soluble guanylyl cyclase (sGC). A common lead single nucleotide polymorphism (SNP) at this locus (rs7692387) is located in an intron of the *GUCY1A3* gene and genome-wide significantly associated with CAD. Furthermore, an extended family with multiple members suffering from premature CAD and MI has been reported to carry a frameshift mutation in the coding sequence of *GUCY1A3* leading to a truncated non-functional protein. Additionally, further rare coding *GUCY1A3* variants have been shown to be enriched in patients suffering from premature CAD and MI. Whereas the loss-of-function mutation in the extended family has been described to influence platelet function, the underlying mechanisms of non-coding variants as well as of further identified coding *GUCY1A3* variants remain to be elucidated.

sGC is the primary receptor for the vascular signal molecule NO and plays a central role in cardiovascular physiology via the production of the intracellular messenger cGMP. sGC is an obligatory heterodimeric protein composed of an α_1 and a β_1 subunit, the latter containing a prosthetic haem group. Binding of NO leads to the activation of sGC triggering the catalysis of cGMP from guanosine-5'-triphosphate. cGMP regulates the activity of various downstream proteins, including cGMP-dependent protein kinase G, cGMP-dependent phosphodiesterases and cGMP-gated ion channels promoting functions like vascular smooth muscle relaxation and inhibition of platelet aggregation. Diminished sGC function contributes to a number of disorders, including cardiovascular diseases. The therapeutic importance of the NO/cGMP signalling pathway has been well recognised for many years with NO donors being used for the treatment of vascular disorders. Recently, so-called sGC modulators have been developed which directly target sGC in an NO-independent manner.

Thus far, eight *GUCY1A3* variants were found to be enriched in patients suffering from CAD and MI and were functionally investigated for protein expression levels, dimerisation capability as well as enzymatic activty. We showed that decreased capability of

cGMP formation due to decreased enzymatic activity and in part due to decreased expression could be rescued by the sGC stimulator BAY 41-2272 which might represent a novel treatment strategy for patients suffering from atherosclerosis secondary to genetic alterations in the *GUCY1A3* gene.

Furthermore we provide functional evidence that the common lead SNP rs7692387 at chromosome 4q32.1 affects *GUCY1A3* gene expression via alteration of a transcription factor binding site. The transcription factor ZEB1 rather binds to the non-risk allele leading to an increase in *GUCY1A3* expression, higher sGC levels, and higher sGC activity after stimulation.

Taken together, our data indicate that impared expression of *GUCY1A3* or dysfunctional sGC are importantly involved in mediating susceptibility of MI and CAD and thus might represent novel targets in the treatment of these disorders.

1 Introduction

1.1 Cardiovascular diseases

Cardiovascular diseases are the leading causes of death worldwide (World Health Organisation 2014), estimated at 15.6 million deaths per year by the The 2010 Global Burden of Disease study (Townsend *et al.* 2015). They include diseases of the heart, vascular diseases of the brain and diseases of blood vessels. A substantial part of cardiovascular diseases results of atherosclerosis as underlying mechanism including coronary artery disease (CAD), cerebrovascular disease (e.g., stroke) and diseases of the aorta and arteries, inclusive of hypertension and peripheral vascular disease.

Amongst these atherosclerosis-related cardiovascular diseases, CAD is the most common one leading to death in both men and women (Finegold *et al.* 2013). In Europe, CAD accounts for 20 % of all cardiovascular diseases (Townsend *et al.* 2015). CAD is determined by both genetic and environmental factors (O'Donnell and Nabel 2011, Kessler *et al.* 2013). The main complication of CAD is myocardial infarction (MI) caused by sudden plaque rupture and coronary atherothrombosis.

1.1.1 Development of atherosclerosis

The development of atheroscerosis as a chronic disease of the arterial wall encompasses serveral stages.

The normal arterial wall comprises three distinct layers: intima, media and adventitia (Figure 1a) (Rhodin 1962, Chen and Kassab 2016). The adventitia (outermost layer of an artery) consists of dense collagen fibers, elastin fibers, some fibroblasts and hydrophilic macromolecules (including glycosaminoglycans, proteoglycans and glycoproteins). It protects the vessel from from over-strech and connects it to the surrounding tissues (Zoumi *et al.* 2004). The media layer is composed of vascular smooth muscle cells (VSMC), elastic lamellae, collagen fibril bundles and elastic fibrils (O'Connell *et al.* 2008). The intima (innermost layer of an artery) is build up of endothelial cells (EC), a few collagen bundles and basal lamina (Zoumi *et al.* 2004).

The initial steps of the development of atherosclerosis include adherence of blood monocytes to intimal endothelial cells, their migration into the intima and their differentiation into macrophages (Figure 1b). Upon uptake of lipids they form foam cells. VSMC migrate from the media to the intima in response to cytokines secreted from damaged EC (Figure 1c). Intimal and media-derived cells proliferate, and extracellular matrix macromolecules are synthesised forming a plaque. Lipid, cholesterol crystals, and microvessels accumulate in the central region of this plaque (Libby *et al.* 2011). Atherosclerotic plaques may remain asymptomatic for decades. When it comes to rupture of the fibrous cap of the atherosclerotic plaque the resulting exposure of blood to the atherosclerotic material triggers thrombus formation, which occludes the artery (Figure 1d) (Finn *et al.* 2010).

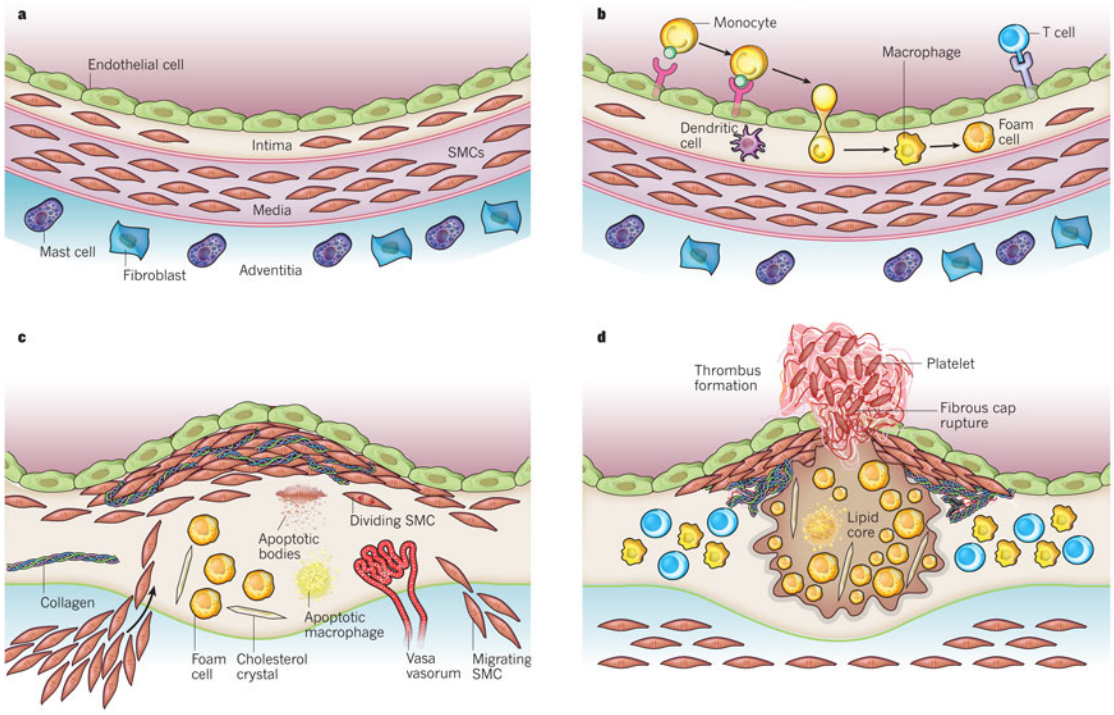

Figure 1 Development of atherosclerosis. Reprinted by permission from Macmillan Publishers Ltd: Figure 1 from *Nature* 2011. 473(7347):317-325 (Libby *et al.* 2011), copyright © 2011.

1.1.2 Risk factors for CAD

A number of lifestyle and environmental factors contribute to the pathogenesis of CAD. They include, for example, blood lipids, blood pressure, diabetes, smoking and obesity and can be summarised under the expression ’modifiable risk factors’ as they can be adressed by lifestyle changes and/or therapeutic intervention (Yusuf *et al.* 2004, Kessler *et al.* 2016). A positive family history respresents a further important risk factor. Twin and family

studies showed that a significant proportion of 40 to 50 % of susceptibility to CAD is heritable (Peden and Farrall 2011). However, the underlying genetic mechanisms and causative genes remained largely unknown for decades until genome-wide association studies (GWAS) of CAD and MI became possible.

Thus far, 56 genomic loci have been shown to be genome-wide significantly associated with CAD with only a minority of them being linked to traditional risk factors like lipid levels, blood pressure or diabetes (Schunkert *et al.* 2011, CARDIoGRAMplusC4D Consortium *et al.* 2013, Nikpay *et al.* 2015) (Figure 2). The (NO)/cyclic guanosine-3',5'-monophosphate (cGMP) signalling pathway thereby seems to play an important role since two key enzymes, the endothelial nitric oxide synthase (eNOS) and the soluble guanylyl cyclase (sGC) have been genome-wide significantly linked to CAD (CARDIoGRAMplusC4D Consortium *et al.* 2013, Nikpay *et al.* 2015). The *NOS3* lead single nucleotide polymorphism (SNP) rs3918226 is located within the promoter region of the *NOS3* gene that encodes eNOS (Salvi *et al.* 2013); the *GUCY1A3* lead SNP rs7692387 located in an intronic region of the gene (CARDIoGRAMplusC4D Consortium *et al.* 2013, Wobst *et al.* 2015a) codes for the α_1 subunit of sGC. The *GUCY1A3* locus had already been previously associated with systolic (SBP) and diastolic (DBP) blood pressure (International Consortium for Blood Pressure Genome-Wide Association Studies *et al.* 2011). Whereas the variant at the *NOS3* locus has already been implicated to influence *NOS3* expression (Salvi *et al.* 2013), the molecular mechanisms affected by common variants at the *GUCY1A3* locus remain elusive.

The risk allele variant G of rs7692387 has a high allele frequency in the population. In fact, ~63 % of all Europeans are homozygous for the risk allele G whereas only ~4 % are homozygous for the non-risk variant A (1000 genomes Project Phase 3; *http://www.ensembl.org/Homo_sapiens/Variation/Population?db=core;r=4:155713657-155714657;v=rs7692387;vdb=variation;vf=4491101*).

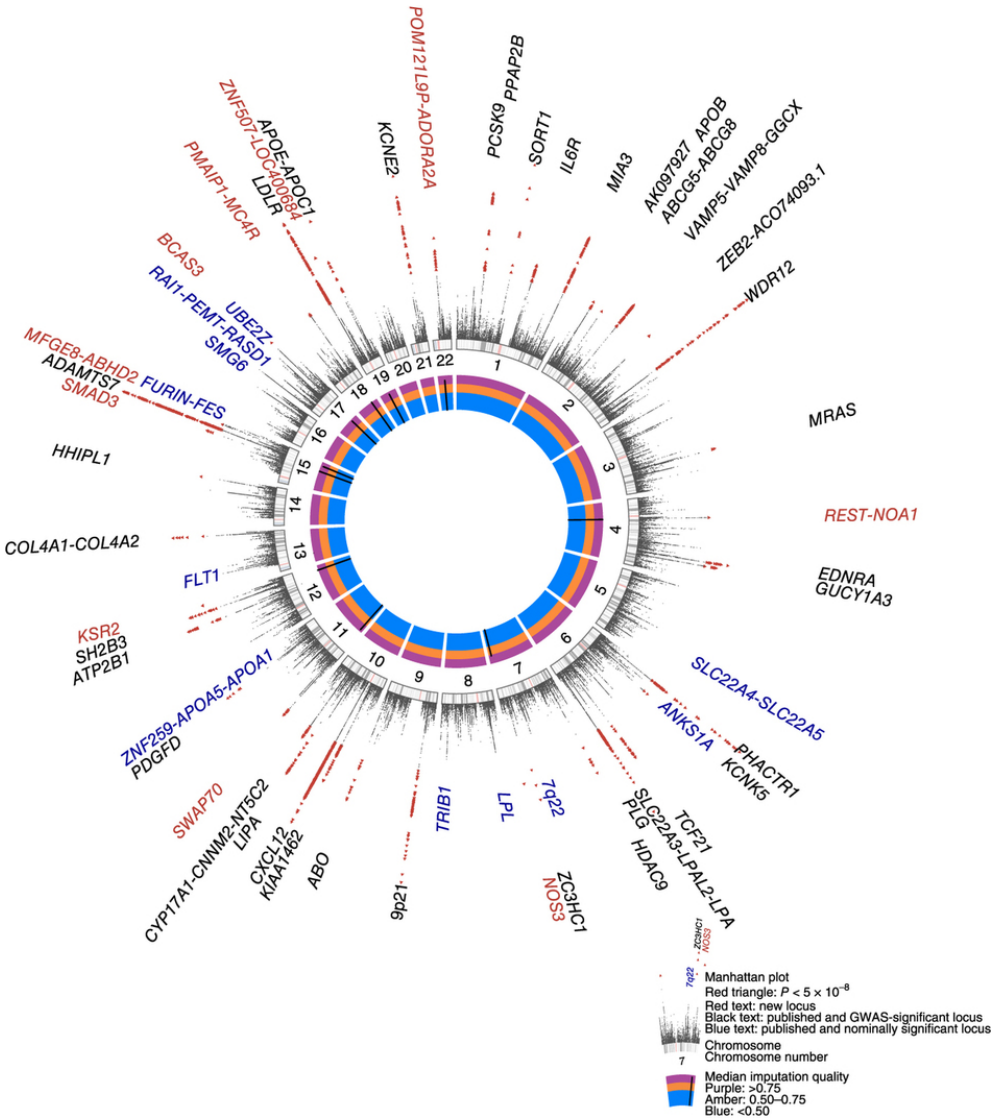

Figure 2 Circular Manhattan plot summarising the current 1000 Genomes Project CAD association results. The *GUCY1A3* locus is genome-widely associated with CAD. Reprinted by permission from Macmillan Publishers Ltd: Figure 2 from *Nat Genet* 2015. 47(10):1121-1130 (Nikpay *et al.* 2015), copyright © 2015.

Furthermore, it has been shown that a loss-of-function mutation in sGC is responsible for premature CAD and MI in an extended family with 32 members of whom 22 had early onset of the disease (≤60 years of age) (Erdmann *et al.* 2013). Whole-exome sequencing in three distantly related family members (III.13, III.24 and III.26; marked with an arrow in Figure 3) revealed cosegregation of two heterozygous private mutations: a frameshift mutation in *GUCY1A3* (p.Leu163Phefs*24) and a missense mutation in *CCT7* (p.Ser525Leu) (Erdmann *et al.* 2013). *CCT7* codes for CCTη, the η subunit of chaperonin-containing T-complex polypeptide 1, for which interaction with sGC has been shown (Hanafy *et al.* 2004). Family members carrying both mutations were affected in 100 % of cases. Experiments on isolated platelets from family members revealed that the combination of both mutations leads to noticeably impaired sGC activity, as shown by significantly lower cGMP levels in platelets

of double-mutation carriers. These results were supported by *in vitro* data showing reduced α_1 and β_1 subunit protein levels after silencing of *CCT7* and *in vivo* experiments in mice lacking the α_1 subunit, which resulted in a decreased time-to-thrombus formation in arterioles initiated by photoexcitation (Erdmann *et al.* 2013).

Whereas it was shown that the digenic mutation in the family affects platelet function, the underlying molecular mechanism involving the lead SNP rs7692387 at the *GUCY1A3* locus in CAD remains elusive.

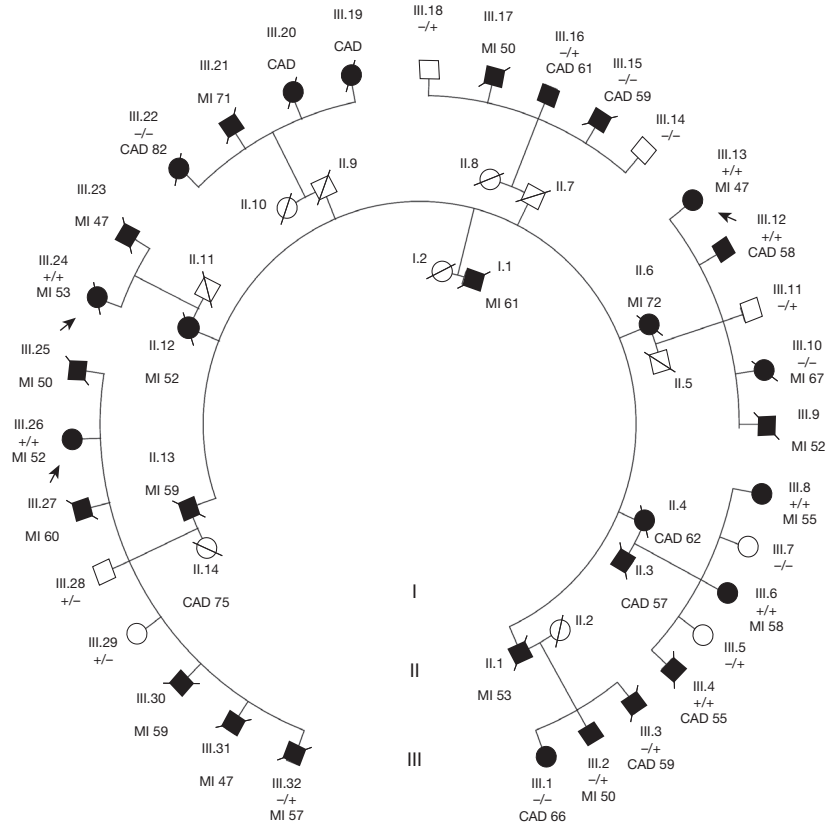

Figure 3 Pedigree of the extended MI family. White symbols indicate healthy, black symbols affected individuals; squares represent males, circles represent females. Crossed symbols represent deceased individuals. Age of onset is given next to the disease. Persons III.13, III.24 and III.26 were exome-sequenced; +/+ denotes double-mutation carriers (p.Leu163Phefs*24/p.Ser525Leu); +/- denotes probands carrying only the p.Leu163Phefs*24 mutation in *GUCY1A3*; -/+ denotes probands carrying only the p.Ser525Leu mutation in *CCT7*. Reprinted by permission from Macmillan Publishers Ltd: Figure 1 from *Nature* 2013. 405(7480):432-436 (Erdmann *et al.* 2013), copyright © 2013.

1.2 NO/cGMP signalling pathway

In 1980 Furchgott and Zawadzki first demonstrated that the endothelium releases a substance that mediates atecylcholine-induced relaxation of blood vessels (Furchgott and

Zawadzki 1980). This ‘endothelium-derived relaxing factor’ was later identified as nitric oxide (NO) (Ignarro *et al.* 1987, Palmer *et al.* 1987).

Most of the physiological functions of NO are mediated through its primary receptor sGC. Activated sGC catalyses the generation of cGMP from guanosine-5’-triphosphate (GTP). cGMP acts as an ubiquitous second messenger in intracellular signalling cascades, which serves to regulate the activity of three main cellular targets: cGMP-dependent protein kinase G (PKG), cGMP-dependent phosphodiesterases (PDE) and cGMP-gated ion channels. The cellular and physiological effects propagated through cGMP are varied and include VSMC relaxation (Warner *et al.* 1994) and inhibited platelet aggregation (Dangel *et al.* 2010), for example (Figure 4).

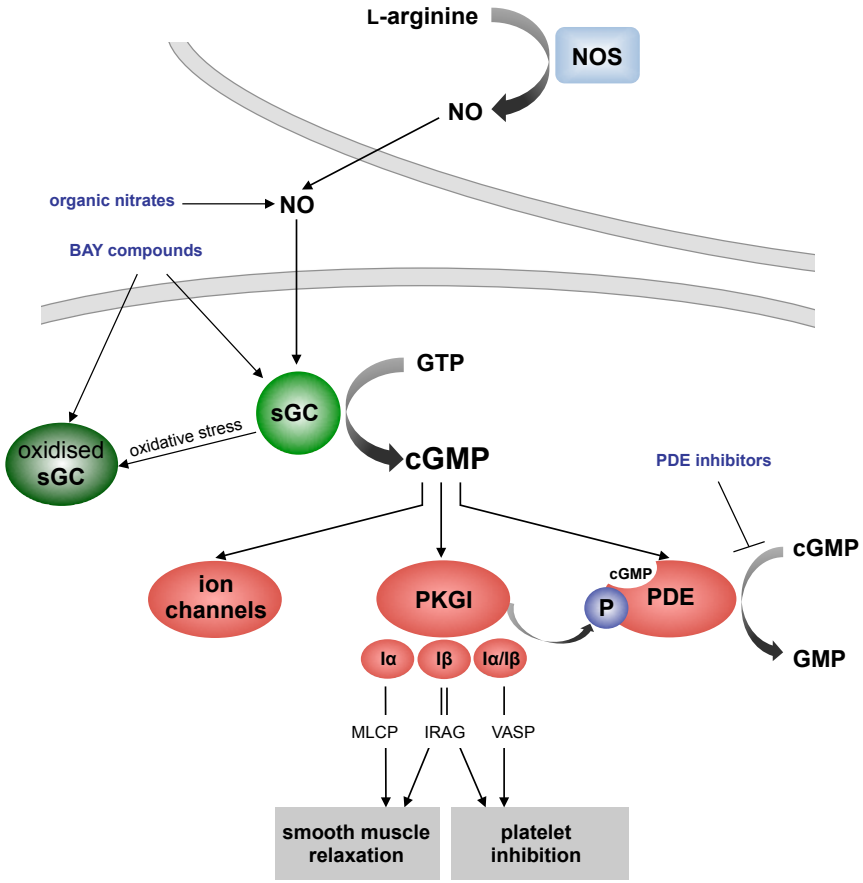

Figure 4 Overview of main components of the NO/cGMP signalling pathway. NO synthases (NOS) catalyse the production of NO from L-arginine. NO binds to soluble guanylyl cyclase (sGC) which consequently catalyses the reaction from guanosine-5’-triphosphate (GTP) to guanosine-3’,5’-monophosphate (cGMP). cGMP acts as an intracellular second messenger activating cGMP-dependent proteinkinase G I (PKGI), cGMP-dependent phosphodiesterases (PDE) and cGMP-gated ion channels. PKGI phosphorylates different effector proteins leading to relaxation of smooth muscle cells and inhibition of platelet aggregation. *MLCP:* myosine light-chain phosphatase; *IRAG:* IP_3 receptor-associated cGMP kinase substrate; *VASP:* vasodilator-stimulated phosphoprotein. Adapted by permission of John Wiley & Sons, Inc: Figure 1 from *EMBO Rep* 2006. 7:149-153 (Feil and Kemp-Harper 2006), copyright © 2006.

1.2.1 NO synthases

NO is biosynthesised endogenously through sequential oxidation of the amino acid L-arginine by nitric oxide synthases (NOS) (Palmer *et al.* 1988). Three NOS isoforms encoded by different genes have been reported and well characterised: neuronal NOS (nNOS/*NOS1*), inducible NOS mainly in macrophages (iNOS/*NOS2*) and endothelial NOS (eNOS/*NOS3*), with about 50 to 60 % homology in protein structure but each with separate functions (Lamas *et al.* 1992). A fourth isoform may occur in mitochondria (mtNOS) (Elfering *et al.* 2002).

NOS enzymes are catalytically active when dimerised (Stuehr 1997). The activity of both constitutively expressed isoforms nNOS and eNOS is Ca^{2+}-dependent. Increasing intracellular Ca^{2+} levels lead to the formation of calcium/calmodulin complexes that facilitate the catalysis of L-arginine. The iNOS isoform functions in a Ca^{2+}-independent manner; it binds calmodulin tightly and is always active (Mattila and Thomas 2014). Its expression is induced under specific conditions such as inflammation (Hamalainen *et al.* 2008). In the cardiovascular system, eNOS is the main source of NO production (Ursell and Mayes 1993, Seddon *et al.* 2009) which occurs in response to chemical stimuli such as platelet-derived factors, acetylcholine, and cytokines (Busse and Fleming 1995) as well as mechanical stimuli like shear stress (Paniagua *et al.* 2001).

1.2.2 Soluble guanylyl cyclase

1.2.2.1 sGC subunits and isoforms

sGC is an heterodimeric ~150 kDa protein composed of a bigger α subunit and a smaller β subunit (Kamisaki *et al.* 1986). In humans, two types of each subunit have been identified: α_1 and α_2 as well as β_1 and β_2. All four proteins are encoded by distinct genes: *GUCY1A3* (α_1), *GUCY1A2* (α_2); *GUCY1B3* (β_1), and *GUCY1B2* (β_2). The genes *GUCY1A3* and *GUCY1B3* are located on chromosome 4 (Giuili *et al.* 1993), *GUCY1A2* and *GUCY1B2* on chromosomes 11 (Yu *et al.* 1996) and 13 (Behrends *et al.* 1999), respectively.

Human α_1, α_2 and β_1 exist as different isoforms due to alternative splicing (Behrends *et al.* 1995, Sharina *et al.* 2008, Martin *et al.* 2014). Seven alternatively spliced *GUCY1A3* transcript variants code for three different isoforms: canonical full-length 690 aa α_1 IsoA (Tr1 to Tr4 and Tr8; 77 kDa), 455 aa α_1 IsoB (N-termΔ235aa; Tr5; 51 kDa) and 624 aa α_1 IsoD (C-termΔ66aa; Tr7; 70 kDa) (Wobst *et al.* 2015b). Tr1 to Tr4 as well as Tr8 coding for the identical α_1 IsoA differ from each other only in their 5' and 3' UTR sequences, which likely

affects mRNA stability (Sharina *et al.* 2011). An overview of transcript variants coding for sGC α_1 subunit isoforms can be appreciated in Table 1.

Table 1 Overview of human sGC α_1 subunit isoforms. The *GUCY1A3* gene which was mapped to chromosome 4q31.3-q33 (Giuili *et al.* 1993) exhibits 7 different transcript variants due to alternative splicing which code for three different sGC α_1 isoforms of different sizes. Data adopted from *NCBI* (*http://www.ncbi.nlm.nih.gov/nuccore*).

Transcript Variant	Total Exons	Coding Exons	Isoform	Protein size (aa)	Accession No. cDNA*	Accession No. Protein#
Tr1	11	8	α_1 IsoA	690	NM_000856.5	NP_000847.2
Tr2	10				NM_001130682.2	NP_001124154.1
Tr3	10				NM_001130683.3	NP_001124155.1
Tr4	9				NM_001130684.2	NP_001124156.1
Tr8	10				NM_001256449.1	NP_001243378.1
Tr5	10	5	α_1 IsoB	455	NM_001130685.2	NP_001124157.1
Tr7	9	7	α_1 IsoD	624	NM_001130687.2	NP_001124159.1

**NCBI Nucleotide*
#NCBI Protein

sGC subunits only exhibit catalytic activity when dimerised (Harteneck *et al.* 1990). Both α subunits (α_1 and α_2) can build up a functional enzyme together with β_1, which means that α_1/β_1 as well as α_2/β_1 heterodimers are activated by NO (Russwurm *et al.* 1998). In contrast, β_2 does not exhibit cyclase activity neither expressed together with α_1 nor with α_2. Though it has been shown that β_2 protein can function as a homodimer *ex vivo* (Koglin *et al.* 2001). The function of β_2 homodimers remains elusive. By contrast, Zabel *et al.* showed that overexpressed α_1/α_1 and β_1/β_1 homodimers in Sf9 cells are both catalytically inactive (Zabel *et al.* 1999).

Whereas α_1 and β_1 are ubiquitously expressed, α_2 is highly expressed in brain, placenta, spleen and uterus (Budworth *et al.* 1999). Moreover, α_1 and α_2 differ in their subcellular localisation: the α_2 subunit enables association of sGC α_2/β_1 to the membrane whereas sGC α_1/β_1 is cytosolic (Russwurm *et al.* 2001). As the α_1/β_1 heterodimer is expressed in most tissues and shows greater activity than α_2/β_1 in both basal and NO stimulated state it is regarded as the major isoform (Harteneck *et al.* 1991). The functional importance of α_1/β_1 sGC was demonstrated by the significantly decreased relaxing effects of major vasodilators such as acetylcholine, NO, YC-1 and BAY 41-2272 in α_1 sGC knock-out mice (Mergia *et al.* 2006, Nimmegeers *et al.* 2007).

1.2.2.2 sGC structure

A comparison of the primary structure shows that each sGC subunit is composed of four functionally different domains: (1) H-NOX (haem-NO/oxygen domain), (2) a Per/Arnt/Sim-like domain (PAS), (3) an α-helical region capable of forming coiled-coils involved in dimerization, and (4) a C-terminal catalytic domain where the GTP is bound and converted to cGMP (Derbyshire and Marletta 2012). These four specified domains form two rigid units within the sGC: the smaller unit comprises the dimeric catalytic domain, and the larger one is built from the clustering of the PAS and H-NOX domains. The helical domains form a dimeric parallel coiled-coil that flexibly connects the two modules (Campbell *et al.* 2014) (Figure 5). Although crystal structures of the independent domains have been reported (Pellicena *et al.* 2004, Ma *et al.* 2010, Allerston *et al.* 2013, Purohit *et al.* 2013) a high-resolution 3D structure of the complete human is still lacking.

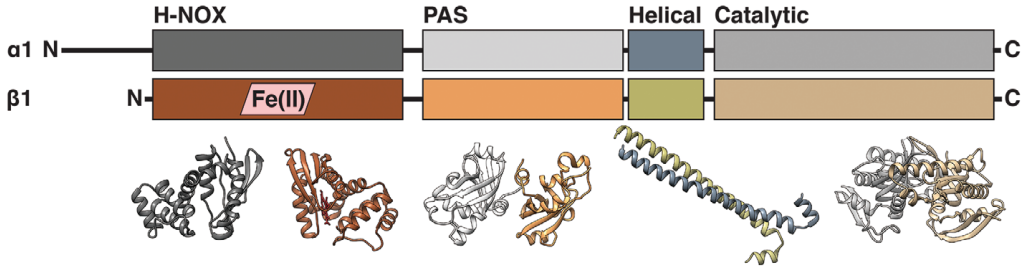

Figure 5 sGC domain organisation and X-ray crystallographic models. Each subunit contains four modular domains; α_1 domains are shown in shades of gray, and β_1 domains are shown in color. The H-NOX domain of the β_1 subunit contains the haem cofactor, shown in red. *H-NOX:* haem-NO/oxygen domain; *PAS:* Per/Arnt/Sim-like domain. Reviewed figure reprinted with permission from Wobst *et al.* Molecular Variants of Soluble Guanylyl Cyclase Affecting Cardiovascular Risk. Circ J 2015. 79:463-469 (Wobst *et al.* 2015b). Original figure (Figure 1) reprinted with permission from Campbell *et al.* Single-particle EM reveals the higher-order domain architecture of soluble guanylate cyclase. *PNAS* 2014. 111(8):2960-2965 (Campbell *et al.* 2014).

1.2.2.3 NO-mediated sGC activation

The H-NOX domain of the β_1 subunit contains the haem cofactor, where NO binding takes place. In contrast, the α_1 subunit cannot bind haem (Allerston *et al.* 2013). When NO binds to haem a transient 6-coordinate complex is formed, which rapidly converts into a 5-coordinate nitrosyl-haem complex because of disruption of the coordinating bond between histidine$_{105}$ and the haem (Stone and Marletta 1996) leading to structural changes of the sGC (Ignarro 1991, Gileadi 2014, Underbakke *et al.* 2014).

The C-terminal catalytic domain of activated sGC then converts GTP to the intracellular second messenger cGMP and pyrophosphate (Waldmann and Murad 1987). In

other words, the formation of the NO-haem complex induces the allosteric transition from basal to activated sGC, which increases sGC activity more than 200-fold (Humbert *et al.* 1990). Once NO dissociates from sGC, basal cGMP production is restored, ensuring sGC activity being quickly up- and downregulated (Derbyshire and Marletta 2012). CO also binds to sGC but only leads to a 2-fold to 5-fold activation of the enzyme (Stone and Marletta 1994).

As NO directly binds to the haem group it cannot activate the enzyme when it is haem-free or when the haem moiety is oxidised (Fe^{3+}). The latter occurs following oxidative stress (Stasch *et al.* 2006) or under the action of inhibitors such as 1H-[1,2,4]-oxadiazolo [4,3-a]quinoxalin-1-one (ODQ) (Zhao *et al.* 2000).

1.2.3 cGMP-dependent phosphodiesterases

Intracellular cGMP concentrations are controlled by a family of cGMP-dependent phosphodiesterases (PDE), enzymes that break the 3'-phosphodiester bond within cGMP hydrolysing it to GMP (Kass *et al.* 2007b). Collectively, 11 different types of isoenzymes, each with several isoforms, exist in humans (Bender and Beavo 2006). Whereas some PDEs are cGMP-selective, because of their 100-fold substrate preference for cGMP over cyclic adenosine-3',5'-monophosphate (cAMP), others are specific for hydrolysing cAMP, and some PDEs can hydrolyse both cAMP and cGMP (Bender and Beavo 2006) (Figure 6). The primary enzymes responsible for cardiac cGMP degradation are PDE1, PDE2 and PDE5 (Kass *et al.* 2007b, Lee and Kass 2012).

Out of these, PDE5 is considered to be the most important one in humans (Francis *et al.* 2009). It acts as a homodimer (Thomas *et al.* 1990) with each monomer containing two subsequent GAF domains at the N-terminus, GAF A and GAF B, and a catalytic cGMP binding site at the C-terminus where cGMP cleavage takes place (Kass *et al.* 2007a). cGMP binding to the GAF A domain increases PDE5 activity by approximately 10-fold (Rybalkin *et al.* 2003a). Activation of PDE5 lowers cGMP concentration leading to vasoconstriction while inhibition of the enzyme prolongs vasorelaxation, making PDE5 an important pharmaceutical target for PDE inhibitors (Rybalkin *et al.* 2003b).

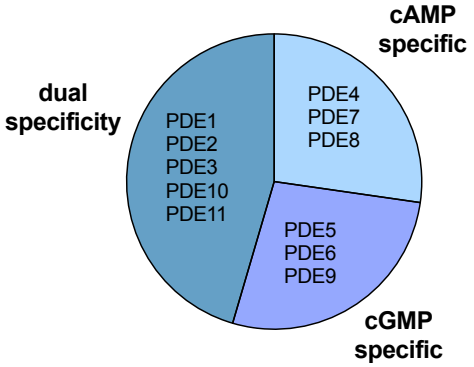

Figure 6 PDE substrate specificity. The 11 phosphodiesterase (PDE) isoenzymes can be grouped into three categories based on their substrate specificity.

1.2.4 cGMP-dependent proteinkinase G

Two types of cGMP-dependent proteinkinase G (PKG) proteins exist in humans which are encoded by different genes (*PRKG1* and *PRKG2*) (Hofmann 2005). Only the PKGI family will be discussed because it is more commonly involved in NO/cGMP signalling in the cardiovascular system. It is a serine/threonine kinase and the primary target of cGMP in the NO/cGMP signalling pathway mediating most of the cGMP functions. Two different PKGI isoforms result from alternative splicing: PKGIα and PKGIβ. They only differ in the N-terminal ~100 amino acids (Ruth *et al.* 1997). Upon activation, PKGI phosphorylates specific serine or threonine residues on target proteins. The three most important ones are myosine light-chain phosphatase (MLCP), IP_3 receptor-associated cGMP kinase susbtrate (IRAG) as well as vasodilator-stimulated phosphoprotein (VASP).

MLCP: PKGIα-dependent phosphorylation of MLCP activates its phosphatase function, which subsequently catalyses the dephosphorylation of myosin light-chain fibers that were phosphorylated by myosin light kinase (MLCK). In doing so, the phosphatase activity of MLCP disrupts the cross-bridge between actin and myosin in the contracted state, and thus promotes smooth muscle cell relaxation (Lincoln 2007).

IRAG: IRAG interacts specifically with the PKGIβ isoform and the inositol 1,4,5-trisphosphate receptor I (Schlossmann *et al.* 2000). When phosphorylated it inhibits Ca^{2+} transport and decreases intracellular Ca^{2+} concentrations, leading to vasodilatation (Desch *et al.* 2010) and inhibition of platelet aggregation (Antl *et al.* 2007). In smooth muscle cells decreased intracellular Ca^{2+} leads to decreased myosin light-chain phosphorylation and therefore to vasorelaxation. In platelets decreased Ca^{2+} concentrations promote inhibition of platelet aggregation by, for example, inhibiting the reorganisation of the actin cytoskeleton necessary for shape change (Hathaway and Adelstein 1979, Varga-Szabo *et al.* 2009).

VASP: VASP is an established substrate of both cAMP- and cGMP-dependent protein kinase. VASP phosphorylation at serine$_{239}$ in response to cGMP-activated PKGIβ closely correlates with platelet inhibition and in particular with the inhibition of fibrinogen binding to the gylcoprotein IIb/IIIa (also known as integrin $\alpha_{IIb}\beta_3$) of human platelets (Smolenski *et al.* 1998).

1.2.5 cGMP-gated ion channels

cGMP-gated ion channels refer to unselective cation channels which, upon activation by cGMP, directly lead to influx of extracellular cations into the cytoplasm and to the depolarisation of the plasma membrane (Biel 2009). They were originally identified in the olfactory and vision system (Fesenko *et al.* 1985). It is now known that they are also expressed in intestinal epithelium, testis, kidney, brain and heart (Biel *et al.* 1994, Distler *et al.* 1994).

1.3 Therapeutic potential of the NO/cGMP signalling pathway

The NO/cGMP signalling pathway has been a target for treating cardiovascular diseases for a long time. Organic nitrates such as nitroglycerine are the preferred NO donors in the treatment of acute ischaemia and heart failure as well as in the treatment of angina. However, prolonged exposure to organic nitrates causes development of dose-dependent tolerance to the compounds which is a major clinical issue (Sage *et al.* 2000, Gori 2002).

For the management of vascular diseases the discovery of new treatments has now focused directly on sGC. Several synthetic compounds have been discovered that stimulate sGC in an NO-independent way. These so-called sGC modulators can be separated into two different classes based on their mechanisms of action: sGC stimulators and sGC activators (Evgenov *et al.* 2006, Stasch *et al.* 2011) (Figure 7). The effectiveness of these compounds differs depending on the redox state of sGC. Like NO sGC stimulators target the reduced form of sGC, i.e., when the haem iron is in its ferrous (Fe^{2+}) state (Ko *et al.* 1994, Evgenov *et al.* 2006). They activate sGC in an NO-independent but haem-dependent manner. sGC stimulators stabilise the nitrosyl-haem complex of the reduced sGC and, as allosteric modulators, markedly enhance NO-dependent cGMP production.

Under various pathophysiological oxidative stress conditions such as hypertension, atherosclerosis, diabetes, and heart failure the sGC redox equilibrium can be shifted to the

oxidised, ferric state (Fe^{3+}) by reactive oxygen species (ROS). ROS like superoxide anion (O_2^-) deplete the bioactivity of NO due to the reaction with NO to peroxynitrite ($ONOO^-$). Subsequently, sGC activity is reduced by oxidation through $ONOO^-$. Oxidation of the sGC haem renders the enzyme insensitive to either endogenous/exogenous NO or sGC stimulators (Meurer *et al.* 2009, Fritz *et al.* 2011). Oxidation of sGC can also result in dissociation of the haem from sGC (Roy *et al.* 2008), after which the enzyme is prone to proteasomal degradation (Meurer *et al.* 2009). In case of oxidised or haem-free sGC NO-independent haem-independent sGC activators are the best choice (Stasch *et al.* 2002b).

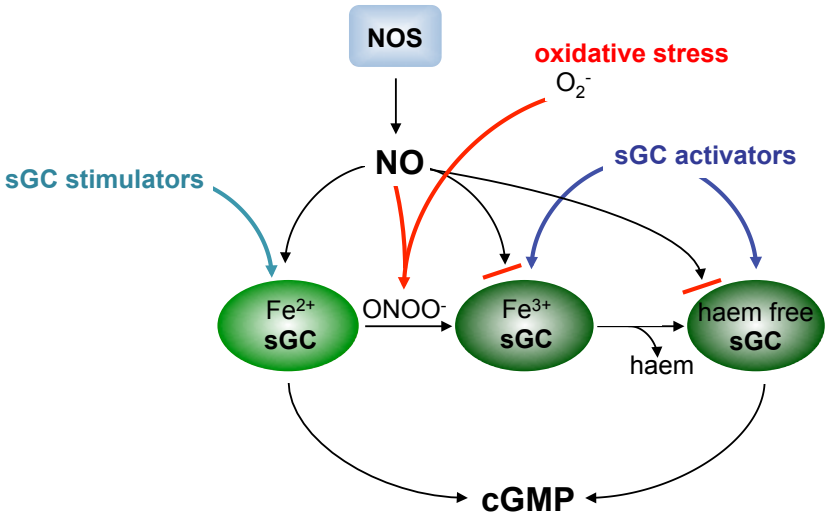

Figure 7 Working mechanisms of sGC stimulators and activators. Generated by NO-synthases (NOS) NO leads to the activation of the reduced (Fe^{2+}) haem-containing sGC and to the subsequent formation of the second messenger cGMP. sGC stimulators target as well this redox state of sGC. Reactive oxygen species like superoxide (O_2^-) impair this pathway by scavenging NO due to the reaction with O_2^- to peroxynitrite ($ONOO^-$) which in turn leads to oxidation of sGC to its ferric (Fe^{3+}) NO-insensitive state. sGC activators are able to bypass the impaired NO/cGMP signalling pathway by activating oxidised and haem-free sGC.

In 1994, the first NO-independent, haem-dependent sGC stimulator YC-1, a synthetic benzylindazole derivate, was described (Ko *et al.* 1994). As YC-1 was a relatively weak vasodilator and had off-target effects, like inhibition of PDE (Friebe *et al.* 1998, Galle *et al.* 1999), more specific sGC stimulators such as the pyrazolopyridines BAY 41-2272 and BAY 41-8543 were invented based on YC-1 as a lead structure (Stasch *et al.* 2001, Stasch *et al.* 2002a). Screening additional compounds led to the discovery of Riociguat (BAY 63-2521) which is already approved for the treatment of pulmonary arterial hypertension (Ghofrani *et al.* 2013b, Pulido *et al.* 2016). The drug also revealed beneficial effects in a clinical trial on patients with inoperable chronic thromboembolic pulmonary hypertension (Ghofrani *et al.* 2013a). As a study investigating the benefit in patients suffering from pulmonary hypertension due to left ventricular dysfunction showed promising results regarding cardiac

measures (Bonderman *et al.* 2013), Riociguat might also play a role in the treatment of heart failure.

The first sGC activator known as Cinaciguat (BAY 58-2667), an amino dicarboxylic acid, is a porphyrin mimetic, that can bind and replace the endogenous haem site in sGC (Schmidt *et al.* 2004). It was discovered in a high-throughput screening in 2002 (Stasch *et al.* 2002b). The cardiovascular effects of Cinaciguat have already been studied in several pre-clinical models of ischaemia reperfusion injury (Korkmaz *et al.* 2009, Methner *et al.* 2013). Cinaciguat also stabilises haem-free sGC, preventing proteasomal degradation (Meurer *et al.* 2009, Stasch *et al.* 2011).

1.4 Aim

It is well established that the NO/cGMP signalling pathway plays a pivotal role in many cardiovascular diseases. Firstly, genome-wide association studies identified the chromosomal locus 4q32.1 being genome-wide significantly associated with CAD (CARDIoGRAMplusC4D Consortium *et al.* 2013) and, secondly, a loss-of-function mutation found in an extended family cosegregated with CAD (Erdmann *et al.* 2013). NO formed by eNOS leads to activation of sGC, which then converts GTP to cGMP. Elevated intracellular cGMP levels activate effector proteins like PKG, PDE or cGMP-gated ion channels leading, for example, to vasodilatation and platelet inhibition. The molecular details involving mutations in *GUCY1A3* in the NO/cGMP pathway remain obscure.

For solving that question two different approaches were pursued:
(1) The functional investigation of eight rare missense variants in the coding sequence of the *GUCY1A3* gene identified by exome sequencing and being enriched in CAD/MI patients, and
(2) the functional investigation of the lead SNP rs7692387 located within an intronic region of the *GUCY1A3* gene.

2 Materials

2.1 Chemicals

Table 2 Listing of chemicals used

Manufacturer	Chemical	Catalogue#	Headquarters
Absource Diagnostics	bortezomib (PS-341)	PS-341	Munich, Germany
AppliChem	3-isobutyl-1-methylxanthin (IBMX) *BioChemica*	A0695	Darmstadt, Germany
	ampicillin sodium salt *BioChemica*	A0839	
	dimethyl sulfoxide (DMSO), cell culture grade *BioChemica*	A3672	
	kanamycin sulfate *BioChemica*	A1493	
	methanol (MeOH)	131091	
	nonfat dry milk powder *BioChemica*	A0830	
	sodium chloride for molecular biology *BioChemica*	A2942	
	Tween® 20 *BioChemica*	A1389	
Beckton Dickinson	BD Bacto™ tryptone	211705	Franklin Lakes, NJ, USA
	BD Bacto™ yeast extract	212750	
	BD Difco™ agar, granulated	214530	
Bio-Rad	2X laemmli	1610737	Hercules, CA, USA
	4X laemmli	1610747	
	10X TRIS/glycine/SDS	161-0772	
Bio/Data Corporation	adenosine diphosphate (ADP), 2 x 10^{-4} M	101312	Horsham, PA, USA
Carl Roth	2-propanol ROTIPURAN® ≥99.8 %	6752	Karlsruhe, Germany
	ethanol denatured ≥96 %	T171	
	glycine PUFFERAN® ≥99 %	3908	
	hydrochloric acid (HCl), 6 mol/l - 6 N	0281	
	Rotiphorese® gel 30 (37.5:1)	3029	
	trichlormethane/choroform ≥99 %, for synthesis	Y015	
	TRIS hydrochloride (TRIS-HCl) PUFFERAN® ≥99 %	9090	
	TRIS PUFFERAN® ≥99.9 %	4855	
Cisbio Bioassays	cellular kinase lysis buffer #1, 4X	64KL1FDF	Codolet, France
	EGFR lysis buffer, 4X	64KL1FDF	
	reconstitution buffer for conjugates	62RB3RDD	
Enzo Life Sciences	S-nitrosoglutathione (GSNO)	420-002	Farmingdale, NY, USA
Lonza	DMEM 4.5 g/l glucose w/ UltraGlutamine	BE12-604F	Basel, Switzerland
	HEPES buffered saline solution	CC-5024	
Merck Millipore	EMPURA® ethanol absolute	1070172511	Billerica, MA, USA
	sodium pyruvate (100 mM)	L 0473	
Merck Millipore/ Biochrom	fetal bovine serum (FBS) superior	S 0615	Billerica, MA, USA
	Dulbecco's PBS solution without Ca^{2+}, Mg^{2+}	L 1825	
New England Biolabs	10X RIPA	9806	Ipswich, MA, USA
	1X super optimal broth with catabolite repression (SOC) outgrowth medium	B9020	
	color prestained protein standard, broad range (11-245 kDa)	P7712	

Manufacturer	Chemical	Catalogue#	Headquarters
New England Biolabs	gel loading dye, purple 6X	B7024	Ipswich, MA, USA
	Quick-Load® 2-Log DNA ladder (0.1-10.0 kb)	N04695	
Promega Corporation	FuGENE® HD transfection reagent	E2312	Madison, WI, USA
PromoCell	endothelial cell growth medium MV	C-22020	Heidelberg, Germany
	endothelial cell growth medium MV SupplementMix	C-39225	
	smooth muscle cell growth medium 2	C-22062	
	smooth muscle cell growth medium 2 SupplementMix	C-39267	
	Hepes BSS	C-40020	
	trypsin-EDTA (0.04 %/0.03 %)	C-41020	
	trypsin neutralising solution (0.05 % trypsin inhibitor in 0.1 % BSA)	C-41120	
Roche Life Science	cOmplete, EDTA-free, *EASYpack*	04693159001	Penzberg, Germany
Rotexmedica GmbH	heparin sodium, 25,000 U/5 ml	03862340	Trittau, Germany
Sigma-Aldrich	ammonium persulfate (APS)	A3678	St. Louis, MO, USA
	amphotericin B solution (250 µg/mL in deionized water)	A2942	
	BAY 41-2272 ≥97 %	B8810	
	CelLytic M cell lysis reagent	C2978	
	chloroform:isoamyl alcohol (24:1)	C0549	
	ethylenediaminetetraacetic acid disodium salt (EDTA-Na_2) solution, 0.5 M	E7889	
	gelatin from porcine skin, powdered	G1890	
	N,N,N',N'-tetramethylethylenediamine (TEMED)	T9281	
	penicillin-streptomycin (10,000 units penicillin/ml, 10 mg streptomycin/ml)	P4333	
	sodium nitroferricyanide(III) dihydrate (sodium nitroprusside, SNP)	228710	
	β-mercaptoethanol	M3148	
Thermo Fisher Scientific	Ambion™ TRIzol® reagent	15596-026	Waltham, MA, USA
	Gibco™ Geneticin® selective antibiotic (G418 Sulfate)	11811031	
	Gibco™ Opti-MEM® I reduced serum medium	31985062	
	Gibco™ PBS (10X), pH 7.4	70011044	
	Gibco™ RPMI 1640 medium	21875034	
	Gibco™ trypan blue solution, 0.4 %	15250061	
	Gibco™ trypsin-EDTA (0.25 %), phenol red	25200056	
	Invitrogen™ GlycoBlue™ coprecipitant (15 mg/ml)	AM9515	
	Invitrogen™ Lipofectamine® RNAiMAX™ transfection reagent	13778150	
	Invitrogen™ UltraPure™ DNase/RNase-free distilled Water	10977035	
	Invitrogen™ UltraPure™ TRIS-borate-EDTA (TBE) buffer, 10X	15581028	
	Novex™ MagicMark™ XP Western protein standard	LC5602	
	Thermo Scientific™ BupH™ phosphate buffered saline packs	28372	
	Thermo Scientific™ Halt™ protease inhibitor cocktail, EDTA-free (100X)	87785	
VWR	universal agarose, peqGOLD	732-2789	Erlangen, Germany

2.2 Buffers, media, solutions

2.2.1 Standard buffers and solutions

1X phosphate buffered saline (PBS)

with a final concentration of 1 mM KH_2PO_4, 0.16 M NaCl, 2.97 mM Na_2HPO_4-$7H_2O$, pH 7.4 at room temperature

100 ml 10X Gibco™ PBS (Thermo Fisher Scientific)

ad 1000 ml Millipore® water

storage at room temperature

1X TRIS-borate-EDTA (TBE)

with a final concentration of 0.1 M TRIS, 90 mM boric acid, 1 mM EDTA, pH 8.3 at 20 °C

100 ml 10X Invitrogen™ UltraPure™ TRIS-borate-EDTA (TBE) buffer (Thermo Fisher Scientific)

ad 1000 ml Millipore® water

storage at room temperature

70 % v/v ethanol

35 ml EMPURA® ethanol absolute (Merck Millipore)

ad 50 ml DNase/RNase-free water

storage at room temperature

2.2.2 Media for cultivation and selection of bacteria

Ampicillin (100 mg/ml)/kanamycin (50 mg/ml) stock solutions

100 mg ampicillin sodium salt/50 mg kanamycin sulfate (both AppliChem)

ad 1 ml Millipore® water

Both, ampicillin and kanamycin solutions were filtered sterile using Stericup® filters (Merck Millipore) and stored at -20 °C.

Lysogeny broth (LB) medium

8 g BD Bacto™ tryptone (BD)

4 g BD Bacto™ yeast extract (BD)

8 g sodium chloride (AppliChem)

ad 800 ml Millipore® water
LB medium was autoclaved for 20 minutes at 121 °C and stored at 4 °C.

LB agar plates
8 g BD Bacto™ tryptone (BD)
4 g BD Bacto™ yeast extract (BD)
8 g sodium chloride (AppliChem)
12 g BD Difco™ agar, granulated (BD)
ad 800 ml Milipore® water
Medium for LB agar plates was autoclaved for 20 minutes at 121 °C. After cooling down to approximately 55 °C the respective antiobotic stock solution was added in a ratio of 1:1000 and the medium was casted into 10 cm dishes. Plates were stored at 4 °C.

2.2.3 Media and solutions for cultivation of human cells

0.1 % w/v gelatin
1 g gelatin (Sigma-Aldrich)
ad 1000 ml Millipore® water
The gelatin was autoclaved for 20 minutes at 121 °C. After cooling down 1 ml penicillin-streptomycin (Sigma-Aldrich) was added and stored at 4 °C.

250 mg/ml geneticin
1.5 g Geneticin® selective antibiotic (Thermo Fisher Scientific)
ad 6 ml Millipore® water
The geneticin solution was filtered sterile using Stericup® filters (Merck Millipore) and stored at 4 °C.

HEK 293 medium
500 ml DMEM 4.5 g/l glucose w/ UltraGlutamine (Lonza)
50 ml FBS superior (Merck Millipore/Biochrom)
5 ml penicillin-streptomycin (Sigma-Aldrich)
5 ml ampothericin B solution (Sigma-Aldrich)
500 µl geneticin (250 mg/ml)
storage at 4 °C

VSMC medium

500 ml smooth muscle cell growth medium 2 (PromoCell)

25 ml smooth muscle cell growth medium 2 SupplementMix (PromoCell)

5 ml penicillin-streptomycin (Sigma-Aldrich)

storage at 4 °C

Meg-01 medium

500 ml Gibco™ RPMI 1640 medium (Thermo Fisher Scientific)

50 ml FBS superior (Merck Millipore/Biochrom)

5 ml penicillin-streptomycin (Sigma-Aldrich)

2 ml sodium pyruvate (Merck Millipore)

storage at 4 °C

EC medium

500 ml endothelial cell growth medium MV (PromoCell)

25 ml endothelial cell growth medium MV SupplementMix (PromoCell)

5 ml penicillin-streptomycin (Sigma-Aldrich)

storage at 4 °C

For freezing cells, media for each cell line was supplemented with 10 % DMSO (AppliChem).

2.2.4 Buffers and solutions for Western blotting

0.5 M TRIS-HCl, pH 6.8

27.23 g TRIS-HCl PUFFERAN® (Carl Roth)

ad 80 ml Millipore® water

pH adjustment was achieved with 6 N HCl (Carl Roth). Afterwards the volume was filled up to 150 ml with Millipore® water.

1.5 M TRIS-HCl, pH 8.8

6 g TRIS-HCl PUFFERAN® (Carl Roth)

ad 60 ml Millipore® water

pH adjustment was achieved with 6 N HCl (Carl Roth). Afterwards the volume was filled up to 150 ml with Millipore® water.

10 % w/v ammonium perfulfate (APS)
1 g APS (Carl Roth)
ad 10 ml Millipore® water

10 % w/v SDS
10 g SDS (Carl Roth)
ad 100 ml Millipore® water
storage at room temperature

12 % v/v SDS-polyacrylamide resolving gels (volume/gel)
4 ml Rotiphorese® gel 30 (37.5:1) (Carl Roth)
2.5 ml 1.5 M TRIS-HCl, pH 8.8
100 µl SDS (10 % w/v)
3353.3 µl Millipore® water
5 µl TEMED (Sigma-Aldrich)
50 µl APS (10 % w/v)
It is important that TEMED and APS are added ad the end.

4 % v/v SDS-polyacrylamide stacking gels (volume/gel)
528 µl Rotiphorese® gel 30 (37.5:1) (Carl Roth)
1008 µl 0.5 M TRIS-HCl, pH 6.8
40 µl SDS (10 % w/v)
2.4 ml Millipore® water
4 µl TEMED (Sigma-Aldrich)
20 µl APS (10 % w/v)
It is important that TEMED and APS are added ad the end.

1X radioimmunoprecipitation assay (RIPA) buffer
10 ml 10X RIPA (New England Biolabs)
ad 100 ml Millipore® water
storage at -20 °C

2X laemmli buffer
with a final concentration of 355 mM β-mercaptoethanol
50 µl β-mercaptoethanol (Sigma-Aldrich)
950 µl 2X laemmli (Bio-Rad)
storage at -20 °C

4X laemmli buffer

with a final concentration of 355 mM β-mercaptoethanol

100 µl β-mercaptoethanol (Sigma-Aldrich)

900 µl 4X laemmli (Bio-Rad)

storage at -20 °C

1X running buffer

100 ml 10X 10X Tri/Glycine/SDS (Bio-Rad)

2 ml Tween® 20 (AppliChem)

ad 1000 ml Millipore® water

storage at room temperature

1X transfer buffer

3,03 g TRIS PUFFERAN® (Carl Roth)

14,4 g glycine PUFFERAN® (Carl Roth)

200 ml methanol (AppliChem)

ad 1000 ml Millipore® water

storage at room temperature

1X PBS-T

with a final concentration of 1 mM KH_2PO_4, 0.16 M NaCl, 2.97 mM Na_2HPO_4-$7H_2O$, 0.2 % v/v Tween® 20, pH 7.4 at room temperature

100 ml 10X Gibco™ PBS (Thermo Fisher Scientific)

2 ml Tween® 20 (AppliChem)

ad 1000 ml Millipore® water

storage at room temperature

5 % w/v milk in PBS

5 g nonfat dry milk powder (AppliChem)

ad 100 ml 1X PBS (diluted from 10X Gibco™ PBS in Millipore® water)

storage at 4 °C for up to two days

2.5 % w/v milk in PBS-T

2.5 g nonfat dry milk powder (AppliChem)

ad 100 ml 1X PBS-T (composition see above)

storage at 4 °C for up to two days

2.2.5 Buffers and solutions for EMSA

1X PBS

with a final concentration of 0.1 M sodium phosphate, 0.15 M NaCl, pH 7.2
1 pouch of Thermo Scientific™ BupH™ PBS (Thermo Fisher Scientific) was dissolved in 500 ml Millipore® water and stored at 4 °C.

0.5X TBE

with a final concentration of 0.05 M TRIS, 45 mM boric acid, 0.5 mM EDTA, pH 8.3 at 20 °C
50 ml 10X Invitrogen™ UltraPure™ TBE buffer (Thermo Fisher Scientific)
ad 1000 ml Millipore® water
storage at 4 °C

4 % polyacrylamide gels (volume/gel)

1.33 ml Rotiphorese® gel 30 (37.5:1) (Carl Roth)
500 µl 10X Invitrogen™ UltraPure™ TBE buffer (Thermo Fisher Scientific)
8.06 ml Millipore® water
100 µl APS (10 % w/v)
10 µl TEMED (Sigma-Aldrich)
It is important to add APS and TEMED at the end.

2.2.6 Further solutions

1 M sodium chloride (NaCl) stock solution

1.17 g sodium chloride (AppliChem)
ad 20 ml DNase/RNase-free water
storage at room temperature

50 U/ml heparin

Heparin sodium, 25,000 U/5 ml (Rotexmedica GmbH) was diluted 1:100 in Dulbecco's PBS solution without Ca^{2+}, Mg^{2+} (Merck Millipore/Biochrom). Dilution was carried out anew for each experiment.

60 mM hydrochloric acid (HCl) working solution

500 µl HCl (6 N) (Carl Roth)
ad 50 ml DNase/Rnase-free water

As the HCl was required to be ice-cold it was stored at -20 °C and thawed on ice just before the experiment.

200 µM adenosine diphosphate (ADP) stock solution

1 vial of lyophilised ADP (2 x 10^{-4} M) was reconstituted in 500 µl DNase/RNase-free water to a stock concentration of 200 µM and stored at 4 °C.

20 µM ADP working solution

The ADP working solution was freshly prepared for every experiment by diluting the stock solution 1:10 in DNase/RNase-free water.

200 mM sodium nitroprusside (SNP) stock solution

30 mg SNP (Sigma-Aldrich)

ad 500 µl DMSO (AppliChem)

Due to its short half-life SNP was prepared freshly for each experiment.

1 mM S-nitrosoglutathione (GSNO) stock solution

0.001 g GSNO (Enzo Life Sciences)

ad 2.97 ml DNase/RNase-free water

Due to its short half-life SNP was prepared freshly for each experiment.

0.5 mM GSNO working solution

The GSNO working solution was freshly prepared for every experiment by diluting the stock solution 1:2 in DNase/RNase-free water.

100 mM 3-isobutyl-1-methylxanthin (IBMX) stock solution

222.25 mg IBMX (AppliChem)

ad 10 ml DMSO (AppliChem)

IBMX was aliquoted to sterile 1.5 ml reaction tubes and stored at -20 °C.

10 mM BAY 41-2272 stock solution

5 mg of BAY 41-2272 (Sigma-Aldrich) were solved in 1.39 ml DMSO (AppliChem), aliquoted to sterile 1.5 ml reaction tubes and stored at -20 °C.

10 mM bortezomib stock solution

5 mg of bortezomib (Abource Diagnostics) were solved in 1.3 ml DMSO (AppliChem), aliquoted to sterile 1.5 ml reaction tubes and stored at -80 °C.

2.3 Primers

Salt free primers were purchased from Eurofins Genomics (Ebersberg, Germany). Primer stocks were liquid in water with a stock concentration of 100 µM. They were diluted in DNase/RNase-free water to working concentrations needed and stored at -20 °C.

2.4 Nucleic acids

Table 3 Listing of nucleic acids used

Manufacturer	Nucleic acid	Catalogue#	Headquarters
BioChain	total RNA – human adult normal tissue: heart	R1234122-50	Newark, CA, USA
Thermo Fisher Scientific	Ambion™ Silencer® select negative control no. 1 siRNA 5 nmol	4390843	Waltham, MA, USA
	Silencer® select ZEB1 siRNA s229971 5 nmol	4392420	
	Silencer® select ZEB1 siRNA s229972 5 nmol	4392420	
	Silencer® select ZEB1 siRNA s229970 5 nmol	4392420	

siRNAs (5 nmol) were diluted in 50 µl DNase/RNase-free water to a stock solution of 100 µM. Besides commercially available nucleic acids listed in Table 3, genomic DNA isolated from CAD patients using the Gentra® Puregene® blood kit from Qiagen (Catalogue# 158389) in the course of a study conducted by Bernhard Wolf (Institute for Cardiovascular Diseases, German Heart Centre Munich, Germany) was used for genotyping.

2.5 Antibodies

2.5.1 Primary antibodies

Table 4 Listing of primary antibodies

Manufacturer	Antibody	Catalogue#	Headquarters
Cell Signaling Technology	GAPDH (D16H11) XP® antibody, rabbit monoclonal	5174	Danvers, MA, USA
	phospho-VASP (Ser239) antibody, rabbit polyclonal	3114	
	TCF8/ZEB1 (D80D3) antibody, rabbit monoclonal	3396	
	VASP (9A2) antibody, rabbit monoclonal	3132	
Novus Biologicals	guanylyl cyclase alpha 1 antibody, rabbit polyclonal	NBP2-13000	Minneapolis, MN, USA
Santa Cruz Biotechnology	ZEB1 antibody (C-20) X	sc-10570 X	Dallas, TX, USA
Sigma-Aldrich	IgG from mouse serum	I8765	St. Louis, MO, USA

Manufacturer	Antibody	Catalogue#	Headquarters
Sigma-Aldrich	monoclonal ANTI-FLAG® M2 antibody, mouse monoclonal	F1804	
Thermo Fisher Scientific	Invitrogen™ HA tag antibody (2-2.2.14), mouse monoclonal	26183	Waltham, MA, USA
	Invitrogen™ V5 Tag Antibody, mouse monoclonal	R960-25	

2.5.2 HRP-conjugated secondary antibodies

Table 5 Listing of HRP-conjugated secondary antibodies used

Manufacturer	Antibody	Catalogue#	Headquarters
Cell Signaling Technology	anti-rabbit IgG, HRP-linked antibody	7074	Danvers, MA, USA
	anti-mouse IgG, HRP-linked antibody	7076	

2.5.3 TR-FRET antibodies

Table 6 Antibodies used for TR-FRET

Manufacturer	Antibody	Catalogue#	Headquarters
Cisbio Bioassays	anti-HA-d2	610HADAA	Codolet, France
	anti-HA-EuK	610HAKLA	
	anti-Flag-d2	61FG2DLA	
	anti-Flag-EuK	61FG2KLA	

2.6 Enzymes

2.6.1 Polymerases

Table 7 Mastermixes and assay containing polymerases

Manufacturer	Mastermix	Catalogue#	Headquarters
New England Biolabs	Q5® high-fidelity 2X master mix	M0492	Ipswich, MA, USA
	OneTaq® Quick-Load® 2X master mix with standard buffer	M0486	
Quanta Biosciences	PerfeCTa® SYBR® Green FastMix®, low ROX™	95074	Gaithersburg, MD, USA
Thermo Fisher Scientific	TaqMan® genotyping assay C__29125113_10	4351379	Waltham, MA, USA

2.6.2 Restriction enzymes

Table 8 Restriction enzymes used in this study

Manufacturer	Enzyme	Catalogue#	Headquarters
New England Biolabs	AlwNI	R0514	Ipswich, MA, USA
	BbsI	R0539	
	BmgBI	R0628	
	BsiWI	R0553	
	EcoNI	R0521	
	HindIII	R0104	
New England Biolabs	NheI	R0131	
	PvuII	R0151	
	XbaI	R0145	

2.6.3 Other enzymes

Table 9 Further enzymes used in this study

Manufacturer	Enzyme	Catalogue#	Headquarters
Thermo Fisher Scientific	DNase I, amplification grade, 1 U/µl	18068015	Waltham, MA, USA
	Invitrogen™ Gateway® BP Clonase® II enzyme mix (incl. Proteinase K, 2 µg/µl)	11789020	
	Invitrogen™ Gateway® LR Clonase® II enzyme mix (incl. Proteinase K, 2 µg/µl)	11791100	

2.7 Cell lines

Human embryonic kidney (HEK) 293 cells as well as human megakaryoblastic leukemia cells (Meg-01) were a kind gift of Steffen Massberg (Medizinische Klinik und Poliklinik I, Ludwig-Maximilians-University Munich, Germany). Scratch wound assays as well as qPCR experiments on vascular smooth muscle cells (VSMC; without knockdown) were conducted in collaboration with Mete Civelek (Center for Public Health Genomics, University of Virgina, Charlottesville, VA, USA). These cells were part of the Systems Genetics Resource at the University of California, Los Angeles (van Nas *et al.* 2013) (*https://systems.genetics.ucla.edu/*) and had been isolated from healthy heart transplant donors. VSMC used for all other experiments as well as endothelial cells (EC) were commercially available.

Table 10 Commercially available cell lines used

Manufacturer	Celline	Order#	Headquarters
PromoCell	human vascular smooth muscle cells	C-12533	Heidelberg,
	human coronary artery endothelial cells	C-12221	Germany

2.8 Chemically competent bacteria

Table 11 Bacteria used in this study

Manufacturer	Bacteria	Catalogue#	Headquarters
New England Biolabs	NEB 5-alpha competent *E. coli*	C2987	Ipswich, MA, USA
Agilent Technologies	XL10-Gold ultracompetent cells	as part of 200522	Santa Clara, CA, USA

2.9 Mice

Eight weeks old male C57Bl/6NCrl mice were obtained from Charles River Laboratories, Sulzfeld, Germany. They were kept in Makrolon® cages type III H and fed with a ssniff® standard diet.

2.10 Cloning vectors

Table 12 Gateway® vectors

Manufacturer	Vector	Description	Catalogue#	Headquarters
Thermo Fisher Scientific	Gateway® pDONR™221	entry vector	12536017	Waltham, MA, USA
	Gateway® pcDNA™-DEST40	expression vector	12274015	

Table 13 Luciferase vectors

Manufacturer	Vector	Description	Catalogue#	Headquarters
Promega Corporation	pGL4.10[*luc2*]	promoterless firefly luciferase reporter vector	E6651	Fitchburg, WI, USA
	pRL-TK	*Renilla* luciferase internal control reporter vector	E2241	

Table 14 Cloned plasmids with inserts of human origin

Vector	Selection	Description of insert	Size
Gateway® pDONR™221	kanamycin	*GUCY1A3* w/o stop	4632
		GUCY1A3 w/ stop	4635

Vector	Selection	Description of insert	Size
Gateway®	kanamycin	*GUCY1B3* w/o stop	4419
pDONR™221		*GUCY1B3* w/ stop	4422
Gateway®	ampicillin	*GUCY1A3* wildtype w/o stop	7576
pcDNA™-DEST40		*GUCY1A3* wildtype w/ stop	7579
		GUCY1A3 wildtype w/ N-terminal HA tag and stop	7606
		GUCY1A3 wildtype w/ C-terminal HA tag and stop	7606
		GUCY1A3 p.Lys53Glu w/o stop	7576
		GUCY1A3 p.Lys53Glu w/ C-terminal HA tag and stop	7606
		GUCY1A3 p.Thr64Ala w/o stop	7576
Gateway®	ampicillin	*GUCY1A3* p.Thr64Ala w/ C-terminal HA tag and stop	7606
pcDNA™-DEST40		*GUCY1A3* p.Leu163Phefs*24 w/o stop	7577
		GUCY1A3 p.Leu163Phefs*24 w/ C-terminal HA tag and stop	7607
		GUCY1A3 p.Thr229Met w/o stop	7576
		GUCY1A3 p.Thr229Met w/ C-terminal HA tag and stop	7606
		GUCY1A3 p.Ser478Gly w/o stop	7576
		GUCY1A3 p.Ser478Gly w/ C-terminal HA tag and stop	7606
		GUCY1A3 p.Gly537Arg w/o stop	7576
		GUCY1A3 p.Gly537Arg w/ C-terminal HA tag and stop	7606
		GUCY1A3 p.Ile571Val w/o stop	7576
		GUCY1A3 p.Ile571Val w/ C-terminal HA tag and stop	7606
		GUCY1A3 p.Val587Ile w/o stop	7576
		GUCY1A3 p.Val587Ile w/ C-terminal HA tag and stop	7606
		GUCY1A3 p.Cys610Tyr w/o stop	7576
		GUCY1A3 p.Cys610Tyr w/ C-terminal HA tag and stop	7606
		GUCY1B3 wildtype w/o stop	7363
		GUCY1B3 wildtype w/ stop	7366
		GUCY1B3 wildtype w/ N-terminal Flag tag and stop	7390
		GUCY1B3 wildtype w/ C-terminal Flag tag and stop	7390
pGL4.10[*luc2*]	ampicillin	lead SNP region rs7692387 w/ non-risk allele A (upstream of *luc2*)	4769
		lead SNP region rs7692387 w/ risk allele G (upstream of *luc2*)	4769
pBiFC-YN155*	ampicillin	*GUCY1A3* w/o stop	7286
pBiFC-YC155#	ampicillin	*GUCY1B3* w/o stop	5921

*,# originally containing coding sequences for rat *Gucy1a3* and *Gucy1b3* (Rothkegel *et al.* 2007), these plasmids were a kind gift of J.-P. Stasch (PharmaResearch Center, Bayer HealthCare, Wuppertal, Germany).

Additionally to the plasmids listed above in Table 14, further plasmids were used in this study which were kindly provided by Frank Kaiser (Institute of Human Genetics, UKSH Lübeck, Germany) as part of a collaborational work; (1) three pGL4.10[*luc2*] constructs with all of them carrying the *GUCY1A3* promoter (2,578 bp; chr4:155,666,380-155,668,957 (GRCh38/hg38)) upstream of the *luc2* gene with two of them additionally carrying a 407 bp fragment flanking the lead SNP (rs7692387; chr4: 155,713,878-155,714,284 (GRCh38/hg38)) downstream of the *luc2* gene and (2) the full length open reading frame of human *ZEB1* inserted into the 3xFLAG® (Sigma-Aldrich) expression plasmid leading to a C-terminal fusion construct.

Cards for vectors listed in Table 12 and Table 13 as well as vector cards for pBiFC-*GUCY1A3 w/o stop*-YN155 and pBiFC-*GUCY1B3 w/o stop*-YC155 listed in Table 14 are depicted in Appendix Section B.

2.11 Commercially available kits

Table 15 Commercially available kits

Manufacturer	Kit	Catalogue#	Headquarters
Agilent Genomics	QuikChange II XL site-directed mutagenesis kit	200522	Santa Clara, CA, USA
Eurofins Genomics	Mix2Seq kit	*online order*	Ebersberg, Germany
IBL International	cGMP RIA	RE29075	Hamburg, Germany
Promega Corporation	Dual-Luciferase® reporter assay system	E1960	Fitchburg, WI, USA
Qiagen	MinElute® gel extraction kit	28604	Hilden, Germany
	QIAGEN® plasmid midi kit	12145	
	QIAshredder™	79656	
	RNeasy® Plus mini kit	74136	
Qiagen	Gentra® Puregene® blood kit	158389	
Roche Life Science	Rapid DNA Dephos & Ligation kit	04898117001	Penzberg, Germany
Sigma-Aldrich	GeneElute™ plasmid miniprep kit	PLN350-1KT	St. Louis, MO, USA
Thermo Fisher Scientific	Thermo Scientific™ LightShift™ chemiluminescent EMSA kit	20148	Waltham, MA, USA
	NE-PER™ nuclear and cytoplasmic extraction Reagents	78833	
	Thermo Scientific™ Pierce™ biotin 3' end DNA labeling kit	89818	
	Pierce™ BCA protein assay kit	23225	
	Pierce™ ECL Western blotting substrate	32106	
	ThermoScript™ RT-PCR system for first-strand cDNA synthesis	11146016	
	Novex™ Dynabeads® co-immunoprecipitation kit	14321D	

2.12 Consumables

Table 16 Listing of consumables used

Manufacturer	Consumable	Catalogue#	Headquarters
5 PRIME GmbH	phase lock gel heavy 1.5 ml	2302810	Hilden, Germany
Bio-Rad	cell counting slides for TC10™	1450011	Hercules, CA, USA
Bio/Data Corporation	test tubes - micro (7.25 x 55 mm) for PAP8	101521	Horsham, PA, USA
	stir bars (micro)	105990	
Merck Millipore	Scepter™ cell counter sensors, 60 µm	PHCC60050	Billerica, MA, USA
	Stericup®-GP, 0.22 µm, polyethersulfone, 150 ml, radio-sterilised	SCGPU01RE	
	Immobilon®-P PVDF membrane, 0.45 µm	IPVH00010	
Thermo Fisher Scientific	Applied Biosystems™ MicroAmp® fast optical 96 well reaction plate, 0.1 ml	4346907	Waltham, MA, USA
	Applied Biosystems™ MicroAmp® optical 384 well reaction plate with barcode	4309849	
	Applied Biosystems™ MicroAmp® optical adhesive film	4311971	
	Thermo Scientific™ Biodyne™ B nylon membrane, 0.45 µm, 8 cm x 12 cm	77016	

2.13 Devices and utensils

Table 17 Listing of devices and utensils used

Manufacturer	Device	Type designation	Headquarters
Berthold Technologies	gamma counter	LB 2111	Bad Wildbad, Germany
Bio-Rad	vertical electrophoresis system	Mini-PROTEAN® tetra cell	Hercules, CA, USA
	blotting module	Mini Trans-Blot® electrophoretic transfer cell	
	horizontal electrophoresis system		
Bio-Rad	cell counter	TC10™	
Bio/Data Corporation	platelet aggregation profiler	PAP8 v2.0	Horsham, PA, USA
GE Healthcare Life Sciences	biomolecular imager	ImageQuant™ LAS 4000	Chicago, IL, USA
Merck Millipore	millipore water system	Milli-Q® Reference	Billerica, MA, USA
	cell counter	Scepter™	
Minitüb GmbH	heating plate	HT 00 W	Tiefenbach, Germany
Nikon	inverted microscope	Eclipse TS100	Tokyo, Japan
Olympus	inverted microscope	IX50	Tokyo, Japan
Sysmex Corporation	haemocytometer	KX-21N	Kobe, Japan
Tecan Group	microplate reader	Infinite® M200 PRO	Männedorf, Switzerland
	microplate reader	Infinite® F200 PRO	
Thermo Fisher Scientific	real-time PCR instrument	Applied Biosystems™ ViiA™ 7 real-time PCR system	Waltham, MA, USA
	inverted microscope	Invitrogen™ EVOS® FL Auto imaging system	

2.14 Software

Table 18 Software and their application

Manufacturer	Software	Application	Headquarter
Bio/Data Corporation	PAP8 v2.0 software	platelet aggregation documentation	Horsham, PA, USA
CLC bio	CLC Main Workbench 6	· sequencing data analysis · cloning · multiple sequence alignments	Arhus, Denmark
GE Healthcare Life Sciences	ImageQuant™ LAS 4000 v1.2	· Western blot documentation · gel electrophoresis documentation	Chicago, IL, USA
	ImageQuant™ TL 1D v8.1	Western blot quantification	
GraphPad Software	GraphPad Prism® software version 6.0 version 6.0 for Mac OS X	statistical analyses	La Jolla, CA, USA
National Institutes of Health	ImageJ 1.47v	scratch wound assay analysis	Bethesda, MD, USA
PerkinElmer	Openlab 3.2.1	2D microscope image processing	Waltham, MA, USA

Manufacturer	Software	Application	Headquarter
Tecan Group	iControl v1.10	· nucleic acid concentration · luciferase assay	Männedorf, Switzerland
	Magellan™ data analysis software v7.2	BCA measurement	
Thermo Fisher Scientific	ViiA™ 7 software v1.2.2	· qPCR measurement · genotyping measurement	Waltham, MA, USA
	TaqMan® Genotyper software v1.3	analysis of genotyping results	
	EVOS® FL Auto software v1.6	2D microscope image processing	

2.15 Databases

Ensembl Genome Browser *http://www.ensembl.org*

National Center for Biotechnology Information (NCBI)
http://www.ncbi.nlm.nih.gov/

SNP Annotation and Proxy Search
http://archive.broadinstitute.org/mpg/snap/ldsearchpw.php

UCSC Genome Browser *https://genome.ucsc.edu*

2.16 Online tools and resources

AliBaba2.1 *http://www.gene-regulation.com/pub/programs/alibaba2/index.html?*

Double Digest Finder *https://www.neb.com/tools-and-resources/interactive-tools/double-digest-finder*

ExPASY PeptideMass *http://web.expasy.org/peptide_mass/*

ExPASy Translate tool *http://web.expasy.org/translate/*

NEBcutter V2.0 *http://nc2.neb.com/NEBcutter2/*

QuikChange Primer Design *http://www.genomics.agilent.com/primerDesignProgram.jsp*

Reverse Complement *http://www.bioinformatics.org/sms/rev_comp.html*

3 Methods

3.1 Primer design

Primers for polymerase chain reaction (PCR), Gateway® cloning and conventional cloning were designed using the online tool *NCBI Primer Blast*. *AttB* sites in the Gateway® primers as well as restriction sites in the primers used for conventional cloning were added manually. Forward primers for Gateway® cloning contained – additonally to the *attB1* site – two short recognition sequences that greatly facilitate the initial binding of mRNA to the small subunit of the ribosome. The Shine-Dalgarno sequence (GAAGGAGATA) is a ribosomal binding site in prokaryotic mRNA whereas the Kozak sequence occurs in eukaryotic mRNA (ACCATG). Exemplary Gateway® primer sequences for the amplification of *GUCY1A3* can bee appreciated in Figure 8. An exemplary primer pair for the amplification of the rs7692387 lead SNP region with recognition sites for NheI and HindIII for conventional cloning is shown in Figure 9. Primers for site-directed mutagenesis were designed using the online tool *QuikChange Primer Design* from Agilent Technologies. If applicable, primers for the amplification of cDNA were designed to span exon-exon junctions. Primers used for sequencing were were designed manually without the use of a primer designing program. All primers used in this study are listed in Appendix Section A.

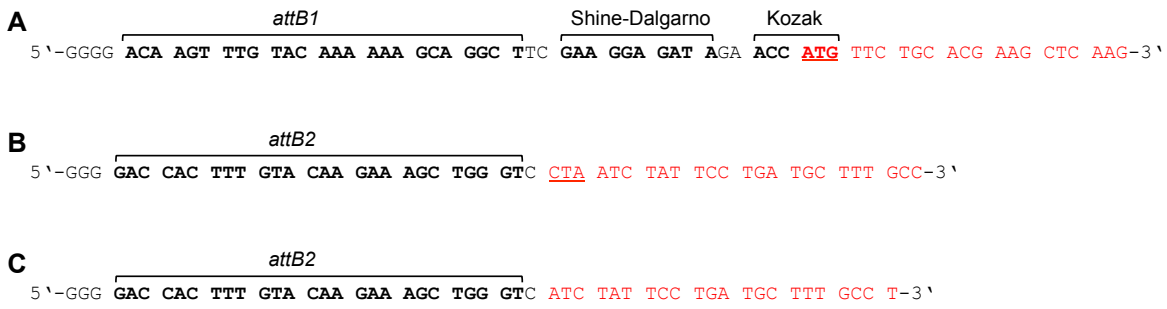

Figure 8 Exemplary forward and reverse Gateway® primers for the amplification of the human *GUCY1A3* coding sequence. *AttB* sites, Shine-Dalgarno as well as Kozak sequences are indicated as bold and start and stop codons are underlined. cDNA-specific nucleotides are marked in red. Forward primer (A), reverse primer with stop codon (B), reverse primer without stop codon allowing the C-terminal fusion with a tag (C).

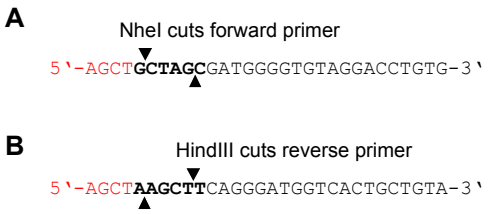

Figure 9 Exemplary forward and reverse primer sequences for conventional cloning of the region flanking the *GUCY1A3* lead SNP rs7692387 into pGL4.10[*luc2*] plasmid. Restriction sites are indicated as bold, four base overhangs for efficient cleavage marked in red. The resulting 597 bp long amplificate spanning the SNP carries a NheI restriction site at the 5' end (A) and a HindIII restriction site at the 3' end (B).

3.2 Polymerase chain reaction

Polymerase chain reaction (PCR) enables the exponential amplification of a defined DNA sequence *in vitro* (Mullis *et al.* 1986, Sambrook *et al.* 1989). In general, a PCR proceeds in three steps which are defined by different temperatures. During the *denaturation step* a temperature of 94-98 °C causes disruption of the hydrogen bonds between complementary bases resulting in single-stranded DNA. During the *annealing step* the temperature is lowered to 50-65 °C. This temperature range is needed for the primers to anneal to the DNA template. The temperature during the *elongation step* is again raised to 68-72 °C depending on the polymerase used. The polymerase synthesises a new DNA strand complementary to the target DNA. All three steps are repeated between 25-fold to 40-fold.

3.2.1 Endpoint PCR

Conventional endpoint PCR was performed when a qualitative detection of a specific target cDNA was required (see primers from Appendix Table 2 and Appendix Table 3). Furthermore, it was applied for amplification of a target cDNA or gDNA sequence prior to cloning (see primers from Appendix Table 4 to Appendix Table 6). For these applications two different PCR setups were applied (Table 19 to Table 22) which were prepared in sterile 200 µl tubes. Water instead of sample served as negative control.

Table 19 PCR reaction mix for qualitative detection of cDNA

Volume	Reagent	Final concentration
12.5 µl	OneTaq® Quick-Load® 2X master mix with standard buffer	
variable	100 cDNA template*	
1 µl	10 µM forward primer	0.4 µM
1 µl	10 µM reverse primer	0.4 µM
ad 25 µl	water	

*amount corresponding to ng of RNA

Table 20 PCR reaction mix for amplification of cDNA/DNA prior to cloning

Volume	Reagent	Final concentration
12.5 µl	Q5® high-fidelity 2X master mix	
variable	100 ng cDNA*/10 ng gDNA template[#]	
1.25 µl	10 µM forward primer	0.5 µM
1.25 µl	10 µM reverse primer	0.5 µM
ad 25 µl	water	

*amount corresponding to ng of RNA for Gateway® cloning
[#]for construction of luciferase plasmids

Table 21 General thermocycling profile for OneTaq® Quick-Load® 2X master mix

Step	Temperature	Duration
Initial denaturation:	95 °C	30 s
40 cycles:	95 °C	15 s
	60 °C	30 s
	68 °C	1 min/kb
Final extension:	68 °C	5 min
Hold:	4 °C	∞

Table 22 Thermocycling profile for Q5® high-fidelity 2X master mix

Step	Temperature	Duration
Initial denaturation:	98 °C	30 s
40 cycles:	98 °C	10 s
	60 °C	30 s
	72 °C	30 s/kb
Final extension:	72 °C	2 min
Hold:	4 °C	∞

PCR products were separated on 1 % w/v agarose gels as described in Section 3.3. Prior to cloning, bands were extracted from the gels following the protocol in Section 3.4.

3.2.2 Real-time quantitative PCR

In contrast to conventional endpoint PCR, real-time quantitative PCR (qPCR) provides the possibility to quantify the PCR products. The quantification is thereby based on fluorescence measurement. For our studies, qPCR was performed using PerfeCTa® SYBR® Green FastMix®, low ROX™ (Quanta Biosciences). SYBR® Green is a non-specific fluorescence dye that intercalates with double-stranded DNA. Oligonucleotide primers used for qPCR are listed in Appendix Table 2. Table 23 shows the setup for qPCR reactions, Table 24 the cDNA amounts used and Table 25 the thermocycle conditions. A non-template control from cDNA first-strand synthesis (Section 3.14) as well as water served as negative controls. Additionally, when qPCR followed overexpression of *GUCY1A3* and *GUCY1B3* in HEK 293 cells, for each sample controls from cDNA first-strand synthesis without reverse transcription were run to access non-digested plasmid contamination levels. Every cDNA sample/control was analysed as technical triplicate upon the Applied Biosystems™ ViiA™ 7 real-time PCR system by use of the ViiA™ 7 software v1.2.2 (both Thermo Fisher Scientific) in 96 well format.

Results for *GUCY1A3*, *GUCY1B3* and *ZEB1* were normalised against *RPLP0* expression. For siRNA experiments, $2^{-\Delta\Delta\mathrm{Ct}}$ values were analysed using One-sample t test with the reference value of 1 for control siRNA treatment. For comparison of gene expression in different individuals, ΔCt values were analysed using Student's unpaired t test (Yuan *et al.* 2006) and plotted as $2^{-\Delta\mathrm{Ct}}$ values. For all qPCR primers used PCR products were first run on an agarose gel to confirm that products of the expected size were detected.

Table 23 qPCR reaction mix setup

Volume	Reagent	Final concentration
10 µl	PerfeCTa® SYBR® Green FastMix®	
variable	cDNA sample	
1 µl	8 µM forward primer	0.5 µM
1 µl	8 µM reverse primer	0.5 µM
ad 20 µl	water	

Table 24 cDNA amounts used for qPCR

Source of cDNA	Target gene	cDNA amount*
HEK 293	*GUCY1A3*	50 ng (1 µl)
	GUCY1A3 (overexpressing HEK 293)	1 ng (1 µl 1:50 in DNase/RNase-free water)
	GUCY1B3	50 ng (1 µl)
	ZEB1	1 ng (1 µl 1:50 in DNase/RNase-free water)
VSMC	*GUCY1A3*	7 ng (2 µl)
	ZEB1	7 ng (2 µl)

*amount corresponding to ng of RNA

Table 25 Cycle conditions for qPCR

Step	Temperature	Duration
Initial denaturation:	95 °C	30 s
40 cycles:	95 °C	15 s
	60 °C	1 min
Melt curve:	95 °C	15 s
	60 °C	1 min
	95 °C	15 s

3.2.3 Genotyping

Genotyping was performed using Universal TaqMan® mastermix II, no UNG in combination with the TaqMan® SNP genotyping assay for rs7692387 (both Thermo Fisher Scientific). The assay contains a PCR primer pair to detect specific SNP targets as well as sequence-specific TaqMan® MGB probes labelled with the fluorescent dyes FAM and VIC. Detection is permitted after hybridisation of the probes to their target sequences. DNA was diluted to a concentration of 10 ng/µl in water. 10 ng of the samples were measured in 384 well format with the Applied Biosystems™ ViiA™ 7 real-time PCR system and analysed with the TaqMan® Genotyper software v1.3 (both Thermo Fisher Scientific). Per 384 well plate three water controls were applied. For reaction mixes, which were prepared in sterile 1.5 ml tubes, and cycle conditions see Table 26 and Table 27.

Table 26 Genotyping reaction mix

Volume	Reagent
3 µl	2X Universal TaqMan® mastermix II, no UNG
0.3 µl	20X TaqMan® SNP genotyping assay for rs7692387
1 µl	DNA (10 ng/µl)
ad 6 µl	DNase/RNase-free water

Table 27 Cycle conditions for genotyping

Step	Temperature	Duration
Initial denaturation:	95 °C	10 min
40 cycles:	95 °C	15 s
	60 °C	1 min
Post-PCR read:	60 °C	30 s

3.3 Agarose gel electrophoresis of DNA

DNA was resolved in horizontal agarose gel electrophoresis at 130 V (1 % w/v in 1X TBE buffer). 1X TBE was used as electrophoresis buffer. If required, DNA was mixed 6:1 with 6X purple loading dye (New England Biolabs) before loading. The 2-Log DNA Ladder (New England Biolabs) ranging from 0.1 to 10.0 kb was used as size reference. Gels were photographed under UV light in the ImageQuant™ LAS 4000 biomolecular imager using the ImageQuant™ LAS 4000 v1.2 software (both GE Healthcare Life Sciences).

3.4 DNA extraction from agarose gels

DNA bands were visualised on a UV transilluminator, excised with a sterile scalpel, and transferred into a sterile 1.5 ml reaction tube. DNA isolation from the gel slice was done using the MinElute® gel extraction kit (Qiagen) according to the manufacturer's instructions. Briefly**,** 100 µl buffer QG were added to the excised band and incubated for 10 min at 50 °C with vortexing in-between. DNA was precipitated by adding 100 µl isopropanol (100 % v/v) to the sample and inverting several times. After loading the sample onto a MinElute® column and centrifugation for 1 min at 17,900 x g, the DNA was washed with 500 µl QG followed by 1 min centrifugation at 17,900 x g. A second wash step was performed by adding 750 µl PE buffer to the column and 1 min centrifugation at 17,900 x g. The column was dried by a further centrifugation step for 1 min at maximum speed before the DNA was eluted in 20 µl DNase/RNase-free water into a fresh sterile 1.5 ml reaction tube. The DNA was stored at -20 °C until required.

3.5 Cloning

3.5.1 Gateway® cloning

The Gateway® technology is a cloning method based on site-specific recombination properties of the bacteriophage *lambda* providing a rapid and efficient way to move DNA sequences into multiple vector systems for functional analysis and investigation of protein expression (Sambrook *et al.* 1989, Katzen 2007). The method proceeds in two steps. In a first step the target CDS is amplified with primers carrying *attB* recombination sites. The *attB* PCR product is inserted into an entry vector equipped with *attP* recombination sites by use of

Gateway® BP Clonase™ II (Thermo Fisher Scientific). Thereby resulting *attL* sites recombine in a second step with *attR* sites within a destination vector by help of Gateway® LR Clonase™ II. For the present study we selected the Gateway® pDONR™221 vector as entry clone and the Gateway® pcDNA™-DEST40 vector as destination vector (both Thermo Fisher Scientific). Vector cards for both plasmids are depicted in Appendix Figure 1 and Appendix Figure 2 in the Appendix Section B.

First, coding sequences of *GUCY1A3* and *GUCY1B3* with and without stop codon were amplified from 100 ng revers transcribed adult human total heart RNA (BioChain) using primers depicted in Appendix Table 4. Then mixes for BP and LR reactions, respectively, were prepared in sterile 1.5 ml reaction tubes as listed in Table 28 and Table 29.

Table 28 BP reaction

Volume	Reagent
1 µl	cleaned *attB* PCR product
1 µl	Gateway® BP Clonase™ II
variable	150 ng Gateway® pDONR™221 vector
ad 5 µl	1X TE buffer

Table 29 LR reaction

Volume	Reagent
1 µl	Gateway® pDONR™221 vector incl. CDS
1 µl	Gateway® LR Clonase™ II
variable	150 ng Gateway® pcDNA™-DEST40 vector
ad 5 µl	1X TE buffer

Both reaction mixes were incubated for 1 h at 25 °C in a thermomixer before 1 µl Proteinase K (2 µg/µl) was added to each reaction and incubated for 10 minutes at 37 °C. Transformation of competent NEB® 5-alpha *E. coli* cells (New England Biolabs) was done following the protocol in Section 3.7.

3.5.2 Conventional cloning

Conventional cloning was achieved by dephosphorylation and ligation reactions using the Rapid DNA Dephos & Ligation kit (Roche) following manufacturer's instructions (Sambrook *et al.* 1989).

The plasmids pBiFC-*Gucy1a3* w/o stop-YN155 and pBiFC-*Gucy1b3* w/o stop-YC155 (Rothkegel *et al.* 2007) were kindly provided by J.-P. Stasch (PharmaResearch Center, Bayer HealthCare, Wuppertal, Germany). Rat coding sequences for *Gucy1a3* and *Gucy1b3* were removed from the vector backbones by double digestion using the enzymes BsiWI and XbaI for *Gucy1a3* and BsiWI and BmgBI for *Gucy1b3*. Sequences that were ligated into the linearised vector backbones coded for human *GUCY1A3* and *GUCY1B3*. They were amplified from 100 ng each reverse transcribed human total heart RNA (BioChain) using primers carring the mentioned restriction sites (Appendix Table 5).

To construct pGL4.10[*luc2*] reporter gene plasmids (Promega Corporation) carrying the putative regulatory lead SNP rs7692387 region upstream of the *luc2* gene, a 559 bp long sequence flanking the lead SNP was amplified from genomic DNA extracted from blood of homozygous allele carriers for the risk allele G and non-risk allele A. For that, 10 ng DNA were amplified with primers containing restriction sites for HindIII and NheI (Appendix Table 6). PCR reaction were performed as described in Section 3.2.1 using Q5® high-fidelity 2X master mix (New England Biolabs).

Double digest of vector and insert for ligation: Suitable enzymes were chosen by use of the online tool *Double Digest Finder*. Reaction mixes for digests were prepared in sterile 200 µl tubes. The composition of a reaction mix is listed in Table 30. Buffers and enzymes as well as the applied temperatures can be appreciated in Table 31. Digests were done over night in a thermocycler. In case of two different temperatures, the lower one was set over night and the next day temperature was raised to the second temperature and incubated for 5 more hours.

Table 30 Reaction mix for double digest

Volume	Reagent
10 µl	vector/PCR product
2 µl	10X buffer
1 µl	enzyme 1
1 µl	enzyme 2
ad 20 µl	RNase/DNase-free water

Table 31 Buffers and temperatures used for double digests

Plasmid	Enzyme	Temperature	Buffer	Activity
pBiFC-*Gucy1a3* w/o stop-YN155	BsiWI	55 °C	NEBuffer 3.1	100 %
	XbaI	37 °C		75 %
pBiFC-*Gucy1b3* w/o stop-YC155	BsiWI	55 °C	NEBuffer 3.1	100 %
	BmgBI	37 °C		100 %
pGL4.10[*luc2*]	HindIII	37 °C	NEBuffer 2.1	100 %
	NheI	37 °C		100 %

Digested PCR products and vector backbones were separated on 1 % w/v agarose gels as described in Section 3.3 and extracted from the gels according to Section 3.4.

Dephosphorylation reaction: Digested DNA typically possesses a 5' phosphate group which is required for ligation. When using restriction enzymes generating two different ends dephosphorylation of linearised vector backbones is in theory not necessary for preventing self-ligation. Nevertheless, a dephosphorylation step was always carried out, independently of the use of blunt end or sticky end cutters.

For that, 500 ng linearised vector were dephosphorylated in a total volume of 20 µl in a sterile 1.5 ml reaction tube. Reactios were incubated for 30 min at 37 °C in a thermomixer. Afterwards the phosphatase was inactivated during a 2 min incubation step at 75 °C. The dephosphorylation reaction setup is depicted in Table 32.

Table 32 Composition of dephosphorylation reaction prior to ligation

Volume	Reagent
variable	500 ng linearised vector
2 µl	10X rAPid alkaline phosphatase buffer
1 µl	rAPid alkaline phosphatase
ad 20 µl	DNase/RNase-free water

Ligation: Dephosphorylated vector and insert DNA were combined to a molar ratio of vector:insert of 1:4 in a sterile 1.5 ml reaction tube. The reaction setup is listed in Table 33.

Table 33 Reaction mix for ligation reaction

Volume	Reagent
2 µl	50 ng dephosphorylated vector
variable	200 ng cut insert DNA
2 µl	5X DNA dilution buffer
ad 10 µl	DNase/RNase-free water

10 µl of 2X T4 DNA ligation buffer and 1 µl of T4 DNA ligase were added to the reaction mix and incubated over night at 16 °C in a thermomixer. Transformation of NEB® 5-alpha *E. coli* cells (New England Biolabs) was carried out as described in Section 3.7.

3.6 *In vitro* site-directed mutagenesis

The principle of site-directed mutagenesis is based on oligonucleotides carrying the desired mutation being complementary to the template DNA at the position where the mutation shall be introduced (Sambrook *et al.* 1989).

Base exchanges in the coding sequence of *GUCY1A3* as well as the insertion of HA and Flag tags into Gateway® pcDNA™-DEST40 plasmids were performed using the QuikChange II XL site-directed mutagenesis kit (Agilent Technologies) according to the supplier's protocol. Primers used for mutagenesis reactions are listed in Appendix Table 7, Appendix Table 8 and Appendix Table 9. Reactions were prepared on ice in sterile 200 µl reaction tubes. The composition of a reaction mix can be appreciated in Table 34.

Table 34 Components of a site-directed mutagenesis reaction

Volume	Reagent
2.5 µl	10X reaction buffer
0.5 µl	dNTP mix
variable	10 ng plasmid DNA
1.5 µl	QuikSolution reagent
1 µl	10 µM forward mutagenesis primer
1 µl	10 µM reverse mutagenesis primer
ad 25 µl	DNase/RNase-free water

0.5 µl *PfuUltra* high fidelity DNA polymerase (2.5 U/µl) were added to the reaction mix and the temperature profile depicted in Table 35 was applied.

Table 35 Temperature profile for site-directed mutagenesis

Step	Temperature	Duration
Initial denaturation:	95 °C	1 min
18 cycles:	95 °C	50 s
	60 °C	50 s
	68 °C	1 kb/min
Final Extension:	68 °C	7 min
Hold:	4 °C	∞

After the PCR reaction 1 µl DpnI (10 U/µl) restriction enzyme was added and incubated for 1 h at 37 °C in a thermomixer. As plasmids generated in *E. coli* are methylated and hemimethylated, DpnI selectively digests the template plasmid. The newly synthesised plasmid carrying the mutations/tags is thereby not affected by DpnI.

Transformation of XL10-Gold ultracompetent *E. coli* bacteria (Agilent Technologies)

was carried out as described in Section 3.7.

3.7 Transformation of competent *E. coli* bacteria

Transformation is a process of horizontal gene transfer by which bacteria take up free, extracellular genetic material from the environment, first reported in *Streptococcus pneumoniae* (Griffith 1928). Transformation enables the expression of multiple copies of DNA resulting in large amounts of protein or enzyme that are not normally expressed by bacteria. Bacteria having the prerequisite to undergo transformation are termed as competent cells. Bacteria can be made competent either chemically or by electroporation. In this study, chemically competent *E. coli* bacteria were used (XL10-Gold ultracompetent cells for transformation with pladmid DNA resulting from site-directed mutagenesis (Agilent Technologies) and NEB® 5-alpha cells for all other reactions (New England Biolabs)).

After thawing bacteria on ice plasmid DNA was added and kept on ice for 30 min. The amounts of plasmid DNA used for transformation are listed in Table 36. Of NEB® 5-alpha cells one vial (50 µl) was used per reaction. Concerning XL10-Gold ultracompetent cells 45 µl were taken from the original vial and transferred to a sterile 1.5 ml reaction tube. Before adding the DNA, XL10-Gold ultracompetent cells were supplemented with 2 µl β-mercaptoethanol and incubated for 2 min on ice in order to permeabilise the cell membrane. After the bacteria-DNA-mix had been incubating for 30 min heatshock was given by placing the mix in a 42 °C waterbath for 30 s followed by snap cooling for 2 min. After addition of 250 µl prewarmed SOC medium the cells were incubated for 1 h at 37 °C and 1000 rpm in a thermomixer. Finally 100 µl of the transformed bacteria were plated on prewarmed LB agar plates containing the respective antibiotic (see Table 14) and were incubated over night in an incubator at 37 °C.

Table 36 Amount of plasmid DNA used for transformation

DNA Amount	DNA Source	Bacteria to be transformed
1 µl	BP recombination reaction	NEB® 5-alpha cells
1 µl	LR recombination reaction	
2 µl	dephos and ligation reaction	
1 µl	site-directed mutagenesis	XL10-Gold ultracompetent cells

3.8 Inoculating overnight cultures

Using sterile inoculating loops single transformed colonies were picked and transferred into LB medium supplemented with respective antibiotics. For a miniprep 5 ml LB containing 5 µl antibiotic working solution were inoculated in a sterile 15 ml reaction tube. For a midiprep 100 ml LB with 100 µl antibiotic working solution were inoculated in a 500 ml Erlenmeyer flask. Cultures were incubated over night at 37 °C and 250 rpm in a bacteria shaker.

3.9 Nucleic acid isolation

3.9.1 Plasmid preparation from *E. coli*

The method used for plasmid extraction was depending on the quantity of DNA required.

Small-scale plasmid preparation (Miniprep): For small-scale plasmid preparation the GenElute™ plasmid miniprep kit (Sigma-Adlrich) was used according to manufacturer's instructions. In brief, from the total volume of 5 ml inoculated overnight culture two times 2 ml were pelleted by centrifugation at maximum speed for 1 min at 4 °C in a 2 ml reaction tube. The pellet was resuspended in 200 µl resuspension buffer containing RNase and vortexed until complete solving. After the addition of 200 µl lysis buffer and inverting several times lysis was maintained for up to 5 min at room temperature and finally stopped by adding 350 µl neutralisation buffer. Once again the tube was inverted several times and then centrifuged for 10 min at maximum speed. In order to bind the plasmids to the columns, the cleared supernatant was applied to columns which were before activated by each 500 µl column preparation solution and centrifuged for 1 min at 12,000 x g. Salts and remaining proteins were removed by two washing steps: the first one with 500 µl optional wash buffer and the second one with 750 µl wash buffer, each followed by 1 min centrifugation at 12,000 x g. After drying the column membrane by a further centrifugation step for 1 min at maximum speed plasmids were eluted in 80 µl DNase/RNase-free water into a fresh sterile 1.5 ml reaction tube. Plasmid DNA was stored at -20 °C.

Large-scale plasmid preparation (Midiprep): Large-scale plasmid preparation was done with the QIAGEN® plasmid midi kit (Qiagen) according to manufacturer's recommendations. For that, 100 ml inoculated overnight culture were allocated to two sterile 50 ml reaction tubes and centrifuged for 15 min at 5000 x g at 4 °C. The pellets were

resuspended in 4 ml P1 buffer including RNase A. After the addition of 4 ml P2 buffer, the tube was inverted several times and incubated for 5 min at room temperature. 4 ml chilled P3 buffer were added to the lysate followed by immediate inversion. The lysate was loaded onto a QIAfilter and incubated for 10 min at room temperature. In the meantime a QIAtip was equilibrated with 4 ml QBT. After 10 min incubation time the lysate was pressed from the QIAfilter into the QIAtip. The column was washed two times with 10 ml of ethanol-containg washbuffer and the DNA afterwards eluted in 5 ml QF buffer into a 15 ml reaction tube. DNA was precipitated by adding 3.5 ml isopropanol (100 % v/v) and then centrifuged for 30 min at 4 °C at 5000 x g. The supernatant was carefully removed, the DNA washed in 70 % v/v ethanol. The DNA-ethanol mixture was transferred to a 1.5 ml reaction tube and then centrifuged for 15 minutes at 15,000 x g. The supernatant was removed, the pellet air dried and finally resolved in 300 µl DNase/RNase-free water. Plasmid DNA was stored at -20 °C.

3.9.2 DNA isolation from cultured cells

For isolating DNA from cultured cells the QIAamp® DNA mini kit (Qiagen) was used according to manufacturer's protocol. Following trypsinisation (see Section 3.15) no more than 5 x 10^6 cells were transferred to a sterile 2 ml reaction tube. Cell were pelleted for 2 min at 1000 x g, the supernatant was discarded and cells were resuspended in 200 µl cold Dulbecco's PBS. 20 µl QIAGEN® Protease were added. Pulse-vortexing for 15 s followed the addition of 200 µl buffer AL. Samples were incubated for 10 min at 56 °C in a thermomixer. DNA was precipitated by adding 200 µl ethanol (100 % v/v). The samples were applied to QIAamp® Mini spin columns and centrifuged for 1 min at 6000 x g. After discarding the flow-through, the column was washed with 500 µl AW1 followed by centrifugation for 1 min at 6000 x g. Then the column was washed with 500 µl buffer AW2 followed by centrifugation for 3 min at maximum speed. The column was placed into a new collection tube and a centrifugation step for 1 min at full speed was applied in order to dry the membrane. The column was placed into a new sterile 1.5 ml reaction tube. Elution was done in 60 µl water and centrifugation for 1 min at 6000 x g. DNA samples were stored at -20 °C.

3.9.3 RNA isolation from cultured cells

Total RNA was extracted from cultured cells using the RNeasy® Plus mini kit in combination with QIAshredder™ homogenizer columns (both Qiagen) following

manufacturer's recommendations. In brief, cells grown in 24 well plates were washed with 500 µl of cold Dulbecco's PBS on ice. Then 350 µl lysis buffer were added. After on freeze-thaw cycle cells were scraped with a pipette tip and the lysate was loaded onto a QIAshredder™ spin column. Samples were centrifuged for 3 min at maximum speed. The flow-throughs were loaded onto gDNA eliminator columns followed by centrifugation at 8000 x g for 30 sec. 350 µl ethanol (70 % v/v in RNase/DNase-free water) were added to the flow-throughs and then loaded onto to RNeasy spin columns and centrifuged for 30 s at 8000 x g. Columns were washed with 700 µl Buffer RW1 followed by centrifugation for 30 s at 8000 x g. Then the columns were washed twice with 500 µl buffer RPE. The first time followed by a centrifugation step for 30 s, the second time for 2 min at 8000 x g. Then an additional centrifugation step for 1 min at maximum speed was applied to dry the membrane. RNA was eluted in 30 µl DNase/RNase-free water into a sterile 1.5 ml reaction tube by centrifugating for 1 min at 8000 x g. RNA was stored at -80 °C.

3.9.4 RNA extraction from leukocyte-depleted platelet concentrate

50 ml leucocyte-depleted platelet concentrate were transferred to a 50 ml reaction tube and isolated with Ambion™ TRIzol® reagent (Thermo Fisher Scientific). For that, a 10 min centrifugation step at 3000 x g was followed by discarding the supernatant and resuspending the pellet in 3 ml TRIzol® reagent. The mixture was frozen two times in liquid nitrogen and thawed at 40 °C in a waterbath. After 5 min incubation at room temperature 600 µl chlorophorm were added. It was vortexed for 15 s and again incubated for 5 min at room temperature. The sample was transferred to a pre-chilled phase lock tube (5 PRIME) and was centrifuged for 15 min at maximum speed and 4 °C. The top aqueous phase was transferred into a sterile 1.5 ml reaction tube. Then 500 µl isoproanol (100 % v/v) followed by 2 µl Invitrogen™ GlycoBlue™ coprecipitant (Thermo Fisher Scientific) were added. The sample was carefully shaked. Due to GlycoBlue™ the RNA was visible in form of bluish threads. It was incubated for 10 min at room temperature and then centrifuged for 10 min at maximum speed and 4 °C. The supernatant was discarded and the RNA pellet washed in 1 ml 70 % v/v ethanol. After 5 min centrifugation at 5000 x g the supernatant was discarded and the pellet air dried. The pellet was resuspended in 15 µl DNase/RNase-free water. The RNA (282 ng/µl) was stored at -80 °C.

3.10 Control digest of plasmid DNA

Plasmid DNA resulting from cloning was digested with restriction enzymes in order to verify that the sequence of interest was (1) inserted into the vector and (2) inserted within the correct orientation. For that, 5 µl plasmid DNA were digested with 0.5 µl restriction enzyme in a total volume of 20 µl in a sterile 200 µl reaction tube over night at 37 °C in a thermocycler and separated in 1 % w/v agarose as described in section 3.3. The enzymes and buffers used as well as the resulting fragment sizes are listed in Table 37.

Table 37 Restriction enzymes, buffers and resulting fragment sizes of vectors with insert

Backbone	Insert	Enzyme	Buffer	Sizes
Gateway® pDONR™221	*GUCY1A3* w/ stop	EcoNI	CutSmart®	2535 bp 1352 bp 751 bp
	GUCY1A3 w/o stop	EcoNI	CutSmart®	2535 bp 1349 bp 751 bp
	GUCY1B3 w/ stop	PvuII	NEBuffer 3.1	1942 bp 1416 bp 1064 bp
	GUCY1B3 w/o stop	PvuII	NEBuffer 3.1	1942 bp 1416 bp 1061 bp
Gateway® pcDNA™-DEST40	*GUCY1A3* w/ stop	AlwNI	CutSmart®	3835 bp 2270 bp 1483 bp
	GUCY1A3 w/o stop	AlwNI	CutSmart®	3832 bp 2270 bp 1483 bp
	GUCY1A3 w/ HA tag and stop	AlwNI	CutSmart®	3862 bp 2270 bp 1483 bp
	GUCY1B3 w/ stop	AlwNI	CutSmart®	3780 bp 2112 bp 1483 bp
	GUCY1B3 w/o stop	AlwNI	CutSmart®	3777 bp 2112 bp 1483 bp
	GUCY1B3 w/ Flag tag and stop	AlwNI	CutSmart®	3804 bp 2112 bp 1483 bp
pGL4.10[*luc2*]	rs7692387 lead SNP region (upstream of *luc2*)	BbsI	NEBuffer 2.1	2827 bp 1950 bp
pBiFC-YN155	*GUCY1A3* w/o stop	AlwNI	CutSmart®	2989 bp 2839 bp 1467 bp
pBiFC-YC155	*GUCY1B3* w/o stop	PvuII	NEBuffer 3.1	2364 bp 1874 bp 1683 bp

3.11 Nucleic acid quantitation

DNA and RNA concentrations were measured in a microplate reader. The ratio of the absorbance at 260 nm and 280 nm gives information on the purity of the nucleic acid. DNA samples with a ratio from 1.7 to 1.9 can be regarded as pure, a lower ratio indicates a contamination with proteins. For RNA, an A260/A280 ratio of 1.8 to 2.1 is indicative of pure RNA. 2 µl of undiluted DNA or RNA samples were measured in the Infinite® M200 PRO microplate reader by use of the software iControl v1.10 (both Tecan Group).

3.12 Sequencing of plasmids

Sequencing of plasmids was performed by Eurofins Genomics. Template and primers were combined as depicted in Table 38 in barcoded sequencing tubes (Mix2Seq kit) provided by Eurofins Genomics. Primers listed in Appendix Table 10, Appendix Table 11 and Appendix Table 12 were used for sequencing reactions.

Table 38 Setup for sequencing

Volume	Reagent
variable	1125 ng plasmid DNA
1 µl	10 µM forward primer
1 µl	10 µM reverse primer
ad 17 µl	DNase/RNase-free water

3.13 DNase I digest

When qPCR analysis followed overexpression of *GUCY1A3* and *GUCY1B3* in HEK 293 cells an 'in-tube' DNA digest with DNase I (Thermo Fisher Scientific) was performed. This step was mandatory as primers designed to target cDNA in qPCR also bind to plasmid DNA due to lacking introns in the coding sequence. The reaction mix (Table 39) was prepared in a sterile 200 µl reaction tube. It was incubated 15 min at room temperature and stopped by adding 1 µl of 25 mM EDTA solution. DNase I digested RNA (21 ng/µl) was stored at -80 °C.

Table 39 Reaction mix for 'in-tube' DNA digest with DNase I

Volume	Reagent
variable	231 ng RNA from overexpressing HEK 293 cells
1 µl	10X DNase I Reaction Buffer
1 µl	DNase I, amplification grade (1 U/µl)
ad 10 µl	DNase/RNase-free water

3.14 cDNA first-strand synthesis

cDNA synthesis was performed using the ThermoScript™ RT-PCR system for first-strand cDNA synthesis kit (Thermo Fisher Scientific) with a mixture of oligo(dT) and random hexamer primers. In a first sample denaturation step RNA, primers and dNTPs were combined in a sterile 200 µl reaction tube as depicted in Table 40 and incubated 5 min at 65 °C in a thermocycler to eliminate possible secondary structures and to accelerate primer hybridysation. The reaction mix was quickly chilled on ice before the cDNA sythesis was started by adding the components listed in Table 41 and incubating for 25 °C for 10 min followed by 50 min at 50 °C. The reaction was stopped by a 85 °C step for 5 min. Afterwards the RNA template was removed by adding 1 µl RNase H and 20 min incubation at 37 °C. cDNA was stored at -20 °C.

Table 40 Sample denaturation reaction mix

Volume	Reagent
variable	RNA*
1 µl	oligo(dT) primers
1 µl	random hexamer primers
2 µl	10 mM dNTP mix
ad 12 µl	water

*transfected HEK 293 from 24 well plates for qPCR: 1050 ng RNA (or 21 ng DNase I-treated RNA from overexpressing cells)
transfected VSMC from 24 well plates for qPCR: 73.5 ng RNA
samples for endpoint PCR: up to 2100 ng RNA

Table 41 cDNA synthesis reaction mix

Volume	Reagent
4 µl	5X cDNA synthesis buffer
1 µl	0.1 M DTT
1 µl	RNaseOUT™ (40 U/µl)
1 µl	ThermoScript™ RT (15 U/µl)
1 µl	DEPC-treated water

3.15 Cell culture

All work was done under a laminar flow hood. Media, Dulbecco's PBS and trypsin-EDTA solution were prewarmed to 37 °C in a water bath before use.

Coating of cell culture flasks and 24 well plates: For the scratch wound assay as well as qPCR analysis of VSMC which were conducted in collaboration with Mete Civelek (Center for Public Health Genomics, University of Virgina, Charlottesville, VA, USA), cell culture flasks and 24 well plates were coated with 0.1 % w/v gelatin. Per T75 cell culture flask coating was done with 5 ml gelatin, per well in a 24 well plate, 0.5 ml were used. Incubation was done for approximately 30 min at room temperature. Just bevor seeding the cells, the gelatin was aspirated.

Revival of frozen cells and maintaining cells: Cell line stocks were kept frozen under liquid nitrogen for long term storage. To revive cells, a frozen aliquot was thawed in a 37 °C waterbath under smooth shaking. Once thawed, cells were transferred to 5 ml of prewarmed media and kept in a humidified incubator at 37 °C supplemented with 5 % CO_2. The next day media was exchanged to get rid of DMSO. In general, fresh media changes were carried out every two to three days.

Passaging cells: Passaging was carried out once the cells were confluent. For detaching HEK 293 cells via trypsinisation, media was aspirated, the cells were washed with Dulbecco's PBS and 0.25 % Gibco™ trypsin-EDTA solution (Thermo Fisher Scientific) was added. The cells were incubated at room temperature for 2 min. The enzymatic reaction was stopped by adding media in a ratio of 4:1. In case of VSMC, washing was performed with Hepes BSS (PromoCell), 0.04 % trypsin-EDTA (PromoCell) was used for trypsinisation and the reaction was stopped by adding trypsin neutralising solution (PromoCell) in a ratio of 1:2.

The cells were transferred to a sterile 50 ml reaction tube and centrifuged at 1000 x g for 2 min. After the supernatant was removed, the pellet was resuspended in media and split into appropriate ratios into cell culture flasks, 10 cm dishes or multiwell plates (for cell numbers seeded see Table 42).

Table 42 Cell numbers seeded

Cell type	24 well plates (0.5 ml)	6 well plates (2 ml)	10 cm dishes (10 ml)
HEK 293	250,000/well	1 million/well	6 million/dish
VSMC	50,000-100,000/well*	-	-

*50,000 VSMC/well for scratch assays and qPCR analysis performed at University of Virginia;
100,000 VSMC/well for all other conducted experiments

Determination of cell counts: For determining cell counts, resuspended cells were diluted 1:10 in a total volume of 1 ml in medium and counted with the Scepter™ cell counter using 60 µM cell counter sensors (both Merck Millipore). In case of determining cell counts prior to the scratch wound assay which was carried out as part of a collaboration with Mete Civelek (Center for Public Health Genomics, University of Virgina, Charlottesville, VA, USA) cells were stained 1:2 in a total volume of 60 µl with 0.4 % Gibco™ trypan blue solution (Thermo Fisher Scientific). 20 µl were then used for measurement with the TC10™ automated cell counter (Bio-Rad).

Freezing cells for storage: Cells were trypsinised as mentioned. Pelleted cells were resuspended in freezing media and aliquoted into cryotubes. The tubes were placed at -80 °C in a freezing container filled with isopropanol (100 % v/v) for at least 24 h before transferring them for long-term storage under liquid nitrogen.

3.16 Transient transfection

Transfection describes the process of introducing exogenous DNA or RNA into eukaryotic cells (Kim and Eberwine 2010).

Transient transfection using FuGENE® HD transfection reagent: For applying expression plasmids into human cells as well as plasmids for luciferase assays, TR-FRET and BiFC experiments, transient transfection was performed with FuGENE® HD transfection reagent (Promega Corporation) in a ratio of 4:1 in Gibco™ Opti-MEM® I reduced serum medium (Thermo Fisher Scientific) 24 h after seeding cells. Reaction mixes for the transfection of cells grown in multiwell plates (volumes per well) as well as 10 cm culture dishes can be appreciated in Table 43.

Table 43 Reaction mixes for transient transfection using FuGENE® HD transfection reagent

	24 well plate			**6 well plate**	**10 cm dish**
Assay:	**BiFC**	· **Western blotting** · **qPCR** · **RIA**	**Luciferase assay**	**TR-FRET**	**Co-IP**
Plasmids:	pBiFC-YN155 625 ng	*GUCY1A3* w/o stop 400 ng	pGL4.10[*luc2*] 500 ng	*GUCY1A3* w/ stop and HA 650 ng to 1 µg	*GUCY1A3* w/ stop and HA 5 µg
	pBiFC-YC155 625 ng	*GUCY1B3* w/o stop 400 ng	pRL-TK 50 ng	*GUCY1B3* w/ stop and Flag 650 ng to 1 µg	*GUCY1B3* w/ stop and Flag 5 µg
FuGENE® HD:	5 µl	3.2 µl	2.2 µl	5.2 to 8 µl	40 µl
Opti-MEM® I:	*ad* 25 µl	*ad* 25 µl	*ad* 25 µl	*ad* 100 µl	*ad* 800 µl

The components were combined in a sterile 1.5 ml reaction tube. After an incubation of 15 min at room temperature the transfection reaction was given dropwise to the cells.

Transient transfection using Invitrogen™ Lipofectamine® RNAiMAX™ transfection reagent: For introducing *ZEB1* siRNA to human cells transient transfection was performed using Invitrogen™ Lipofectamine® RNAiMAX™ transfection reagent in Gibco™ Opti-MEM® I reduced serum medium (both Thermo Fisher Scientific) 24 h after seeding cells to 24 well plates. First, siRNAs were diluted in DEPC-treated water from 100 µM to a working concentration of 10 µM in sterile 1.5 ml reaction tubes. Then reaction mixes were prepared in sterile 1.5 ml reaction tubes as listed in Table 44. Transfection with equal amounts of scrambled siRNA (Silencer® select negative control no. 1 siRNA) was done for controls.

Table 44 Reaction mixes for transient transfection with Invitrogen™ Lipofectamine® RNAiMAX™ transfection reagent using different amounts of siRNA

		siRNA amount/well		
		1.25 pmol	2.5 pmol	5 pmol
Mix1	**Opti-MEM® I:**	25 µl	25 µl	25 µl
	Lipofectamine® RNAiMAX™:	1.5 µl	1.5 µl	1.5 µl
Mix2	**Opti-MEM® I**	25 µl	25 µl	25 µl
	10µM siRNA	0.125 µl	0.25 µl	0.5 µl

25 µl each from *Mix1* and *Mix2* were pipetted together into a sterile 1.5 ml reaction tube, incubated for 5 min at room temperature and then the total of 50 µl was given dropwise to the cells.

In case siRNA knockdown followed transfection with luciferase plasmids, first transfection with FuGENE® HD transfection reagent was done as described above. After an incubation time of 6 hours transfection with siRNAs and Lipofectamine® RNAiMAX™ transfection reagent was performed.

3.17 Proteasome inhibition

Proteasome inhibition experiments were conducted by treating HEK 293 cells overexpressing *GUCY1A3* w/o stop and *GUCY1B3* w/o stop with bortezomib (Absource Diagnostics). The boron atom within bortezomib catalytically binds the active site of the 26S proteasome with high affinity and specificity which leads to cell cycle arrest and apoptosis (Bonvini *et al.* 2007).

For proteasome inhibition experiments, HEK 293 cells grown in 24 well plates were incubated with bortezomib. In brief, 24 h after transfecting HEK 293 cell with plasmids coding for *GUCY1A3* w/o stop and *GUCY1B3* w/o stop, bortezomib was added to the medium to a final concentration of 0.1 µM. For that, it was first serially diluted from a stock solution of 10 mM in DMSO to a working solution of 2.2 µM in medium in sterile 1.5 ml reaction tubes. Then 25 µl of the 2.2 µM solution were used to treat the cells in a total volume of 525 µl (500 µl medium, 25 µl transfection reaction). Incubation was done for 8 hours. A concentration of 0.001 % v/v of DMSO used as a vehicle for bortezomib served as control.

Lysates were prepared as described in Section 3.18 and protein levels of sGC α_1 subunit and GAPDH were investigated by immunoblotting following the protocol in Section 3.21.

3.18 Preparation of cell lysates

To prepare lysates, cells grown in 24 well plates were placed on ice, washed with 500 µl cold Dulbecco's PBS and then 100 µl RIPA were added. After the plate had been frozen at -80 °C, cells were thawed on ice, scraped and transferred to a sterile 1.5 ml reaction tube. Disruption was done by sonification. For that, cells were placed three times for 30 s into an ultrasonic bath and chilled on ice for 30 s in between. Cellular debris was spun down for 30 min at maximum speed and 4 °C. The supernatant was transferred to a fresh sterile 1.5 ml reaction tube. Cleared lysates were stored at -20 °C.

3.19 Determination of protein content in cell lysates

For protein quantification in lysates the Pierce™ BCA protein assay kit (Thermo Fisher Scientific) was used. The method is based on the combination of the reduction of Cu^{2+} to Cu^{1+} by protein in an alkaline medium (the biuret reaction) with the colorimetric detection of formed Cu^{1+} using a bicinchoninic acid (BCA)-containing reagent.

Per reaction 200 µl BCA reagent A were mixed with 4 µl BCA reagent B and incubated with either 2 µl of standard or sample for 30 min at 37 °C in a 96 well microplate. Measurement was done at 562 nm in the Infinite® M200 PRO microplate reader (Tecan Group) using the software Magellan™ data analysis software v7.2 (both Tecan Group). Each sample and standard were measured as duplicates.

3.20 Co-immunoprecipitation

Co-immunoprecipitation (Co-IP) assays were performed in order to investigate protein-protein interactions. For that, HEK 293 cells grown in 10 cm dishes and overexpressing HA tagged *GUCY1A3* and Flag tagged *GUCY1B3* (Table 43) were harvested 24 h post transfection and subsequently used for Co-IP using Novex™ Dynabeads® co-immunoprecipitation kit (Thermo Fisher Scientific).

Antibody coupling: Per reaction 1.5 mg beads were weighed and transferred into a sterile 1.5 ml reaction tube. Beads were washed accordingly with 1 ml C1 buffer and afterwards coupled with antibody (HA and IgG). Per mg beads, 5 µg antibody were used. C1 and C2 buffers were combined with the antibody to a total volume of 100 µl per mg beads ((50 µl C1 - antibody) + 50 µl C2). The samples were incubated over night at 37 °C in a rotating device. The next day, beads were washed with each 800 µl HB and LB wash buffers both supplemented with 0.05 % v/v Tween® 20 as well as with 800 µl SB buffer and finally resuspended in 100 µl SB buffer/mg beads. Antibody-coupled beads (10 mg/ml) were stored at 4 °C for short term until needed.

Cell sample preparation: On ice, cells were washed once with 1 ml cold Dulbecco's PBS, resuspended in 1 ml PBS and transferred to a previous weighed sterile 1.5 ml reaction tube. Cells were spun down at 500 x g and 4 °C for 5 min. The supernatant was discarded and the reaction tube including pellet was weighed again in order to calculate the required volume for resuspension in a 1:9 ratio. 450 µl 1X IP extraction buffer (diluted from 5X in DNase/RNase-free water) supplemented with a final concentration of 100 mM NaCl (from 1M stock solution) were taken for the resuspension of 50 mg cells. Cells were incubated for 15 min on ice and centrifuged at 2600 x g and 4 °C for 5 min. The supernatant was transferred to a fresh sterile 1.5 ml reaction tube and it was directly proceeded with the Co-IP protocol.

Co-IP protocol: Per Co-IP reaction 1.5 mg antibody-coupled beads were transferred into a new 1.5 ml resction tube. They were washed with 900 µl 1X IP buffer supplemented with 100 mM NaCl, resuspended in 450 µl cell lysate and incubated for 30 min at room temperature on a roller. The beads were then washed three times with 200 µl 1X IP buffer w/ NaCl and afterwards with 200 µl 1X LWB buffer (diluted from 5X in DNase/RNase-free water and supplemented with 0.02 % v/v Tween® 20). After the beads were incubated for 5 min at room temperature on a roller, they were resuspended in 60 µl EB buffer and again incubated for 5 min at room temperature on a roller. The supernatant (=purified protein complex) was transferred to a new sterile 1.5 ml reaction tube and stored at -20 °C.

3.21 Western blotting

Western blotting, also known as immunoblotting, is a technique for the detection and analysis of proteins. The method is based on building an antibody-protein complex via specific binding of antibodies to proteins immobilised on a membrane and detecting the bound antibody.

Gel casting: Gels for electrophoresis were casted in two steps. First, the 12 % resolving gel was casted and the surface was covered with isopropanol (100 % v/v). After the resolving gel had gelled, the isopropanol was removed by use of cellulose filter paper and replenished by 4 % stacking gel.

Sample preparation: Before loading onto the gel cleared lysates were mixed with RIPA and laemmli buffer (either 2X or 4X) in a sterile 1.5 ml reaction tube to a maximum volume of 30 µl and denaturated by boiling 5 min at 95 °C in a thermomixer. Protein amouts used for Western blotting are mentioned in the *Western blot protocol* part below. Co-IP eluates were mixed 1:2 with 2X laemmli. Human and mouse platelets had already been mixed with a 1:2 mixture of RIPA and 2X laemmli as described in Section 3.29.

Western blot protocol: Samples were separated on 12 % v/v SDS-polyacrylamide gels in 1X running buffer. First, the samples were run at 100 V. After they entered into the resolving gel, voltage was raised to 150 V. Samples were then transferred electrophoretically to methanol-activated Immobilon®-P polyvinylidene difluoride (PVDF) membranes (Merck Millipore) at 100 V for 1.5 h 1X transfer buffer. The membranes were briefly rinsed in 1X PBS and blocked for at least 1 h at room temperature with 5 % w/v milk in 1X PBS on a shaking decive at 30 rpm. Blots were incubated with primary antibodies over night at 4 °C in 2.5 % milk in 1X PBS-T in a 50 ml reaction tube on a roller. Following antibody concentrations were used: (1) 10 µg lysate from *GUCY1A3* and *GUCY1B3* overexpression in HEK 293 with anti-V5 1:5000/anti-GAPDH 1:25,000; (2) 10 µl Co-IP with 1:2000 anti-Flag/1:5000 anti-HA; (3) 15 µl mouse platelets with 1:5000 anti-P-VASP$_{Ser239}$/1:50,000 anti-GAPDH; (4) 10 µg lysate from *ZEB1* knockdown in HEK 293/VSMC with 1:1000 anti-ZEB1 (D80D3)/1:100,000 anti-GAPDH; (5) 10 µg lysate from stimulated VSMC with 1:1000 anti-P-VASP$_{Ser239}$/1:100,000 anti-GAPDH; (6) 8 µl human platelets with anti-sGCα_1 1:2000/1:50,000 anti-GAPDH; (7) 8 µl human platelets with anti-VASP 1:5000/1:100,000 anti-GAPDH.

After 5 washing steps in 1X PBS-T for each 5 min on a shaking decive at 30 rpm and room temperature blots were incubated with secondary horseradish peroxidase-conjugated antibodies (Sigma-Adlrich) at 1:100,000 dilutions in 2.5 % milk in 1X PBS-T for at least 1 h at room temperature on the shaking device. Protein bands were visualised by enhanced chemiluminescence Pierce™ ECL Western Blotting Substrate (Thermo Fisher Scientific) and were developed in the ImageQuant™ LAS 4000 biomolecular imager by use of the

ImageQuant™ LAS 4000 v1.2 software (both GE Healthcare Life Sciences).

Western blot analysis: Analysis was performed with ImageQuant™ TL 1D v8.1 (GE Healthcare Life Sciences). Background was substracted with the *rolling ball* method. Normalisation was done by dividing the band volume of the target protein by the band volume of the endogenous housekeeping control GAPDH, where the band volume is the raw volume of the uncalibrated quantity of material in the image feature excluding background (=the sum of the pixel intensity).

3.22 Electrophoretic mobility shift assay

Electrophoretic mobility shift assay (EMSA) enables the investigation of protein-DNA interactions (Hellman and Fried 2007). For that, labelled oligos are incubated with nuclear extracts and run in a native polyacrylamide gel to see if binding of protein to the DNA leads to a size shift. Additionally samples can be incubated with competitor oligos to assess the most favourable binding site or with an antibody to achieve a supershift of the protein-DNA-antibody complex.

3' end labeling of oligonucleotides: For visualisation single-stranded oligonucleotides (Appendix Table 13) were 3' end labelled with biotin using the Thermo Scientific™ Pierce™ 3' end biotin labelling kit (Thermo Fisher Scientific). Labelling reactions were prepared in sterile 1.5 ml reaction tubes as depicted in Table 45 without vortexing. All steps were performed on ice.

Table 45 Reaction mix for biotin labelling of oligonucleotides

Volume	Reagent
25 µl	DNase/RNase-free water
10 µl	5X TdT reaction buffer
5 µl	1 µM single-stranded unlabelled oligonucleotides
5 µl	5 µM biotin-11-UTP
5 µl	TdT (1.5 U/µl)*

*diluted from 15 U/µl in 5X TdT reaction buffer and DNase/RNase-free water

After the reaction had been incubated for 30 min at 37 °C in a thermomixer it was stopped by adding 1 µl EDTA-Na_2 (Sigma-Aldrich). To extract the TdT 50 µl chlorophorm:isoamyl alcohol (24:1; Sigma-Aldrich) were added followed by brief vortexing and centrifugation at maximum speed for 2 min. The top aqueous phase containing the

labelled oligonucleotides at a concentration of 100 nM was transferred to a fresh sterile 1.5 ml reaction tube.

To create 3′ end biotin-labelled double-stranded probes, corresponding forward and reverse primers were dimerised. For that, equal amounts of complementary labelled oligos were incubated together in a sterile 1.5 ml reaction tube for 1 h at room temperature to a final concentration of 50 nM each. Afterwards they were diluted 1:5 in DNase/RNase-free water to a final concentration of 10 nM each. Unlabelled oligos (100 µM stock) were pairwise diluted 1:100 in DNase/RNase-free water and incubated likewise 1 h at room temperature to a final concentration of 1 µM each. Annealed oligos were stored at -20 °C.

Extraction of nuclear extract: Nuclear extraction was done with the NE-PER™ nuclear and cytoplasmic extraction reagents (Thermo Fisher Scientific). All steps were performed on ice. 10 x 10^6 HEK 293 cells were pelleted after trypsinisation as described in Section 3.15. Cells were resuspended in 2 ml Thermo Scientific™ BupH™ PBS (Thermo Fisher Scientific), transferred to a sterile 2 ml reaction tube and centrifuged at 1000 x g for 2 min at 4 °C. The supernatant was removed by pipet and cells were lysed in 1 ml ice-cold CER I buffer supplemented with 1X Thermo Scientific™ Halt™ protease inhibitor cocktail, EDTA-free (Thermo Fisher Scientific). 15 s vortexing was followed by 10 min incubation on ice. The addition of 55 µl ice-cold CER II was followed by 5 s vortexing, 1 min incubation on ice, again 5 s vortexing and 5 min centrifugation at maximum speed and 4 °C. The supernatant (=cytoplasmic extract) was transferred to a sterile pre-chilled 1.5 ml reaction tube and immediately stored at -80 °C. The pellet was resuspended in 500 µl ice-cold NER supplemented with 1X Thermo Scientific™ Halt™ protease inhibitor cocktail, EDTA-free (Thermo Fisher Scientific). It was vortexed for 15 s and incubated on ice for 40 min. After every 10 min it was vortexed again. Finally, a centrifugation step at maximum speed was performed for 10 min at 4 °C. The supernatant (=nuclear extract) was transferred to a sterile pre-chilled 1.5 ml reaction tube. Before using nuclear extract for EMSA, it was subjected to one freeze-thaw cycle at -80 °C.

EMSA protocol: For EMSA the LightShift® chemiluminescent EMSA kit (Thermo Fisher Scientific) was used according to manufacturer's recommendations. Reaction mixes were prepared in sterile 1.5 ml reaction tubes as depicted in Table 46. They were incubated for 20 min at room temperature. Additionally, samples containing the components of reaction #2 were supplemented with 1 µl ZEB1 antibody (C-20X) and incubated further 20 min at room temperature. In parallel to preparing the reaction mixes, a native 4 % v/v polyacrylamide gel was pre-run in 0.5X TBE buffer at 100 V for 1 h. Before loading onto the gel, 5 µl loading dye were added to the reactions. Samples were then separated for approximatley 50 min at 100 V (so that the lower (=dark blue) band of the loading dye passed ¾ of the gel). The samples were then blotted onto Thermo Scientific™ Biodyne™ B

nylon membranes (Thermo Fisher Scientific) which were before incubated in 0.5X TBE buffer for at least 10 min. Blotting was done for 45 min at 380 mA in 0.5X cold TBE buffer. Afterwards, crosslinking was done for 15 min. For that, the blot was placed face-down on the UV transmitted light source (with 312 nm bulbs) of the ImageQuant™ LAS 4000 biomolecular (GE Healthcare Life Sciences). The membrane was then incubated for 15 min in 20 ml blocking buffer on a shaking device at 30 rpm followed by a second incubation for 15 min in 20 ml blocking buffer supplemented with 66.7 µl stabilised streptavidin-horseradish peroxidase conjugate. The blot was rinsed with 20 ml 1X washing buffer (in Millipore® water) followed by four washing steps for 5 min in 20 ml 1X washing buffer. The blot was then equilibrated for 5 min in 30 ml equilibration buffer before it was incubated for 7 min in a mixture of 6 ml luminol/enhancer solution and 6 ml stable peroxide solution.

The blot was developed for 10 min in the ImageQuant™ LAS 4000 biomolecular imager using the ImageQuant™ LAS 4000 v1.2 software (GE Healthcare Life Sciences).

Table 46 EMSA reaction mixes

		Reaction		
Component	**Final amount**	**#1**	**#2**	**#3**
DNase/RNase-free water		12.9	7.9	5.9 µl
10X binding buffer		2 µl	2 µl	2 µl
50 % glycerol		1 µl	1 µl	1 µl
100 mM $MgCl_2$		1 µl	1 µl	1 µl
Poly dI•dC (1µg/µL)		0.1 µl	0.1 µl	0.1 µl
1 % NP-40		1 µl	1 µl	1 µl
1 µM unlabelled oligos	2 pmol	-	-	2 µl
nuclear HEK 293 extract		-	5 µl	5 µl
10 nM biotin-labelled oligos	20 fmol	2 µl	2 µl	2 µl

3.23 Bimolecular fluorescence complementation microscopy

Bimolecular fluorescece complementation (BiFC) is a technique that enables direct visualisation of protein interaction in living cells based on reconstitution of an intact fluorescent protein brought together by a pair of interacting proteins (Kerppola 2006, Kerppola 2009). For that, putative interaction partners are fused to two fragments (YN155 and YC155) of enhanced yellow fluorescent protein (EYFP). Upon interaction of the target proteins, ideally also the YN and YC fragments come to close proximity which is measureable in form of fluorescence.

BiFC constructs were cloned as described in Section 3.5.2. HEK 293 cells grown in 24 well plates were transfected according to Table 43. Prior to microscopy the cells were incubated at 4 °C for 30 min to increase the signal. Microscopy was performed 12 to 36 h

post transfection in the IX50 inverted microscope system (Olympus). For detection of complementation between YFP fragments an excitation filter with 500 ± 10 nm transmission and an emission filter with 535 ± 15 nm transmission are appropriate (Kerppola 2006). We used a YFP filter with an excitation range of 488-512 nm and an emission range of 488-554 nm.

3.24 Time-resolved fluorescence resonance energy transfer

Fluorescence resonance energy transfer (FRET) is based on the transfer of energy between two fluorophores, a donor and an acceptor, when they are in close proximity (Shrestha *et al.* 2015). Molecular interactions between biomolecules can be assessed by coupling each partner with a fluorescent label and by detecting the level of energy transfer. Traditional FRET chemistries are impeded by background fluorescence from sample components such as buffers, proteins, chemical compounds and cell lysate. As background fluorescence is extremely transient with a lifetime in the nanosecond range it can be easily eliminated using time-resolved FRET (TR-FRET). For our studies, lysates were tested with two different combinations of antibody-fluorophor complexes: anti-HA-d2 + anti-Flag-EuK and anti-HA-EuK + anti-Flag-d2 (Cisbio Bioassays).

24 h post transfection, transfected HEK 293 cells grown in 6 well plates (Table 43) were washed with 1 ml cold Dulbecco's PBS on ice and either lysed in 500 µl EGFR lysis buffer or 500 µl cellular kinase lysis buffer #1 (both buffers diluted from 4X in DNase/RNase-free water, Cisbio Bioassays). Lysates were incubated for 30 min on ice, transferred to sterile 1.5 ml reaction tubes and centrifuged for 30 min at maximum speed. Cleared lysates were transferred to new sterile 1.5 ml reaction tubes. Dilution series of lysates were prepared in buffer EGFR and buffer #1 ranging from 100 % lysate to 3.125 % lysate (five 1:2 dilution steps).

For anti-HA-d2 and anti-Flag-d2 solutions with a concentration of 4 µg/ml were prepared in reconstitution buffer. Anti-HA-EuK was diluted to a concentration of 240 ng/ml in reconstitution buffer, anti-Flag-EuK to a concentration of 280 ng/ml.

50 µl lysate each were pipetted into white 96 well plates supplemented with either 25 µl each anti-HA-d2 and anti-Flag-EuK or 25 µl each anti-HA-EuK and anti-Flag-d2. Samples were measured as duplicates in the Infinite® F200 PRO microplare reader at wavelengths 620 nm and 665 nm using the iControl v1.10 software (both Tecan Group). Measurements were performed after 15, 30 and 60 min incubation time at room temperature. The *TR-FRET ratio* was calculated using the formula $\frac{665\ \text{nm}}{620\ \text{nm}} \text{x}\ 10{,}000$.

3.25 Scratch wound assay

Scratch wound assays were performed with VSMC grown to confluence in 24 well plates. The cell monolayer was scratched in a straight line in the middle of the well using a 200 µl pipette tip in order to create the scratch. The detatched cells were removed by washing with 500 µl warm Dulbecco's PBS. Then 500 µl medium either supplemented with BAY 41-2272 at a final concentration of 10 µM or the respective amount of DMSO (0.1 % v/v) which was used as vehicle for the stimulator was given to the cells. Cells were subsequently (=t_0) photographed under the Invitrogen™ EVOS® FL Auto imaging system in the phase-contrast mode with the 10X objective using the EVOS® FL Auto software v1.6 (both Thermo Fisher Scientific). The 24 well plates were placed back to the incubator at 37 °C and 5 % CO_2. After 5 h (=t_1) a second image was acquired. With the microscope used it was possible to obtain exactly the same field during the image acquisition at t_1 as compared to t_0. In each experiment cells were investigated as triplicates for each treatment.

The images acquired were further analysed quantitatively by use of ImageJ 1.47v (National Institutes of Health) by measuring the the pixels of the scratch area at t_0 and t_1. The pixels of each treatment within an experiment were averaged and then pixels at t_0 were substracted from pixels at t_1 for DMSO and for BAY 41-2272. ΔDMSO and ΔBAY 41-2272 (=t_0-t_1) values were both divided by 100,000 and then depicted against each other as *reclosure [10^5 pixels]*. For comparing migration as *foldchange to vehicle*, following formula was applied: $\frac{\Delta\text{BAY 41}-2272/\text{BAY 41}-2272\ t_0}{\Delta\text{DMSO}/\text{DMSO}\ t_0}$.

3.26 Stimulation of soluble guanylyl cyclase

100 mM IBMX stock solution was diluted to a 10 mM working solution in HEPES buffered saline solution. S-nitrosoglutathione (GSNO) was diluted in DNase/RNase-free water to two different working solutions of 0.5 and 1 mM. DMSO was diluted in DNase/RNase-free water to a working solution of 1 % v/v. BAY 41-2272 (10 mM) was diluted 1:100 in DNase/RNase-free water (=100 µM BAY 41-2272; 1 % v/v DMSO) and further diluted 1:10 in 1 % v/v DMSO (=10 µM BAY 41-2272; 1 % v/v DMSO).

Stimulation of HEK 293 cells for cGMP measurement: 250,000 HEK 293 cells were grown in 24 well plates and transfected according to Table 43. Cells were placed on a heating plate set at 37 °C and washed with 500 µl warm Dulbecco's PBS. Cells were equilibrated for 15 min with 350 µl warm HEPES buffered saline solution. Afterwards 50 µl of 10 mM IBMX working solution were added follwed by a further incubation step for 5 min. For comparing cGMP production between different time points of GSNO administration 100 µl

0.5 mM GSNO working solution or in case of t_0 100 µl DNase/RNase-free water were added to the cells. For comparing cGMP amounts between the administration of GSNO, BAY 41-2272 and a combination of both cells were treated according to Table 47. DMSO used as vehicle for BAY 41-2272 was thereby adapted to a final concentration of 0.1 % v/v in every sample (excluding the DMSO being contained in the IBMX).

Reactions were stopped by adding 100 µl ice-cold HCl working solution to a final concentration of 10 mM. Samples were scraped with a pipette tip, transferred to sterile 1.5 ml reaction tubes and subjected to one freeze-thaw cycle before measuring the cGMP amount as described in Section 3.27. Every sample was transfected and stimulated in duplicates.

Table 47 GSNO and BAY 41-2272 dilutions for stimulating HEK 293 cells

Treatment	Final concentration	Mix equal amounts of		
vehicle	0.1 % v/v DMSO	1 % v/v DMSO	+	water
BAY 41-2272	1 µM; 0.1 % v/v DMSO	10 µM BAY 41-2272	+	water
	10 µM; 0.1 % v/v DMSO	100 µM BAY 41-2272	+	water
GSNO	100 µM; 0.1 % v/v DMSO	1 mM GSNO	+	1 % v/v DMSO
BAY 41-2272 + GSNO	1 µM + 100 µM; 0.1 % v/v DMSO	10 µM BAY 41-2272	+	1 mM GSNO
	10 µM + 100 µM; 0.1 % v/v DMSO	100 µM BAY 41-2272	+	1 mM GSNO

Stimulation of VSMC for WB analysis of P-VASP$_{Ser239}$: 100,000 VSMC were seeded in 24 well plates and grown to confluence. Cells were placed on a heating plate set at 37 °C and washed with 500 µl warm Dulbecco's PBS. Cells were equilibrated for 15 min with 350 µl warm HEPES buffered saline solution. Afterwards 50 µl of 10 mM IBMX working solution were added follwed by a further incubation step for 5 min. Cells were treated with a final concentration of 10 µM BAY 41-2272, 100 µM GSNO and a combination of both according to Table 47 (each 100 µl). Also here DMSO used as vehicle for BAY 41-2272 was adapted to a final concentration of 0.1 % v/v in every sample (excluding the DMSO being contained in the IBMX). Treatment was applied for 15 min. Then the supernatant was replaced by 100 µl ice-cold RIPA buffer.

Cells were scraped and transferred to sterile 1.5 ml reaction tubes. Lysates were prepared as described in 3.18 and investigated for P-VASP$_{Ser239}$ as mentioned in Section 3.21.

3.27 cGMP measurement

cGMP was measured in a cGMP radioimmunoassay (IBL International) according to supplier's recommendations. The assay is based on the principle of radioimmunoassays for cyclic nucleotides described by Steiner *et al*. (Steiner *et al.* 1972). The effectivness of the assay relies on competition between radioactive ^{125}I-labelled cGMP and non-radioactive cGMP from the samples for a fixed number of antibody binding sites. The amount of bound cGMP to the antibody is inversely proportional to the cGMP concentration of the sample.

Radioimmunoassay: HEK 293 lysates from stimulation with GSNO and/or BAY 41-2272 were thawed on ice and diluted 30-fold in assay buffer in a total volume of 60 µl. 100 µl of standard or 20 µl of diluted sample were transferred to FACS tubes. Two extra tubes each were provided for NSB and B_0 tubes. Except for the standards 100 µl assay buffer were given to any other tube. 200 µl NSB solution were added to the NSB tubes. 100 µl ^{125}I-tracer were pipetted to every tube. Except NSB every tube was supplemented with 200 µl of antiserum. Tubes were capped, vortexed and incubated over night at 4 °C. The next day 1 ml cool separation reagent was pipetted to every tube. After vortexing tubes were centrifuged for 15 min at 2500 x g and 4 °C. Tubes were carefully decanted and beaten on paper towels. Counts per minute (cpm) were measured in a gamma counter (Berthold Technologies). Every sample, standard and control was prepared and measured as duplicate.

cGMP calculation: For each standard and sample B/B_0 % was calculated using following formula: $\mathrm{B/B_0\ \%} = \frac{\mathrm{cpm\ (standard/sample) - cpm\ (NSB)}}{\mathrm{cpm\ (B_0) - cpm\ (NSB)}}\ \mathrm{x}\ 100$. The concentration of the samples was red from the standard curve and multiplyed by 5 as the amount of cGMP within the samples was measured in 20 µl, the amount within the standards in 100 µl. For cGMP estimation as pmol per 10^6 cells, one additional well of cells was transfected for each variant. At the time point of harvesting cells for radioimmunoassay, these extra transfected wells were washed with 500 µl ice-cold Dulbecco's PBS and then scraped in 1 ml ice-cold Dulbecco's PBS and counted as described in Section 3.15. The mean of all cell counts within one experiment was used for calculation. Basal cGMP formation was substracted (t_0 or DMSO control, respectively).

3.28 Luciferase assay

Luciferase activity was measured with the Dual-Luciferase® reporter assay system (Promega Corporation). The activities of firefly and *Renilla* luciferases are measured one after another from the same sample. First, the firefly luciferase reporter is measured to generate a stabilised luminescent signal. Luciferin is added as a substrate. The more firefly

luciferase is produced the more luciferin is oxydised to oxyluciferin under the production of luminescence. After quantifying the firefly luminescence, the reaction is quenched and the *Renilla* luciferase reaction is simultaneously initiated. *Renilla* luciferase serves as a control for normalisation.

HEK 293 cells were seeded at 250,000 cells per well in 24 well plates and cultured to confluence for 24 h. Cells were cotransfected with 500 ng pGL4.10[*luc2*] plasmids and 50 ng pRL-TK plasmid according to Table 43. If necessary, a knockdown with siRNA was performed 6 h after transfection with luciferase plasmids. 24 or 48 h after transfection cells were washed in 500 µl cold Dulbecco's PBS and harvested in 50 µl 1X PLB (diluted from 5X in DNase/RNase-free water). Cells were subjected to one freeze-thaw cycle. The were scraped and homogenised by pipetting. 20 µl were used for measurement in white 96 well plates in the Infinite® M200 PRO microplate reader equipped with an auto-injector system by use of the iControl v1.10 software (Tecan Group). Well-wise, first 100 µl LAR II were injected. After a 2 s pre-read delay a 10 s firefly measurement period followed. Then 100 µl Stop & Glo® Reagent were injected to the well. Again a 2 s pre-read delay was followed by a 10 s measurement period for *Renilla*.

Luciferase activities were calculated by normalising firefly to *Renilla* signals. Values were expressed as fold of the non-risk variant. Untransfected cells in PLB were analysed for substraction background signals of firefly and *Renilla*.

3.29 Isolation of mouse platelets and aggregation experiments

Male C57Bl/6NCrl mice (10 to 12 weeks) were sacrificed by isofluran inhalation. Approximately 800 µl blood were collected from the orbital sinus using a glas capillary and drawn into 200 µl heparin solution (50 U/ml) in a sterile 2 ml reaction tube. After dilution with 1 ml Dulbecco's PBS and centrifugation for 10 min at 100 x g without active deceleration and 20 °C, the upper phase (platelet rich plasma, PRP) was transferred to a sterile 1.5 ml reaction tube. A second centrifugation step for 10 min at 700 x g and 20 °C provided platelet poor plasma (PPP) which was used for blanking.

Aggregation of 200 µl PRP (247-446 x 10^3 platelets/µl) was measured at 37 °C in an 8-channel turbidimetric aggregometer (PAP8 v2.0, Bio/Data Corporation) in glass cuvettes containing a disposable stir bar (both Bio/Data Corporation) for constant stirring. Aggregation was elicited by 25 µl ADP at a final concentration of 2 µM. DMSO, BAY 41-2272, sodium nitroprusside (SNP) and a combination of BAY 41-2272 and SNP (each 25 µl) were administered 2 min before the addition of ADP. The used dilutions can be appreciated Table

48 and Table 49. The concentration of DMSO used as a vehicle for SNP and BAY 41-2272 was adapted to a final concentration of maximum 0.305 % v/v in every sample.

DMSO was diluted in DNase/RNase-free water to concentrations of 2, 3, 4 and 6 % v/v. The 200 mM SNP stock solution was serially diluted in DNase/RNase-free water to a concentration of 200 µM (0.1 % v/v DMSO). The 10 mM BAY 41-2272 stock solution was diluted in DNase/RNase-free water to a working solution of 600 µM (6 % v/v DMSO). The 600 µM BAY 41-2272 working solution was further diluted in 6 % v/v DMSO to concentrations of 200 µM, 60 µM and 20 µM all with a DMSO concentration of 6 % v/v (used for dilutions in Table 48).

Furthermore, 10 mM BAY 41-2272 stock solution was diluted in DMSO to a concentration of 5 mM and then in DNase/RNase-free water to a working solution of 200 µM (4 % v/v DMSO) and again in DNase/RNase-free water to a working solution with a concentration of 100 µM (2 % v/v DMSO) (used for dilutions in Table 49).

Table 48 Dilution scheme for the administration of 10 µM SNP in combination with different concentrations of BAY 41-2272

Treatment	Final concentration	Volume	Chemical
vehicle	0.3 % v/v DMSO	25 µl	3 % v/v DMSO
SNP +	10 µM + 30 µM; 0.305 % v/v DMSO	12.5 µl each	200 µM SNP + 600 µM BAY 41-2272
BAY 41-2272	10 µM + 10 µM; 0.305 % v/v DMSO		200 µM SNP + 200 µM BAY 41-2272
	10 µM + 3 µM; 0.305 % v/v DMSO		200 µM SNP + 60 µM BAY 41-2272
	10 µM + 1 µM; 0.305 % v/v DMSO		200 µM SNP + 20 µM BAY 41-2272

Table 49 Dilution scheme for the administration of 10 µM BAY 41-2272, 10 µM SNP and a combination of both

Treatment	Final concentration	Volume	Chemical
vehicle	0.2 % v/v DMSO	25 µl	2 % v/v DMSO
BAY 41-2272	10 µM; 0.2 % v/v DMSO	25 µl	100 µM BAY 41-2272
SNP	10 µM; 0.2 % v/v DMSO	12.5 µl each	200 µM SNP + 4 % v/v DMSO
BAY 41-2272 + SNP	10 µM + 10 µM; 0.2 % v/v DMSO	12.5 µl each	200 µM SNP + 200 µM BAY 41-2272

Area under the curve (AUC) was recorded over 5 min. Platelets from aggregation experiments were transferred from the glas cuvettes to sterile 1.5 ml reaction tubes and spun down for 15 min at maximum speed and 4 °C. Supernatant was removed, platelets were resuspended in 50 µl of a 1:2 mixture of RIPA and 2X laemmli buffer and stored at -80 °C.

3.30 Measurement of platelet count

Platelet count in whole blood and PRP was determind in a haemocytometer (Sysmex Corporation).

3.31 Data analyses

Distribution of data was assessed using the D'Agostino-Pearson omnibus normality test. Normally distributed data is presented as mean ± SEM, not normally distributed data as median with interquartile range. Normally distributed data was analysed using Student's unpaired/paired t test or One-sample t test, as appropriate. For comparison of more than two groups of normally distributed data, Ordinary/RM one-way analysis of variance (ANOVA) or 2way ANOVA followed by Bonferroni's, Tukey's or Dunnett's multiple comparison test were used followed by post test for linear trend, if applicable. Not normally distributed data was analysed by Mann-Whitney test. For comparison of more than two groups of not normally distributed data Kruskal-Wallis or Friedman test followed by Dunn's multiple comparison were used. Dose-dependent effects of BAY 41-2272 on mouse platelet aggregation as well as the correlation between human sGC α_1 expression and inhibition of platelet aggregation were analysed using linear regression. Categorical data was analysed using Fisher's exact test.

Statistical significance was set as $p<0.05$. Calculations were performed with GraphPad Prism® software version 6.0 for Mac OS X.

4 Results

4.1 Rare coding variants in *GUCY1A3*

4.1.1 Selection of variants

In total, nine rare coding missense variants in the *GUCY1A3* gene were identified by exome sequencing in extended families with high prevalence of premature coronary artery disease (CAD)/myocardial infarction (MI), by screening exome sequencing data of 252 young MI cases (age of onset between 24 and 49 years, 24 % women) with a positive family history of CAD and MI (Erdmann *et al.* 2013) and in data of the Exome Sequencing Project Early-Onset Myocardial Infarction (ESP-EOMI) study (Do *et al.* 2015) (Table 50). It has been shown previously that coding variants in the *GUCY1A3* gene are overrepresented in CAD and MI patients compared to patients suffering from other diseases and healthy controls (Erdmann *et al.* 2013). Of the nine variants one had already been functionally characterised before (Erdmann *et al.* 2013). Figure 10 shows the location of these nine variants within the *GUCY1A3* transcript and the soluble guanylyl cyclase (sGC) α_1 protein.

Table 50 Rare coding missense variants found in *GUCY1A3*. Overall, nine variants have been identified: five variants found in young MI patients (Erdmann *et al.* 2013), two variants found in extended families with high prevalence of premature MI (Erdmann *et al.* 2013), and two variants identified by the Exome Sequencing Project Early-Onset Myocardial Infarction (ESP-EOMI) study conducted by the National Heart, Lung, and Blood Institute (Do *et al.* 2015, Wobst *et al.* 2016) with predicted damaging impact in the PolyPhen-2 prediction (Adzhubei *et al.* 2010). Reprinted with permission of Springer: Table 1 from Wobst *et al.* Stimulators of the soluble guanylyl cyclase: promising functional insights from rare coding atherosclerosis-related *GUCY1A3* variants. *Basic Res Cardiol* 2016. 111(4):51 (Wobst *et al.* 2016), copyright © 2016.

Variant	Identified in	Predicted effect (PolyPhen-2)
p.Leu163Phefs*24	MI family	frameshift
p.Gly537Arg	MI family	probably damaging
p.Lys53Glu	young MIs	possibly damaging
p.Thr64Ala	young MIs	benign
p.Thr229Met	young MIs	possibly damaging
p.Ser478Gly	young MIs	benign
p.Ile571Val	ESP-EOMI	possibly damaging
p.Val587Ile	young MIs	benign
p.Cys610Tyr	ESP-EOMI	probably damaging

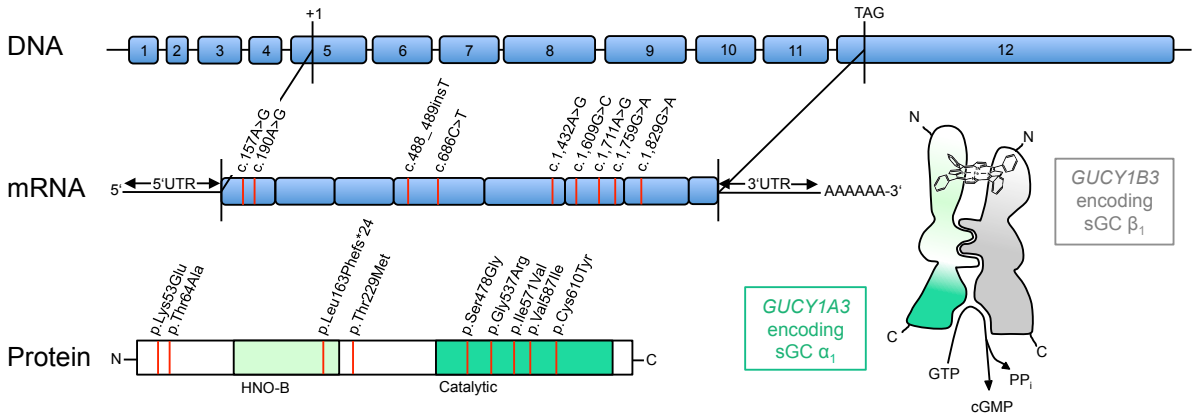

Figure 10 Location of rare coding *GUCY1A3* variants found in MI patients and extended families with high prevalence of premature CAD and MI. The nine variants are distributed over the entire *GUCY1A3* transcript. Whereas the previously described loss-of-function mutation (p.Leu163Phefs*24) is located in the NO-binding domain of the sGC α_1 subunit, five variants, i.e., p.Ser478Gly, p.Gly537Arg, p.Ile571Val, p.Val587Ile, and p.Cys610Tyr, are located in the catalytic domain and three variants, i.e., p.Lys53Glu, p.Thr64Ala, and p.Thr229Met, reside within intermediate regions. Protein annotation according to *NCBI protein* (Accession: NP_001243378.1). *HNO-B:* haem-NO-binding. Reprinted with permission of Springer: Figure 1 from Wobst *et al.* Stimulators of the soluble guanylyl cyclase: promising functional insights from rare coding atherosclerosis-related *GUCY1A3* variants. *Basic Res Cardiol* 2016. 111(4):51 (Wobst *et al.* 2016), copyright © 2016.

4.1.2 Influence of coding *GUCY1A3* variants on subunit protein levels

To investigate the influence of the rare variants in *GUCY1A3* on protein expression of sGC α_1 protein levels, HEK 293 cells were transfected with plasmids coding for the sGC α_1 and β_1 subunits followed by Western blotting. Both, *GUCY1A3* and *GUCY1B3* constructs were fused to a V5 tag at the C-terminus.

The p.Leu163Phefs*24 variant which was previously described (Erdmann *et al.* 2013) results in a frameshift and premature stop of translation after 185 amino acids. Due to the lack of the V5 tag, it could not be detected by immunoblotting and was carried as negative control (Figure 11A). Except for the variant p.Gly537Arg, which led to a 72 % reduction in α_1 subunit protein amount compared to the wildtype α_1 subunit ($p<0.01$), all other coding *GUCY1A3* variants did not result in significant changes of α_1 subunit protein levels (Figure 11B). Protein levels of the β_1 subunit changed concordantly with the α_1 subunit protein levels (Figure 11C). Therefore, a significant reduction in β_1 subunit protein level was only detectable for the p.Leu163Phefs*24 variant (59 %; $p<0.0001$).

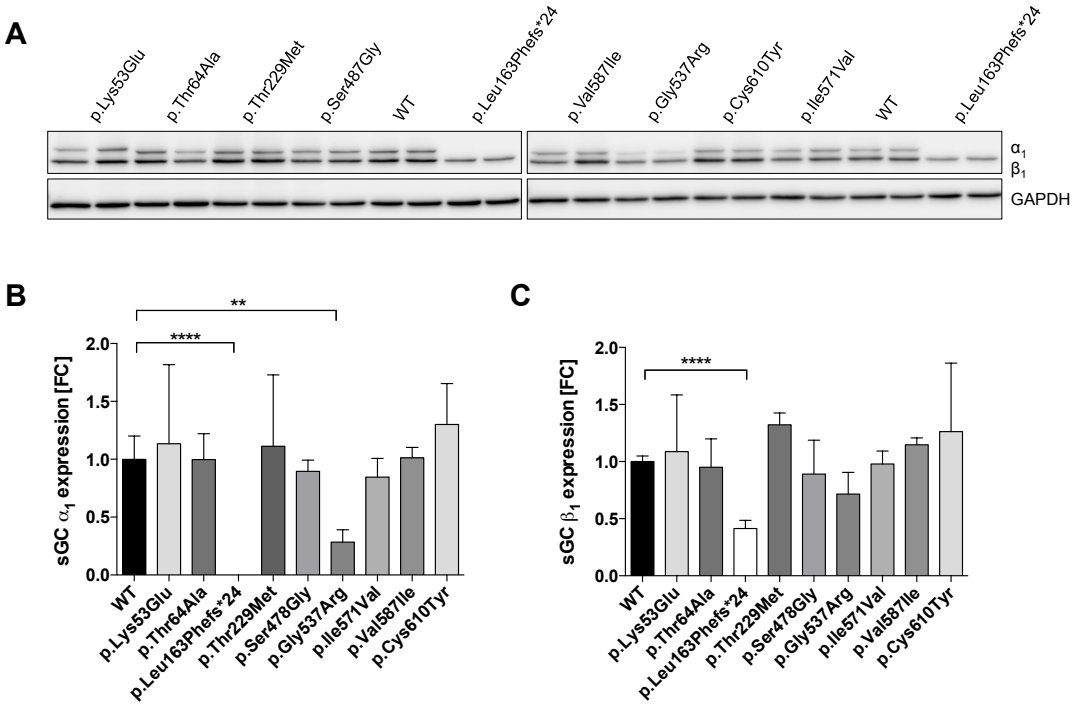

Figure 11 Impact of rare coding *GUCY1A3* variants on sGC α_1 and β_1 protein levels. (A) Representative immunoblot of sGC α_1 wildtype (WT) and rare variants as well as the β_1 subunit overexpressed in HEK 293 cells. (B) Quantification of protein levels revealed, as it had been shown previously (Erdmann *et al.* 2013), a significant reduction of α_1 subunit protein amount for the p.Gly537Arg and p.Leu163Phefs24* variants. (C) Protein levels of β_1 subunit changed concordantly. Data are median with interquartile range of five independent experiments with each variant transfected in duplicates. Statistical significance was assesed by Kruskal-Wallis test with Dunn's multiple comparisons test. **: p<0.01; ****: p<0.0001. Reprinted with permission of Springer: Part of Figure 2 from Wobst *et al.* Stimulators of the soluble guanylyl cyclase: promising functional insights from rare coding atherosclerosis-related *GUCY1A3* variants. *Basic Res Cardiol* 2016. 111(4):51 (Wobst *et al.* 2016), copyright © 2016.

4.1.3 p.Gly537Arg sGC α_1 levels are likely influenced by reduced mRNA stability

To further investigate the reason for decreased protein levels of the sGC α_1 variant p.Gly537Arg, proteasome inhibition and mRNA quantification experiments were performed.

For proteasomal degradation experiments, HEK 293 cells were transfected with plasmids coding for *GUCY1A3* and *GUCY1B3* carrying a C-termial V5 tag and were either treated with 0.1 µM bortezomib or respective amounts of DMSO which was used as vehicle for bortezomib. Since proteasome inhibition with bortezomib led to a significant increase in wildtype sGC α_1 subunit protein levels but not in p.Gly537Arg α_1 subunit protein levels (Figure 12A, B) a second experiment was performed, in which the amount of *GUCY1A3* mRNA was measured by qPCR.

Hence, HEK 293 cells were again co-transfected with the respective plasmids followed by qPCR. Results suggest that the reduction of p.Gly537Arg is likely to be due to reduced mRNA stability rather than enhanced degradation as p.Gly537Arg was already

reduced on mRNA level (Figure 12C). In contrast, mRNA levels of the variant carrying the frame-shift mutation leading to the truncated sGC α_1 protein (p.Leu163Phefs*24) were not decreased (Figure 12D).

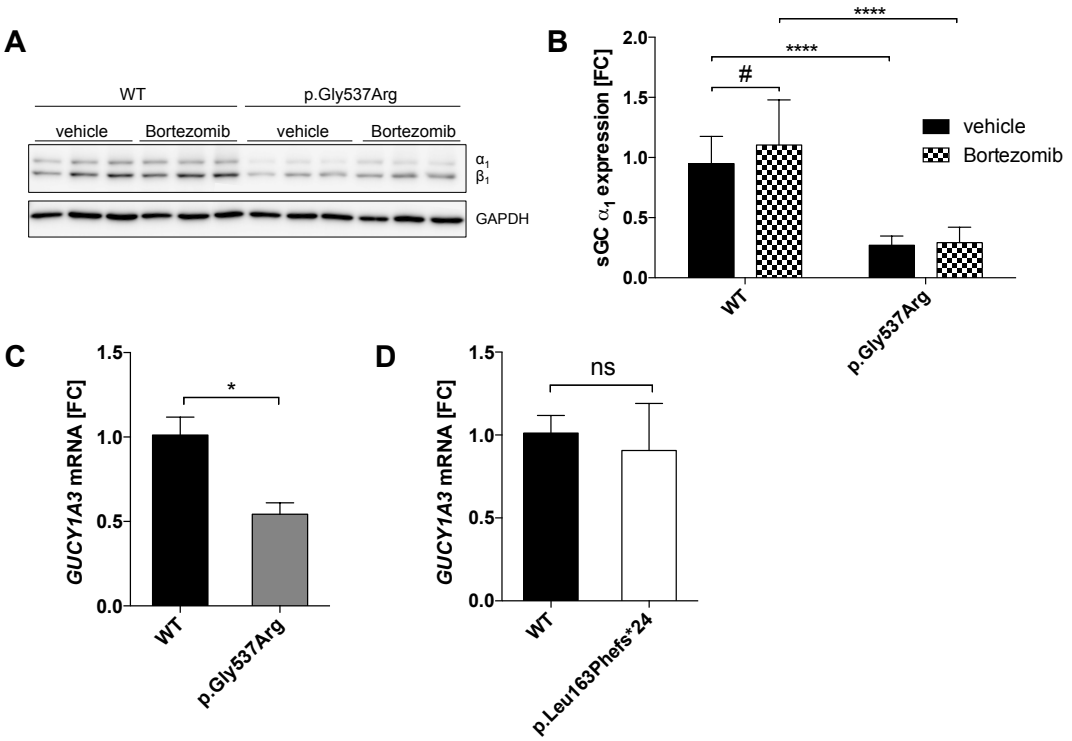

Figure 12 Decreased p.Gly537Arg α_1 subunit protein levels are likely caused by reduced mRNA stability. (A) Representative immunoblot of sGC α_1 and β_1 subunits after transfection of HEK 293 cells and treatment with bortezomib. (B) Proteasome inhibition with bortezomib led to a significant increase in WT sGC α_1 subunit protein levels but not in p.Gly537Arg α_1 subunit protein levels. (C) After transfection with constructs containing the p.Gly537Arg *GUCY1A3* variant, mRNA levels were reduced by almost 50 % compared to mRNA levels after transfection of the WT *GUCY1A3* construct. (D) In comparison, the p.Leu163Phefs*24 variant did not influence mRNA levels as compared to WT *GUCY1A3*. Data are median with interquartile range (B) or mean ± SEM (C, D) of three independent experiments each. Statistical significance was assessed by using Mann-Whitney test (B) or Student's unpaired t test (C, D). *: WT vs. variant; #: intravariant; *, #: p<0.05; *: p<0.05; ****: p<0.0001. (B), (C) and (D) reprinted with permission of Springer: Supplemental Figure 1 from Wobst *et al.* Stimulators of the soluble guanylyl cyclase: promising functional insights from rare coding atherosclerosis-related *GUCY1A3* variants. *Basic Res Cardiol* 2016. 111(4):51 (Wobst *et al.* 2016), copyright © 2016.

4.1.4 Variants in sGC α_1 do not influence protein-protein interaction with β_1

sGC is composed of α_1 and β_1 subunits and can only exhibit enzymatic activity if both subunits are dimerised.

In a first experiment, dimerisation of the sGC α_1 subunit with the β_1 subunit was investigated by bimolecular fluorescence complementation (BiFC). Plasmids containing coding sequences for interaction partners out of the bZIP family *bJun* and *bFos* were used as positive controls (Nakagawa *et al.* 2014). Whereas HEK 293 cells overexpressing the control

plasmids exhibited strong fluorescence (Figure 13C) the co-transfection of *GUCY1A3* and *GUCY1B3* did not elicit any light (Figure 13B).

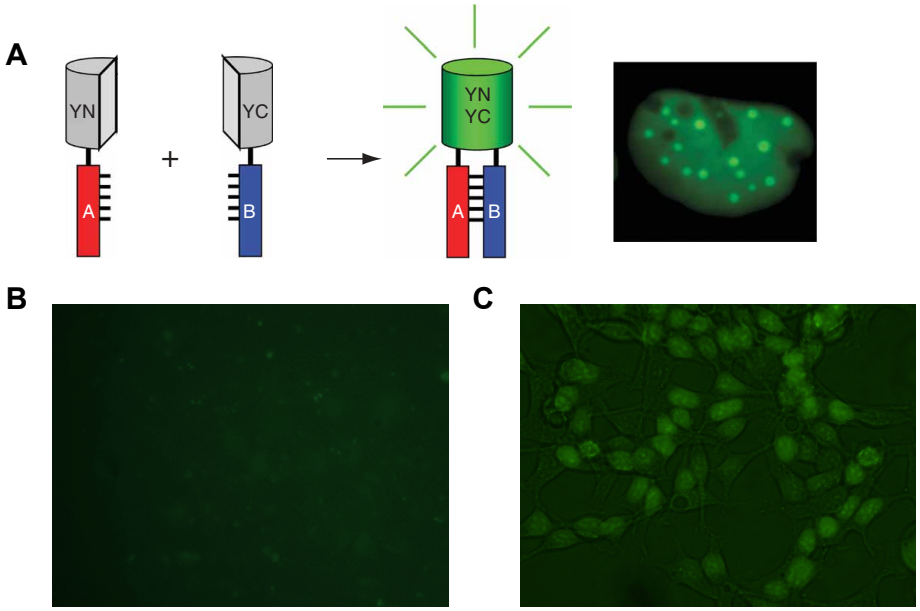

Figure 13 Principle and live cell imaging of BiFC. (A) Two fragments (YN and YC) of enhanced yellow fluorescent protein (EYFP) are fused to two putative interaction partners (A and B). An interaction between the proteins facilitates association between the fragments to produce a bimolecular fluorescent complex. (B) Microscopy of HEK 293 cells overexpressing pBiFC-*GUCY1A3*-YN155 and pBiFC-*GUCY1B3*-YC155 showing no fluorencent signal. (C) Microscopy of HEK 293 cell overexpressing the positive control plasmids pBiFC-*bJun*-YN155 and pBiFC-*bFos*-YC155 exhibiting strong fluorescence. Microscopy done 36 h post transfection. (A) reprinted by permission from Macmillan Publishers Ltd: Figure 1 from *Nat Protoc* 2006. 1(3):1278-1286 (Kerppola 2006), copyright © 2016.

In a second experiment, time-resolved fluorescence resonance energy transfer (TR-FRET) was applied. HEK 293 cells were co-transfected with all four possible TR-FRET construct combinations (*GUCY1A3* with HA at N- and C-terminus as well as *GUCY1B3* with Flag at N- and C-terminus). Cells were lysed in two different buffers and lysates were investigated using different combinations of antibody-fluorophor complexes (anti-HA-d2 + anti-Flag-EuK or anti-HA-EuK + anti-Flag-d2). Measurements were performed after 15, 30 and 60 min incubation time. As compared to the positive control, none of the tested combinations resulted in a measurable TR-FRET signal. Figure 14 gives an overview on an exemplary TR-FRET measurement.

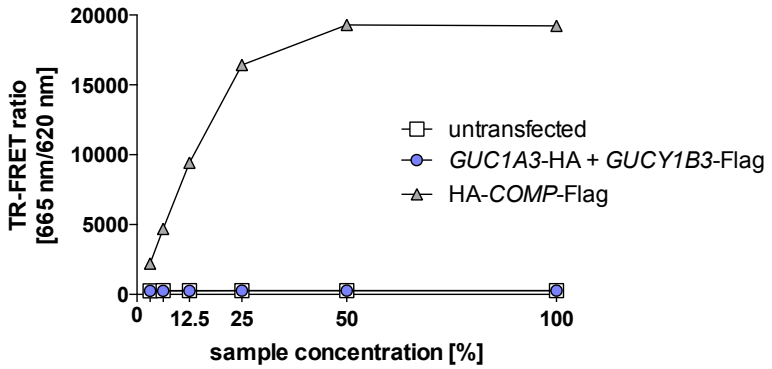

Figure 14 Exemplary TR-FRET measurement data. In this exemplary measurement, lysates in buffer EGFR from HEK 293 cells overexpressing C-terminally HA tagged *GUCY1A3* and C-terminally Flag tagged *GUCY1B3* were investigated with a HA antibody fused to the fluorophore d2 and a Flag antibody fused to the fluorophore EuK. No signal could be observed for the interaction of sGC α_1 with sGC β_1. As positive control a HA-*COMP*-Flag construct was used. *EuK:* europium cryptate.

In a third experiment, the influence of *GUCY1A3* variants on dimerisation of the respective sGC α_1 subunit with the β_1 subunit was assessed by co-immunoprecipitation experiments. Expression of the β_1 subunit was thereby used as readout after immunoprecipitation of the α_1 subunit with HA-coupled beads. In a preliminary experiment, all four combinations of constructs from the TR-FRET approach were tested on protein-protein interactions after overexpression in HEK 293 cells. As the combination of C-terminally HA tagged wildtype *GUCY1A3* with C-terminally Flag tagged wildtype *GUCY1B3* gave the most reliable results in Western blotting (data not shown), subsequent experiments testing the influence of coding variants in *GUCY1A3* were performed with these C-terminally tagged constructs.

As is has been shown before, the p.Leu163Phefs*24 variant resulting in a truncated protein lacking the tag could not be detected. For all other α_1 variants we detected bands for both subunits. In case of the variant p.Gly537Arg both bands appeared weaker. Otherwise we saw similar band intensities as compared to bands resulting from wildtype transfection (Figure 15).

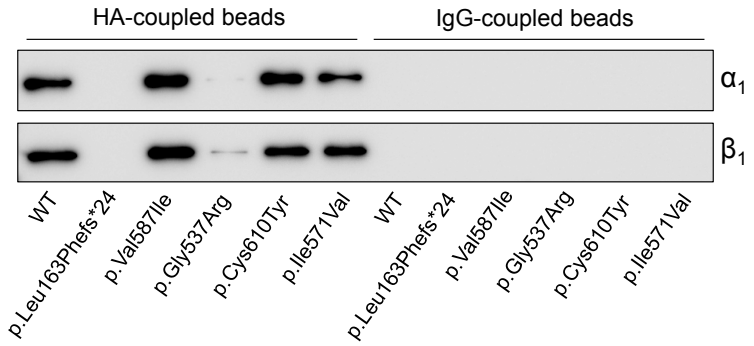

Figure 15 Impact of rare coding *GUCY1A3* variants on dimerisation capability with the β_1 subunit. Representative immunoblot showing protein-protein interaction assessed by co-immunoprecipitation. Immunoprecipitation of all investigated sGC α_1 variants, excepting the p.Leu163Phefs24* variant, enabled detection of β_1 subunit signals. IgG-coupled beads were used as negative control. Reprinted with permission of Springer: Part of Figure 2 from Wobst *et al.* Stimulators of the soluble guanylyl cyclase: promising functional insights from rare coding atherosclerosis-related *GUCY1A3* variants. *Basic Res Cardiol* 2016. 111(4):51 (Wobst *et al.* 2016), copyright © 2016.

4.1.5 Influence of rare coding *GUCY1A3* variants on sGC activity

To investigate the impact of *GUCY1A3* variants on sGC enzymatic activity, HEK 293 cells were transfected with constructs carrying the *GUCY1A3* variants as well as the *GUCY1B3* construct, both C-terminally tagged with V5. In a preliminary experiment cyclic guanosine-3',5'-monophosphate (cGMP) production of wildtype sGC and the two MI family mutations p.Gly537Arg and p.Leu163Phefs*24 after stimulation with the nitric oxide (NO) donor S-nitrosoglutathione (GSNO; 100 µM) was analysed between time points 0 and 10 min in order to determine suitable time points for further experiments. The highest cGMP production was detectable between 30 s and 2 min (Figure 16A). Hence, production of cGMP after stimulation with GSNO (100 µM) was analysed in all investigated variants between 0 and 2 min (Figure 16B).

To investigate difference in enzymatic activity between variants we compared cGMP levels measured after 2 min (Figure 16C). Six variants displayed significantly reduced cGMP levels compared to the wildtype protein with the most prominent effect being observed for p.Leu163Phefs*24 representing endogenous HEK 293 cell sGC. The p.Gly537Arg variant also displayed significantly reduced cGMP formation which can be explained by reduced protein level of the α_1 subunit. The other four variants resulting in significantly reduced cGMP formation, p.Lys53Glu (34 %, $p<0.001$), p.Thr64Ala (40 %, $p<0.0001$), p.Ile571Val (37 %, $p<0.0001$), and p.Val587Ile (50 %, $p<0.0001$), did not display reduced protein levels suggesting a direct influence on enzymatic activity whereby only the latter two variants are located in the catalytic domain of the sGC (Figure 10).

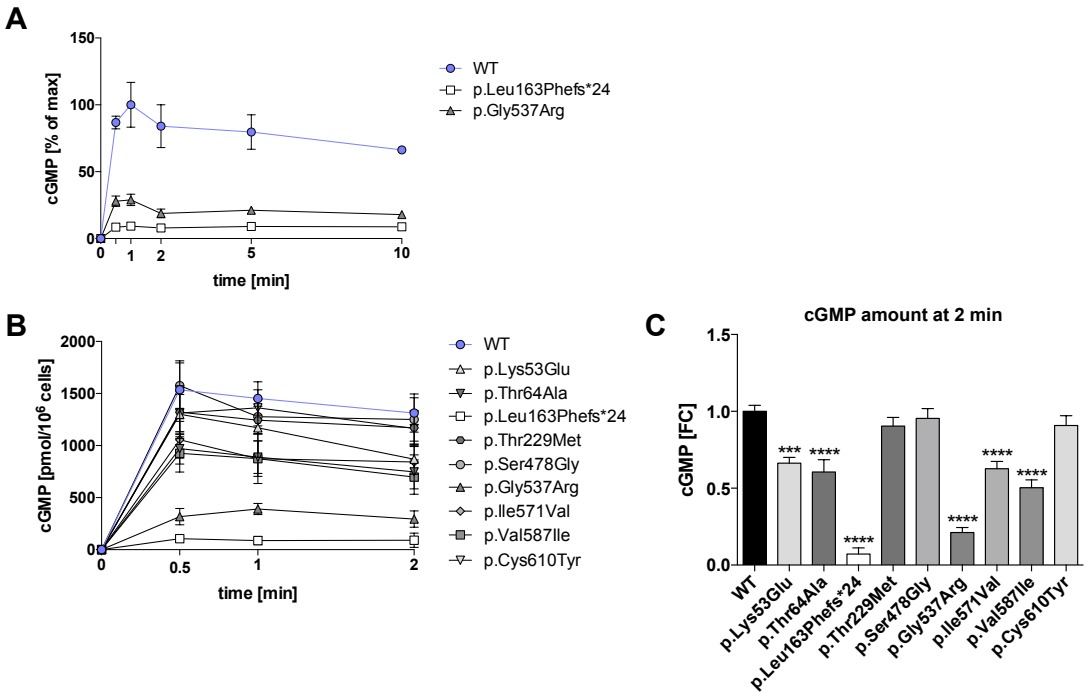

Figure 16 NO-dependent cGMP formation by sGC. (A) Time course of cGMP formation for empiric determination of most suitable time points for subsequent experiments. (B) Rare coding *GUCY1A3* variants displayed altered cGMP formation between 0 and 2 min of stimulation with the NO donor GSNO. As it had been shown previously (Erdmann *et al.* 2013), the p.Leu163Phefs24* variant leads to a loss-of-function. (C) Quantitative analysis at 2 min revealed significant reduction in cGMP formation in five rare coding *GUCY1A3* variants in addition to the p.Leu163Phefs24* variant. Of note, the p.Gly537Arg variant also displayed reduced protein levels. Data are mean ± SEM of five independent experiments with each variant transfected in duplicates (B, C). Statistical significance was assesed by Ordinary one-way ANOVA followed by Bonferroni's test for multiple comparisons. ***: p<0.001, ****: p<0.0001. (B) and (C) reprinted with permission of Springer: Figure 3 from Wobst *et al.* Stimulators of the soluble guanylyl cyclase: promising functional insights from rare coding atherosclerosis-related *GUCY1A3* variants. *Basic Res Cardiol* 2016. 111(4):51 (Wobst *et al.* 2016), copyright © 2016.

4.1.6 Rescue of diminished sGC activity by the stimulator BAY 41-2272

As outlined in Section 1.3 two classes of sGC modulators have been developed for the treatment of cardiovascular diseases, which activate sGC in an NO-independent manner: sGC stimulators and sGC activators. We chose to use the sGC stimulator BAY 41-2272 as stimulators activate purified sGC but mainly exhibit syngergistic effects together with endogenous NO thereby enhancing NO-dependent cGMP production (Evgenov *et al.* 2006, Stasch *et al.* 2011). In this way, a direct comparison between NO-dependent cGMP production and cGMP production upon additional administration with BAY 41-2272 can be drawn.

4.1.7 Effect of NO and BAY 41-2272 on mouse platelet aggregation

Using optical aggregometry we tested the effect of different concentrations of BAY 41-2272 in mouse platelet aggregation.

In preliminary experiments, it was established that a final concentration of 10 µM for the NO donor sodium nitropsusside (SNP) was the most suitable concentration for aggregation of human platelets allowing the analysis despite interindividual differences in platelet inhibition, i.e., a significant but not complete inhibition was achieved with this concentration (data not shown). Therefore, all experiments on mouse platelets presented in this study were also performed using SNP with a final concentration of 10 µM.

In order to determine suitable concentrations of BAY 41-2272, four different concentrations (1 µM, 3 µM, 10 µM and 30 µM) were tested in combination with 10 µM SNP. As shown in Figure 17A, the addition of BAY 41-2272 to the NO donor sodium nitroprusside led to a concentration-dependent inhibition of platelet aggregation elicited by ADP (n=10) as measured by area under the curve (AUC) of platelet aggregation (R^2=0.28, $p<0.001$; Figure 17A). The lowest dose producing a significant aggregation was identified for subsequent experiments, i.e., 10 µM BAY 41-2272.

We then compared the inhibition of platelet aggregation after preincubation with SNP alone (10 µM), with BAY 41-2272 alone (10 µM) or with the combination of both substances (n=10). BAY 41-2272 alone did not show an influence on platelet aggregation ($p>0.99$) whereas the addition of BAY 41-2272 to the NO donor SNP led to a significant decrease in platelet aggregation compared to control ($p<0.001$) and a further decrease compared to SNP alone ($p<0.01$; Figure 17B).

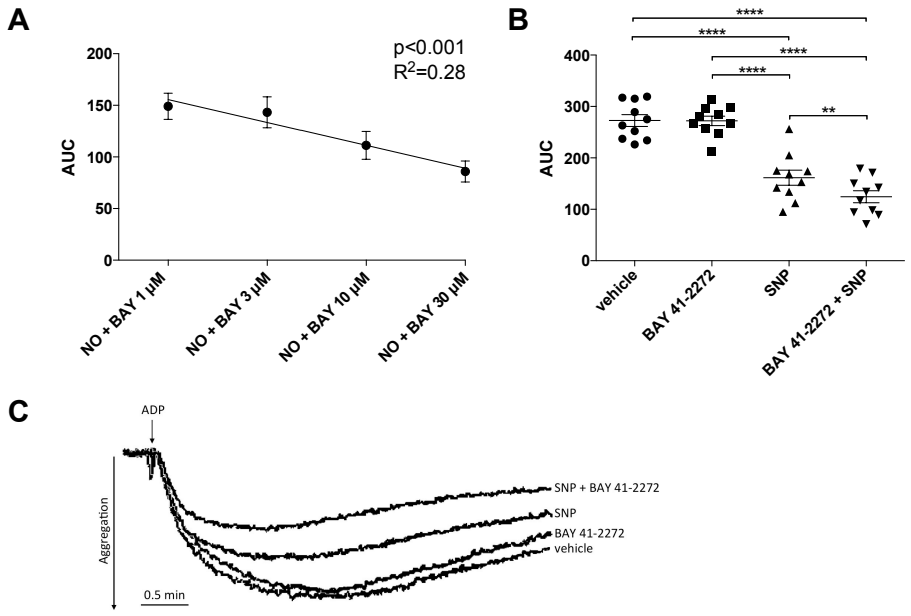

Figure 17 Addition of BAY 41-2272 translates into further inhibition of platelet aggregation. (A) In platelet rich plasma from WT mice, BAY 41-2272 in addition to the NO donor SNP led to a dose-dependent inhibition of platelet aggregation. (B) Whereas the addition of BAY 41-2272 did not have an effect on platelet aggregation alone, the combination with SNP resulted in significantly reduced platelet aggregation. Of note, the addition of BAY41-2272 further inhibited platelet aggregation as compared to SNP alone. Data are mean ± SEM of n=10 in each experiment. Statistical analysis was assesed by (A) linear regression and (B) RM one-way ANOVA with Bonferroni's multiple comparisons test. **: p<0.01; ****: p<0.0001. BAY: BAY41-2272; *SNP*: sodium nitroprusside; *ADP*: adenosine diphosphate. (A) and (B) reprinted with permission of Springer: Part of Figure 4 from Wobst *et al.* Stimulators of the soluble guanylyl cyclase: promising functional insights from rare coding atherosclerosis-related *GUCY1A3* variants. *Basic Res Cardiol* 2016. 111(4):51 (Wobst *et al.* 2016), copyright © 2016.

4.1.8 VASP phosphorylation in mouse platelets

As a further readout, we analysed cGMP-dependent phosphorylation of vasodilator-stimulated pophosphoprotein (VASP) by Western blotting. cGMP thereby activates proteinkinase G Iβ (PKGIβ) to phosphorylate VASP at its PKGIβ specific phosphorylation site serine$_{239}$ (Ser$_{239}$) (Figure 4). The addition of BAY 41-2272 to the NO donor sodium nitroprusside (SNP) led to significantly enhanced VASP phosphorylation over treatment with vehicle (Figure 18).

When detecting P-VASP at Ser$_{239}$ two bands are observed in Western blot. This is due to a additional phoyphorylation of VASP at Ser$_{157}$ by proteinkinases A and C leading to a shift from 46 to 50 kDa.

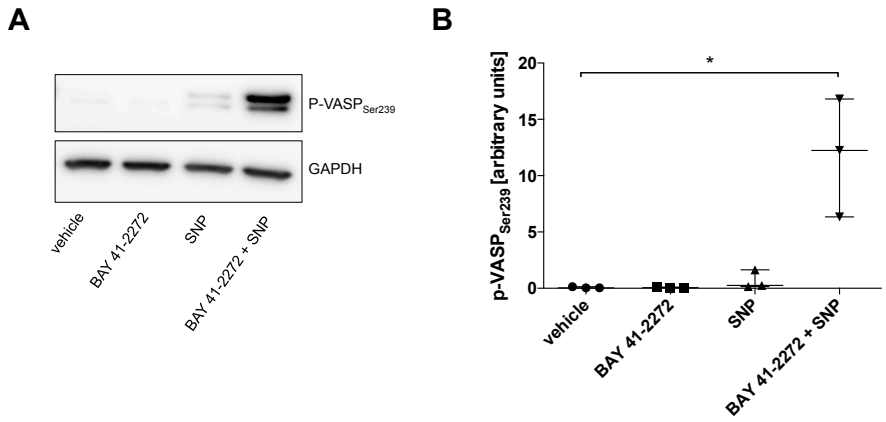

Figure 18 Influence of BAY 41-2272 on cGMP formation in mouse platelets. (A) Representative immunoblot showing the extent of VASP phosphorylation. (B) The combination of SNP and BAY 41-2272 resulted in significantly stronger phosphorylation compared to control. Data are median with interquartile range of n=3. Statistical analysis was done with Friedman test followed by Dunn's multiple comparisons test. *: p<0.05. (A) reprinted with permission of Springer: Part of Figure 4 from Wobst *et al.* Stimulators of the soluble guanylyl cyclase: promising functional insights from rare coding atherosclerosis-related *GUCY1A3* variants. *Basic Res Cardiol* 2016. 111(4):51 (Wobst *et al.* 2016), copyright © 2016.

4.1.9 Rescue of impaired cGMP formation by BAY 41-2272

As shown in Figure 16, six of the investigated variants displayed reduced cGMP formation including the p.Leu163Phefs*24 loss-of-function variant. For experiments testing the potential of BAY 41-2272 to rescue impaired cGMP formation we focused on the five variants displaying reduced cGMP levels but detectable protein levels. For that, cGMP levels were measured after 2 min in the presence of two different concentrations of BAY 41-2272 (1 µM and 10 µM) enabling a direct comparison to cGMP amounts generated after administration of GSNO only (Figure 19).

BAY 41-2272 led to a dose-dependent increase in cGMP formation of the sGC wildtype protein. Same was true for all tested variants except for p.Gly537Arg, where the addition of 1 µM BAY 41-2272 led to a significant increase in cGMP production (31 %, p<0.01; Figure 19D) whereas an increase in BAY 41-2272 concentration (10 µM) did not lead to a further increase in cGMP levels. The α_1 variants p.Thr64Ala and p.Ile571Val both reached the cGMP levels of the wildtype protein stimulated with the NO donor only already at a concentration of 1 µM BAY 41-2272 (1.009 of $WT_{100\mu M\ GSNO}$ and 1.233 of $WT_{100\mu M\ GSNO}$, respectively; Figure 19C and E). For the p.Lys53Glu and p.Val587Ile variants, cGMP levels of the the wildtype protein stimulated with NO only were reached at final concentrations of 10 µM BAY 41-2272 (0.996 of $WT_{100\mu M\ GSNO}$ and 1.185 of $WT_{100\mu M\ GSNO}$, respectively; Figure 19B and F). In summary, all variants displaying reduced cGMP formation *in vitro* and normal protein levels of the α_1 subunit could be functionally rescued by the addition of the sGC stimulator BAY 41-2272.

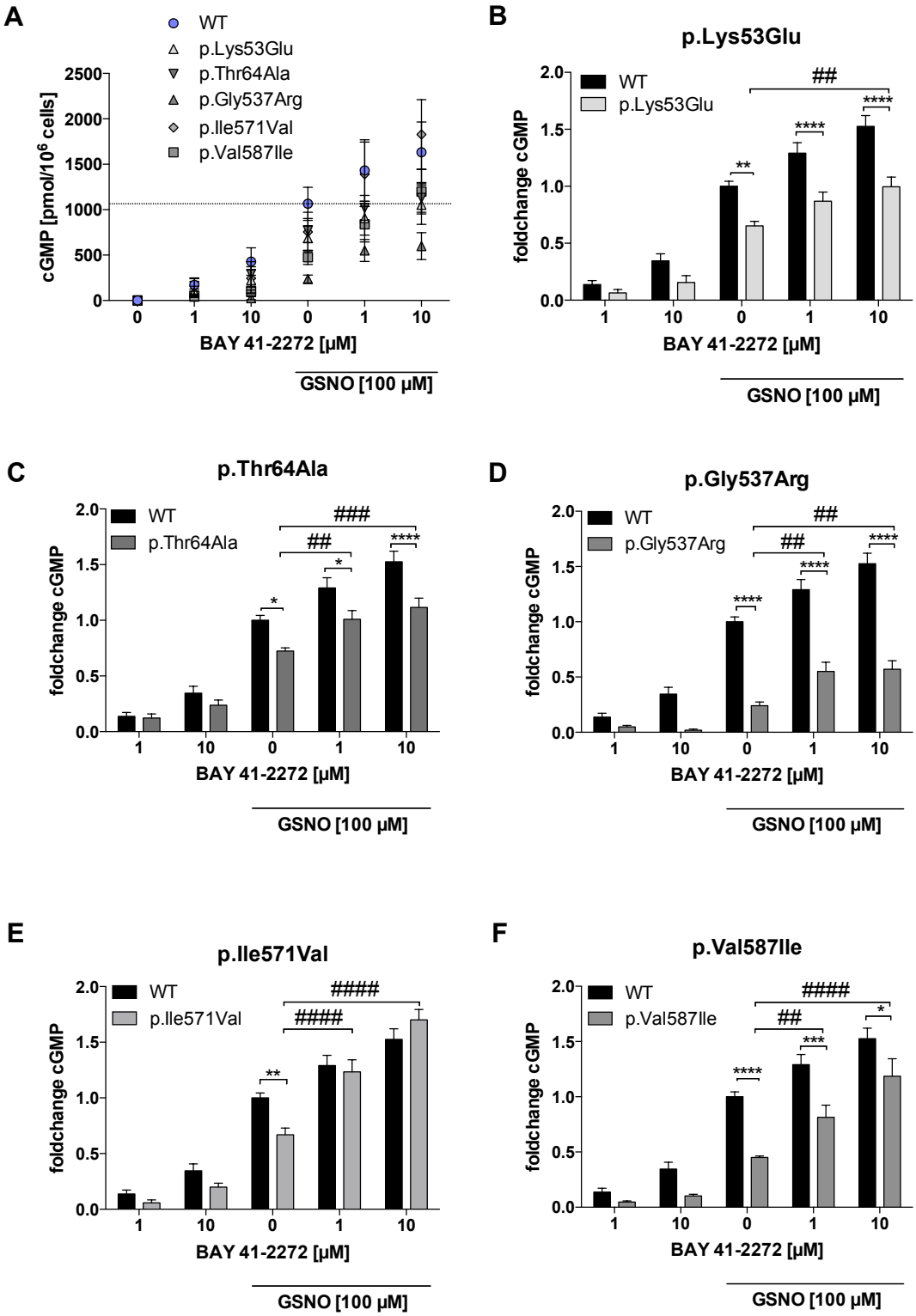

Figure 19 Rescue of reduced cGMP formation by BAY 41-2272. Whereas the addition of BAY 41-2272 to the NO donor GSNO led to a dose-dependent increase in cGMP formation in WT sGC as well as the p.Lys53Glu (B) p.Thr64Ala (C), p.Ile571Val (E), and p.Val587Ile (F) variants, the effect in the p.Gly537Arg (D) variant was weaker: cGMP levels were increased in the presence of 1 µM BAY 41-2272, however, 10 µM did not further enhance cGMP formation. Additionally, cGMP levels were still significantly reduced compared to WT sGC in presence of the NO donor only. In all other variants, the addition of 10 µM BAY 41-2272 was able to rescue cGMP formation to the level of WT sGC in presence of the NO donor only. Data are mean ± SEM of five independent experiments with each variant transfected in duplicate. Statisctical calculation was done by use of 2way ANOVA followed by Bonferroni's multiple comparisons test. *: WT vs. variant; #: intravariant; *, #: p<0.05; **, ##: p<0.01; ***, ###: p<0.001; ****, ####: p<0.0001. (B)-(F) reprinted with permission of Springer: Figure 5 from Wobst *et al.* Stimulators of the soluble guanylyl cyclase: promising functional insights from rare coding atherosclerosis-related *GUCY1A3* variants. *Basic Res Cardiol* 2016. 111(4):51 (Wobst *et al.* 2016), copyright © 2016.

4.2 Common *GUCY1A3* lead SNP rs7692387

4.2.1 *In silico* analyses

4.2.1.1 Localisation of rs7692387 and SNPs in linkage disequilibrium

The human CAD lead SNP rs7692387 is located within the ninth intron of the *GUCY1A3* gene (NC_000004.12 Reference GRCh38.p7 Primary Assembly) on chromosome 4 (Figure 20). Using SNP Annotation and Proxy Search (Johnson *et al.* 2008) we assessed properties of all variants in high linkage disequilibrium (LD; $R^2 \geq 0.8$) with the lead SNP variant based on UCSC Genome Browser annotations (Speir *et al.* 2016) (Table 51). Like rs7692387 none of these variants was located in the coding region of *GUCY1A3*. Of them, rs7692387 was the only variant pointing to regulatory relevance by being located within a DNase I hypersensitivity site (chr4:156635141-156635310 (Hg19)) (Boyle *et al.* 2008) (Figure 20).

Table 51 Proxy SNPs for rs7692387 ($R^2 \geq 0.8$). Prediction was done using SNP Annotation and Proxy Search (Johnson *et al.* 2008). Supplemental Table 1 from Kessler/Wobst *et al.* Functional Characterization of the *GUCY1A3* Coronary Artery Disease Risk Locus. *Circulation* 2017. 136(5):476-489 (Kessler *et al.* 2017).

Proxy SNP	Distance (bp)	R^2	D'
rs3796587	2764	1.000	1.000
rs2306556	3264	1.000	1.000
rs3796581	7575	1.000	1.000
rs10517620	41249	0.950	1.000
rs3796592	3964	0.861	1.000

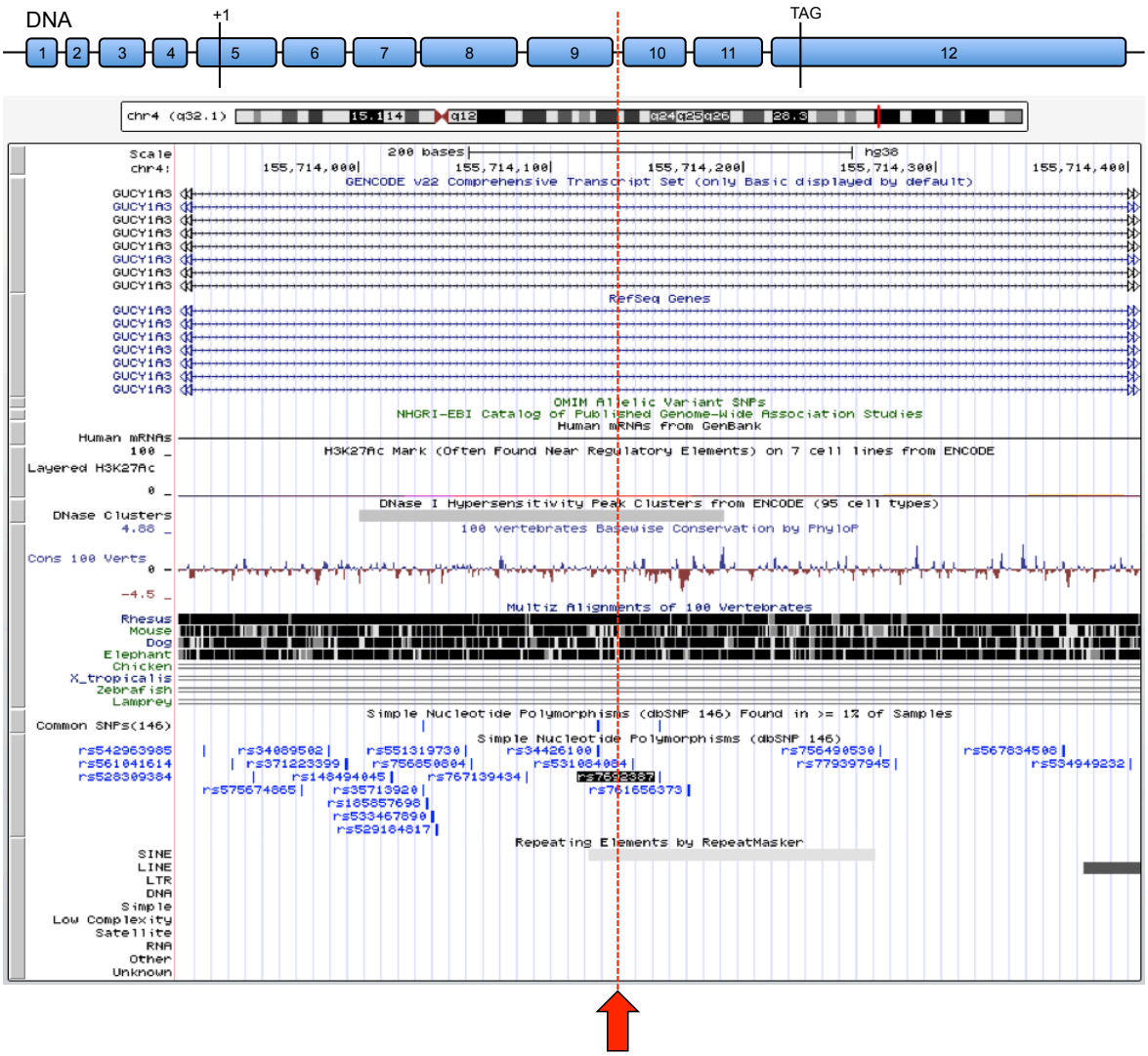

Figure 20 Localisation of the *GUCY1A3* lead SNP rs7692387. According to ENCODE annotation data (Rosenbloom *et al.* 2013, Rosenbloom *et al.* 2015) from the UCSC Genome Browser (*http://genome.ucsc.edu*) (Kent *et al.* 2002, Speir *et al.* 2016), the *GUCY1A3* lead SNP (rs7692387; black) is located within a DNase I hypersensitivity site (chr4: 156,635,141-156,635,310 (Hg19)) in fibroblasts.

4.2.1.2 Putative allele-specific transcription factors

We screened *in silico* for putative transcription factor binding sites affected by rs7692387 using the online tool *AliBaba2.1 (http://www.gene-regulation.com/pub/programs/alibaba2/index.html)* (Grabe 2002). In addition to the rather unspecific C/EBP transcription factor family, IRF8 was predicted to differentially bind to the risk allele G whereas ZEB1 was predicted to differentially bind to the non-risk allele A of the lead SNP rs7692387 (Figure 21).

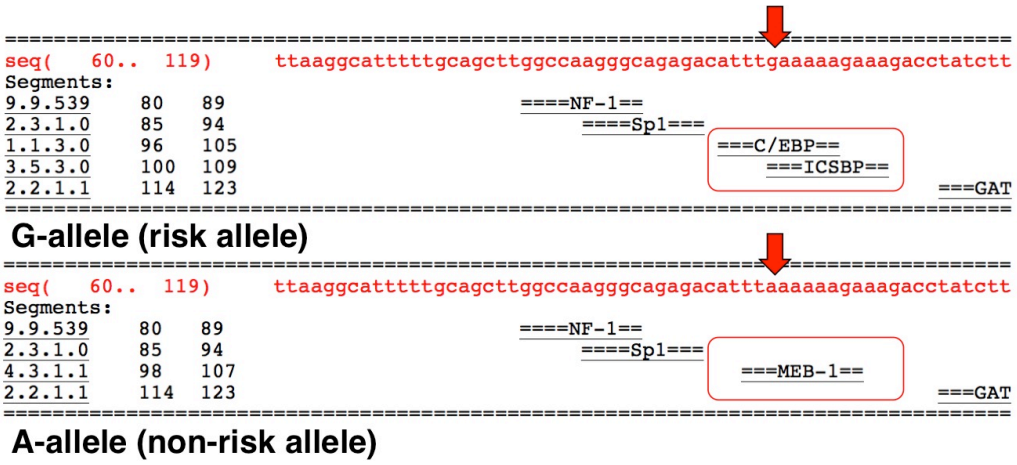

Figure 21 Results of *in silico* transcription factor binding prediction using the online tool *AliBaba2.1*. The transcription factor prediction tool (*http://www.gene-regulation.com/pub/programs/alibaba2/index.html*) (Grabe 2002) revealed two factors binding to the risk allele G of the lead SNP rs7692387, namely C/EBP and ICSBP (better known as IRF8). Concerning binding to the non-risk allele A only one candidate, MEB-1, also termed as ZEB1, was predicted.

We then looked up the expression of the transcription factors IRF8 and ZEB1 in relevant tissues in the Stockholm Atherosclerosis Gene Expression (STAGE) study data. Both of them were found to be expressed in whole blood, internal mammary artery and atherosclerotic arterial wall, i.e., tissues relevant for sGC function (Hagg *et al.* 2009) (Table 52). C/EBP was not investigated further as it is found to be ubiquitously expressed playing a role in many processes. Furthermore, there are at least six isoforms which are encoded by six different genes located on different chromosomes (Ramji and Foka 2002).

Table 52 Characteristics of putative allele-specific transcription factors. Listing of expression in relevant tissues of transcription factors IRF8 and ZEB1. Table from Kessler/Wobst *et al.* Functional Characterization of the *GUCY1A3* Coronary Artery Disease Risk Locus. *Circulation* 2017. 136(5):476-489 (Kessler *et al.* 2017).

Transcription factor	**Predicted allele**		**Expression in relevant tissue***
	A-allele	G-allele	
IRF8	-	+	WB/IMA/AAW
ZEB1	+	-	WB/IMA/AAW

*expression according to STAGE study (Hagg *et al.* 2009) data. *WB:* whole blood; *IMA:* internal mammary artery; *AAW:* atherosclerotic arterial wall; *STAGE:* Stockholm Atherosclerosis Gene Expression.

We further investigated the expression of *IRF8* and *ZEB1* in different cell lines *in vitro*. *ZEB1* was abundantly expressed in human endothelial cells (EC), human vascular smooth muscle cells (VSMC), human megakaryoblastic leukemia cells (Meg-01) and human embryonic kidney (HEK) 293 cells. By contrast, *IRF8* was not found to be expressed in VSMC and Meg-01. Due to the lack of *IRF8* expression in the two most important cell types of the ones investigated with regard to CAD and MI, namely VSMC and Meg-01, we focused on the influence of only ZEB1 for subsequent experiments.

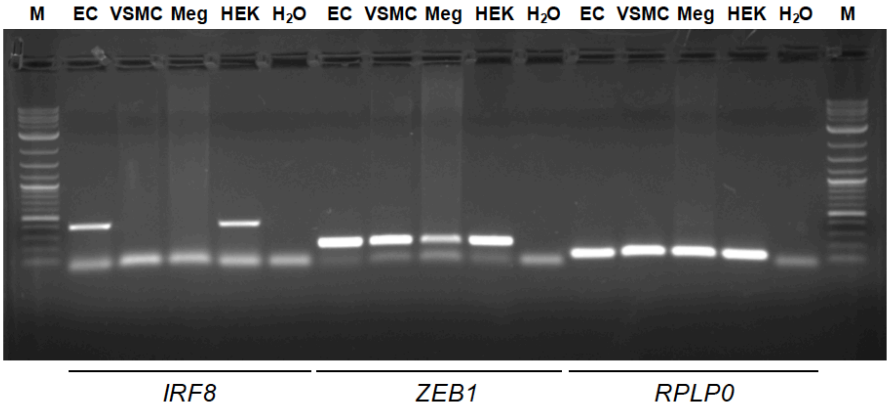

Figure 22 Detection of *IRF8* and *ZEB1* in human cell lines. ZEB1 predicted to bind to the non-risk A allele of the lead SNP rs7692387 is highly abundant on mRNA level in all four investigated cell lines, whereas IRF8 predicted to bind to the non-risk allele G was not detectable in VSMC and Meg-01. *EC:* human coronary artery endothelial cells; *VSMC:* human vascular smooth muscle cells; *Meg:* human megakaryoblastic leukemia cells Meg-01; *HEK 293:* human embryonic kidney 293 cells; *H_2O:* water control; *RPLP0:* ribosomal protein lateral stalk subunit P0, served as housekeeping gene; *M:* marker, size standard. Supplemental Figure 3 from Kessler/Wobst *et al.* Functional Characterization of the *GUCY1A3* Coronary Artery Disease Risk Locus. *Circulation* 2017. 136(5):476-489 (Kessler *et al.* 2017).

A further hint for rs7692387 playing a putative regulatory role was given by publicly available genome-wide chromatin immunoprecipitation (ChIP) sequencing data generated on liver hepatocellular carcinoma (HepG) cells (Boyle *et al.* 2008). They revealed binding of the transcription factor ZEB1 within the *GUCY1A3* intronic region directly adjacent to rs7692387 (Figure 23).

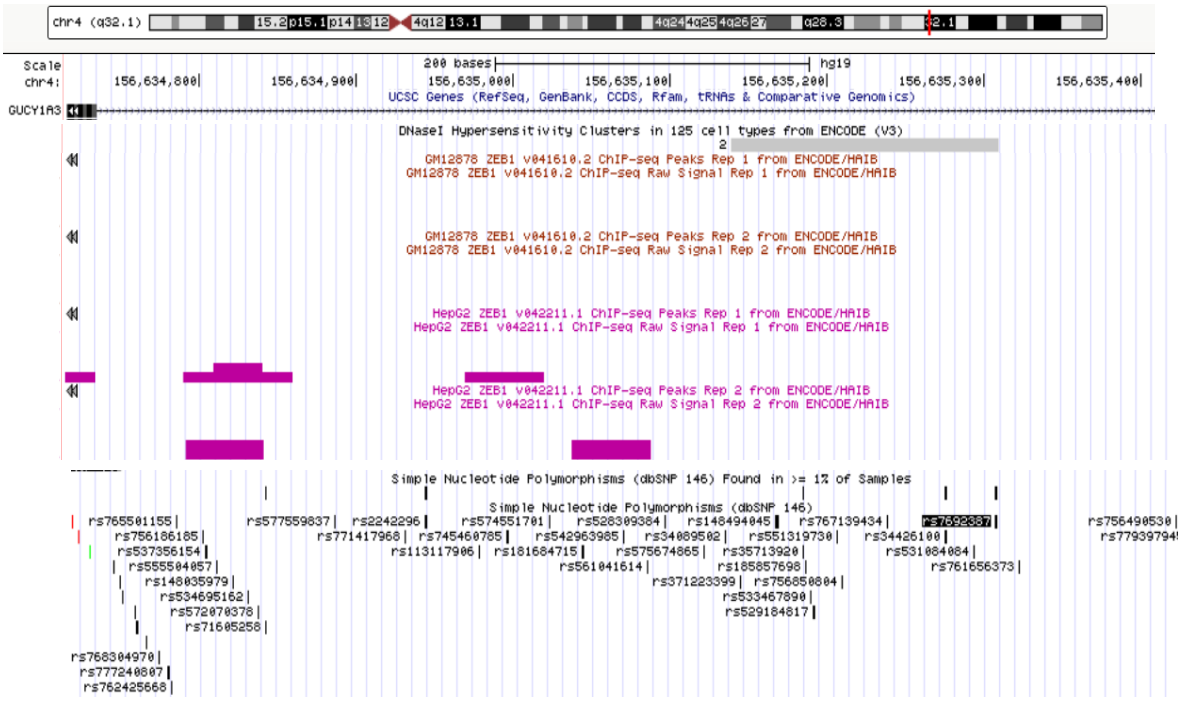

Figure 23 Binding of ZEB1 to the *GUCY1A3* lead SNP (rs7692387) region According to ENCODE chromatin immunoprecipitation data (Rosenbloom *et al.* 2013, Rosenbloom *et al.* 2015) generated on liver hepatocellular carcinoma cells (HepG) from the UCSC Genome Browser (*http://genome.ucsc.edu*) (Kent *et al.* 2002, Speir *et al.*

2016), ZEB1 binds to the *GUCY1A3* lead SNP (rs7692387; black) region in hepatoblasts. Part of Supplemental Figure 4 from Kessler/Wobst *et al.* Functional Characterization of the *GUCY1A3* Coronary Artery Disease Risk Locus. *Circulation* 2017. 136(5):476-489 (Kessler *et al.* 2017).

4.2.2 Regulatory properties of the lead SNP region

4.2.2.1 Genotype-dependent reporter gene expression

To test whether the lead SNP region plays a role in regulation of the *GUCY1A3* gene, we performed reporter gene assays with constructs carrying a 559 bp long nucleotide sequence flanking the non-risk (A) and risk (G) allele variants cloned upstream of the *luc2* gene in the promoterless luciferase pGL4.10[*luc2*] vector (Figure 24A). Results revealed the risk allele G displaying a 50 % reduction of luciferase activity compared to the non-risk allele A (p=0.018; Figure 24B).

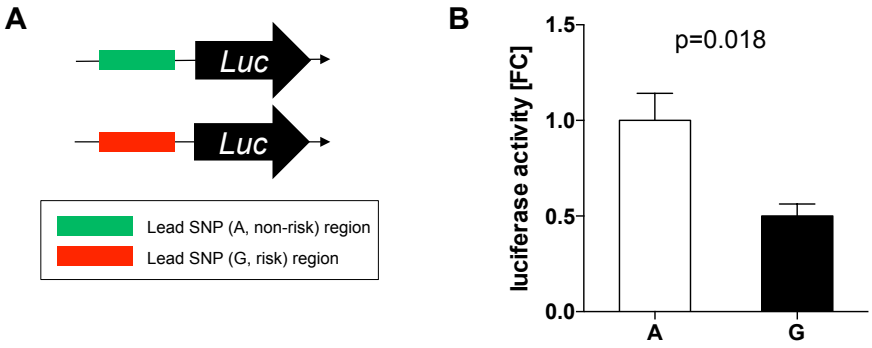

Figure 24 Regulatory properties of region flanking *GUCY1A3* lead SNP rs7692387. (A) Within the luciferase plasmid pGL4.10[*luc2*] a 559 bp long region either flanking the non-risk allele A or the risk allele G was cloned upstream of the *luc2* gene. (B) Compared with the A allele, the risk-carrying G allele in rs7692387 was associated with almost 50 % lower transcriptional activity of the *luc2* gene. Data are mean ± SEM of four independent experiments with every variant transfected in triplicates each. Samples were analysed 24 h post transfection. Statistical analysis was done with Student's unpaired t test.

To further confirm these results we performed additional luciferase assays in collaboration with Frank Kaiser (Institute of Human Genetics, UKSH Lübeck, Germany). Three different constructs were used with all of them containing the *GUCY1A3* promoter (2,578 bp; chr4:155,666,380-155,668,957 (GRCh38/hg38)) upstream of the *luc2* gene. Two of the constructs additionally carried a 407 bp fragment flanking the lead SNP (rs7692387; chr4:155,713,878-155,714,284 (GRCh38/hg38)) downstream of the *luc2* gene (Figure 25A).

Comparing the three constructs, the *GUCY1A3* non-risk allele construct (P+A) led to a 25 % increase of luciferase activity (p=0.0001) whereas the risk allele construct (P+G) displayed a 20 % reduction of luciferase activity compared to the construct carrying the promoter only (P; p=0.0005). Comparing P+A with P+G, the risk-allele constructs displayed a 44 % reduction of luciferase activity (p<0.0001; Figure 25).

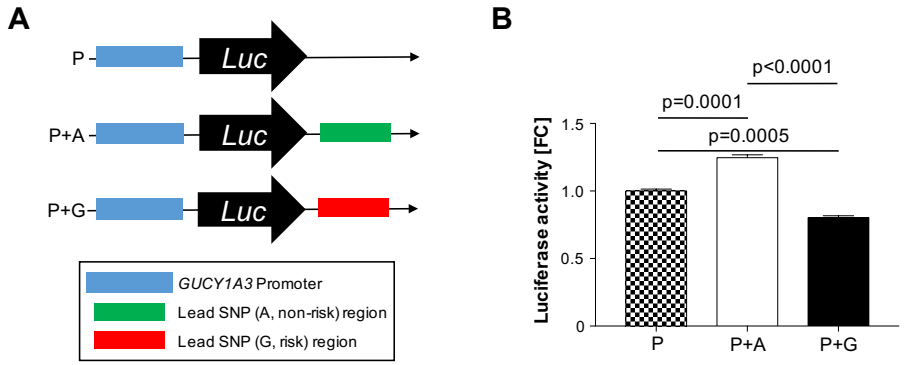

Figure 25 Enhancer properties of the *GUCY1A3* lead SNP region. (A) Into the luciferase plasmid pGL4.10[*luc2*] carrying the *GUCY1A3* promoter upstream of the *luc2* gene a 407 bp long region either flanking the non-risk allele A (P+A) or the risk allele G (P+G) was cloned downstream of the *luc2* gene. (B) The P+A construct led to significantly increased luciferase activity as compared to the construct carrying the promoter only (P). In contrast, the P+G construct led to significant decrease of luciferase activity as compared to P and to P+A. Data are mean ± SEM of three independent experiments. Samples were analysed 48 h after transfection. Statistical analysis was done with Ordinary one-way ANOVA with Tukey's multiple comparisons test. Part of Figure 1 from Kessler/Wobst *et al.* Functional Characterization of the *GUCY1A3* Coronary Artery Disease Risk Locus. *Circulation* 2017. 136(5):476-489 (Kessler *et al.* 2017). The experiment was performed by our collaboration partner Frank Kaiser (Institute of Human Genetics, UKSH Lübeck, Germany).

4.2.2.2 Influence of *ZEB1* knockdown on reporter gene expression

As we concluded from the *in silico* transcription factor binding prediction that the transcriptional modulator ZEB1 should rather bind to the A than to the G allele we aimed to test the influence of ZEB1 on reporter gene expression. We hypothesised that upon knockdown of *ZEB1* A allele-mediated luciferase activity should decrease.

For that, we first conducted a preliminary experiment in order to determine one out of three siRNAs leading to the most effective knockdown of *ZEB1* in HEK 293 cells 24 to 72 h after transfection. As depicted in Figure 26A all three tested siRNAs resulted in a decrease of *ZEB1* mRNA of approximately 45 %. As siRNA #3 (Catalogue# 229972) significantly decreased *ZEB1* mRNA levels at all three time points tested it was chosen for further experiments. The efficiency of the *ZEB1* knockdown by *ZEB1* siRNA #3 was also verified in VSMC 24, 48 and 72 h post transfection. Like in HEK 293 cells *ZEB1* siRNA also led to a significant decrease of *ZEB1* mRNA in VSMC at all three tested time points (Figure 26B).

The knockdown was further confirmed on protein level in cell lysates of both HEK 293 and VSMC harvested 72 h after transfection (Figure 26C-F).

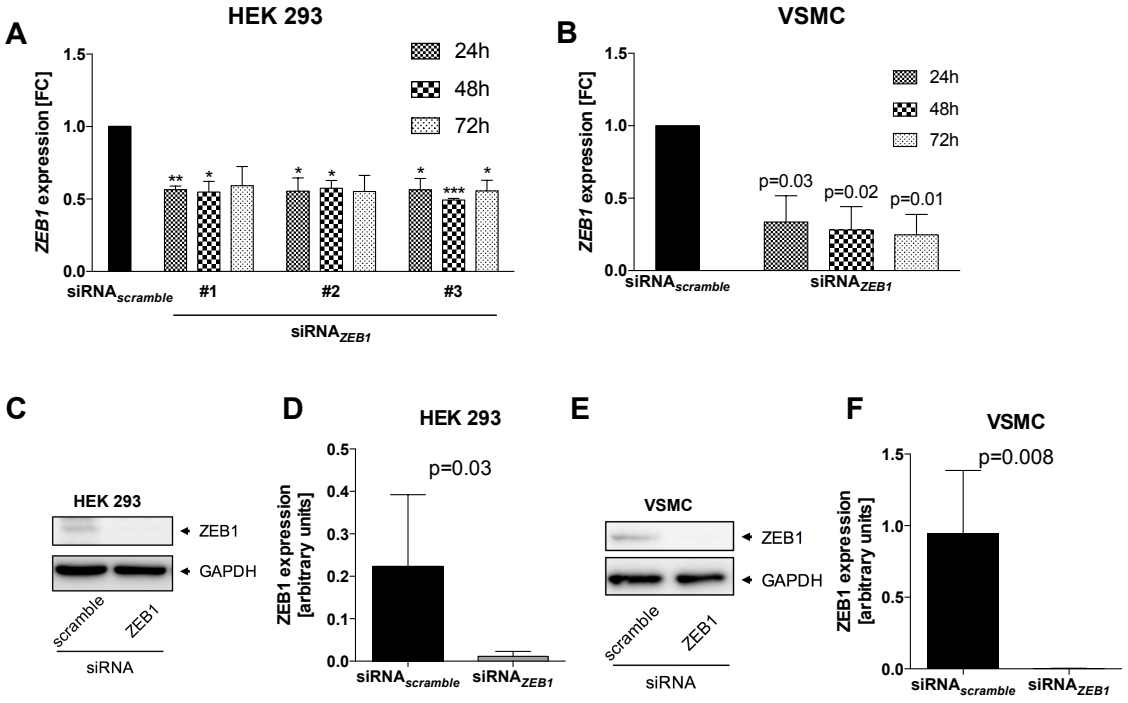

Figure 26 Knockdown of *ZEB1* on mRNA and protein levels in HEK 293 cells and VSMC. (A) Three different siRNAs for the knockdown of *ZEB1* were tested in HEK 293 cells over time ranging from 24 to 72 h post transfection. siRNA #3 was chosen for subsequent experiments as it significantly reduced *ZEB1* mRNA at all three time points tested. (B) Efficacy of siRNA #3 was further verified in VSMC. Knockdown of *ZEB1* 72 h post transfection on protein level was shown in HEK 293 cells (C, D) and in VSMC (E, F). Data are mean ± SEM of three (A) and four (B) independent experiments or median with interquartile range of four (D) and five (F) independent experiments. Statistical significance was assessed by One-sample t test (A and B) or Mann-Whitney test (D and F). *: p<0.05; **: p<0.01; ***: p<0.001. Supplemental Figure 6 (B) and part of Figure 2 (C and E) from Kessler/Wobst *et al.* Functional Characterization of the *GUCY1A3* Coronary Artery Disease Risk Locus. *Circulation* 2017. 136(5):476-489 (Kessler *et al.* 2017).

The effect of ZEB1 on reporter gene expression was then tested using the different types of constructs.

Constructs with lead SNP region only: Knockdown of *ZEB1* led to a 21 % reduction in luciferase expression of the non-risk variant A (p<0.01; Figure 27A) while no significant effect was detectable for the risk variant G (p=0.25; Figure 27B).

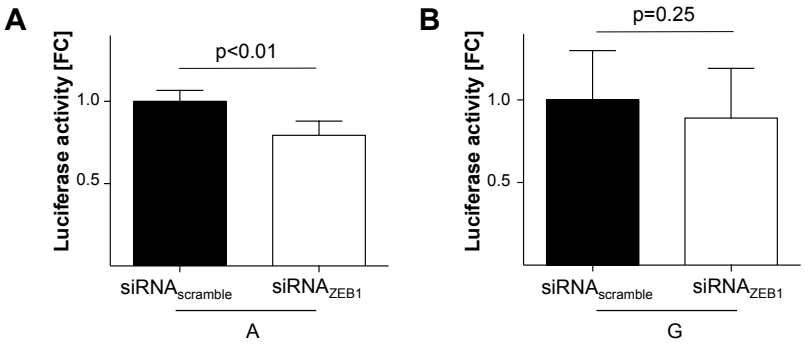

Figure 27 Influence of ZEB1 on luciferase activity from plasmids carrying the lead SNP region only. Only in case of the non-risk allele A an effect was detectable (A) while no difference in luciferase activity was detectable after *ZEB1* knockdown in case of the risk allele G (B). Data are mean ± SEM of five independent experiments with every construct transfected in triplicates. Measurements were done 24 h after transfection with siRNA. Statistical significance was calculated by Student's paired t test.

Constructs with lead SNP region plus GUCY1A3 promoter: Results of *ZEB1* knockdown revealed a significant reduction in luciferase activity rather for the non-risk allele (P+A) construct (15 %; p<0.01; Figure 28A) than for the risk allele (P+G) construct (8 %; p=0.05; Figure 28B). In contrast, overexpression of *ZEB1* resulted in an increase of *GUCY1A3* promoter activity for both reporter plasmids. This gain in reporter gene expression was more prominent for the construct containing the regulatory element with the non-risk allele (P+A; Figure 28C) compared with the risk allele (P+G; Figure 28D).

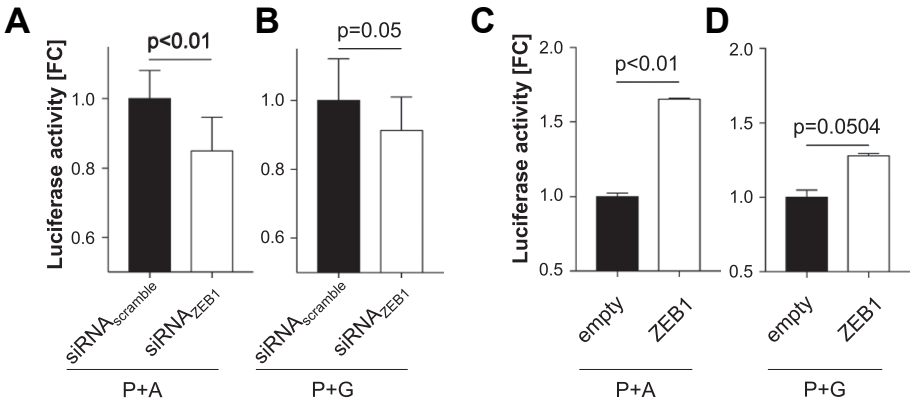

Figure 28 Influence of ZEB1 on luciferase activity from plasmids carrying the *GUCY1A3* promoter in addition to the lead SNP region. siRNA-mediated knockdown of *ZEB1* significantly decreased luciferase activity rather in the non-risk allele A construct (P+A) (A) than in the risk allele G construct (P+G) (B). Overexpression of *ZEB1* (100 ng plasmid) led to an increase of luciferase activity for both reporter plasmids (C, D) which was more prominent for the non-risk allele (P+A) (C). Data are mean ± SEM of nine (A,B) or three (C,D) independent experiments. Measurements were done 48 h after transfection. Statistical significance was assessed by Student's paired t test. Part of Figure 2 from Kessler/Wobst *et al.* Functional Characterization of the *GUCY1A3* Coronary Artery Disease Risk Locus. *Circulation* 2017. 136(5):476-489 (Kessler *et al.* 2017). The overexpression was done by transfection of HEK 293 cells with full length *ZEB1* cloned into 3xFLAG® (100 ng plasmid) and performed by our collaboration partner Frank Kaiser (Institute of Human Genetics, UKSH Lübeck, Germany).

To investigate whether ZEB1-mediated alterations of reporter gene expression are dosage-dependent, we compared the results from the overexpression with knockdown of *ZEB1* with different siRNA concentrations in combination with the luciferase plasmids carrying the *GUCY1A3* promoter plus the lead SNP region.

Increased levels of ZEB1 correlated with increased luciferase activity for both constructs (Figure 29). The effect was more pronounced for the non-risk allele construct (Figure 29B).

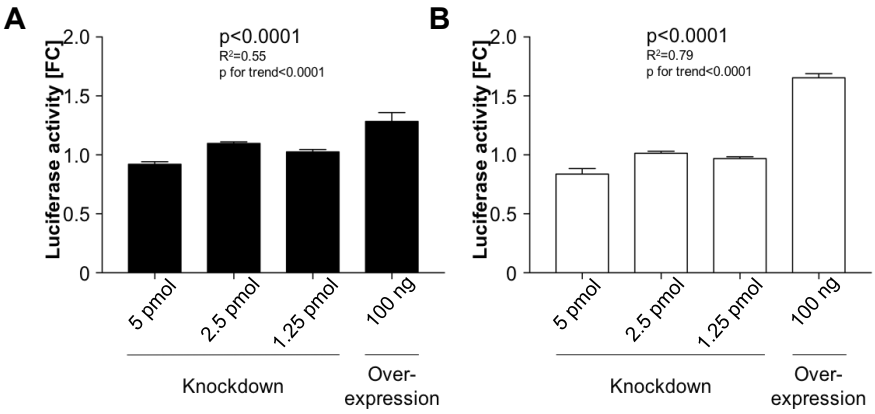

Figure 29 Correlation of ZEB1 dosage and luciferase activity for the *GUCY1A3* risk (rs7692387, P+G) (A) and non-risk (P+A) allele (B) constructs. Luciferase activity after knockdown of *ZEB1* (using doses of 1.25-5 pmol $siRNA_{ZEB1}$) or overexpression of *ZEB1* (100 ng plasmid) was normalised to $siRNA_{scramble}$ or empty vector transfection, respectively. Increasing doses of ZEB1 led to significant increases in both the P+G (A, risk allele) and P+A (B, non-risk allele) constructs. The relationship tends to be weaker in the risk allele construct than in the non-risk allele construct (R^2=0.55 vs. R^2=0.79). Data are mean ± SEM of nine (knockdown) and three independent experiments (overexpression), respectively. Measurements were done 48 h after transfection. Calculations were performed using Ordinary one-way ANOVA with post test for linear trend. Supplemental Figure 7 from Kessler/Wobst *et al.* Functional Characterization of the *GUCY1A3* Coronary Artery Disease Risk Locus. *Circulation* 2017. 136(5):476-489 (Kessler *et al.* 2017).

4.2.3 Investigation of the ZEB1 binding site

As outlined in Section 4.2.1, *in silico* analyses predicted binding of ZEB1 within the regulatory region whose binding affinity might be directly correlated with rs7692387 genotype. Publicly available ChIP sequencing data (Figure 23) already indicated binding of ZEB1 adjacent to the *GUCY1A3* lead SNP region. In order to confirm binding, we performed electrophoretic mobility shift assays (EMSA) with nuclear protein extracted from untransfected HEK 293 cells and oligonucleotides with a ZEB1 consensus sequence E-box 1 (E1) (Wellner *et al.* 2009) and the lead SNP region, respectively.

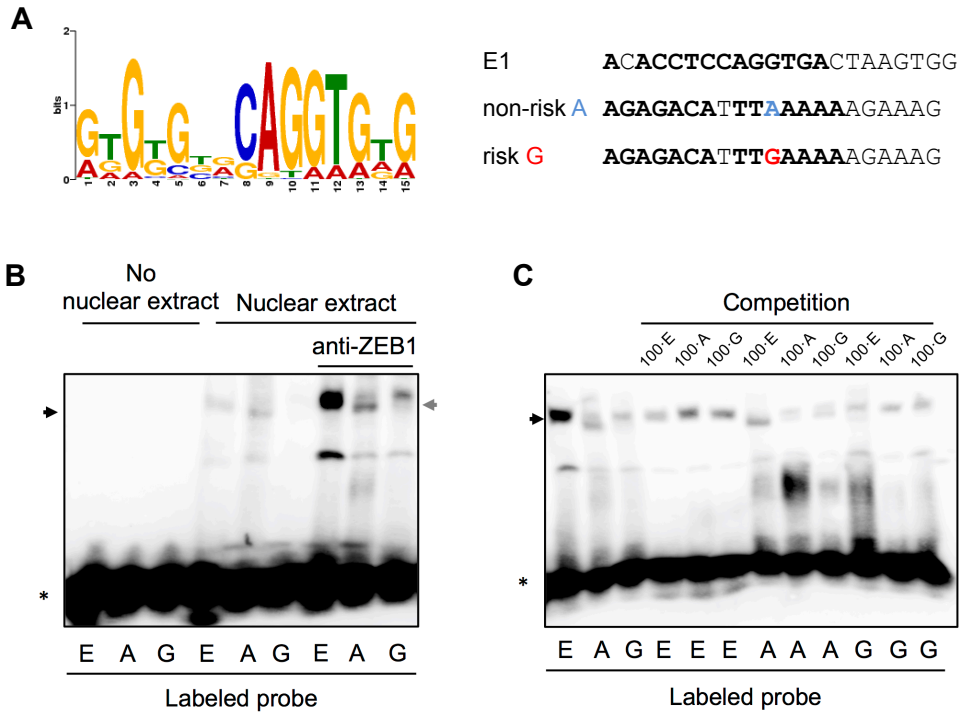

Figure 30 ZEB1 binds to the *GUCY1A3* lead SNP region. (A) Consensus sequence of ZEB1 determined by ChIP sequencing by the HudsonAlpha Lab (Wang *et al.* 2012) and oligonucleotide sequences used for electrophoretic mobility shift assay (EMSA). Overlaps with the ZEB1 consensus sequence are marked in bold. (B) EMSA with labelled probes matching the ZEB1 consensus binding site (Wellner *et al.* 2009), the rs7692387 non-risk allele A sequence, and the rs7692387 risk allele G sequence (E, A and G). A ZEB1 antibody (C-20X) was used to supershift the protein-DNA complex. Different signal intensities are due to different incubation times with and without antibody. (C) Competition assays were performed with 100-fold excess of unlabelled probe (100·E, 100·A, 100·G). EMSA indicated preferential binding of ZEB1 to the non-risk allele variant A probes as compared to G probes. The black arrows indicates the ZEB1 complex. The grey arrow indicates supershift of the ZEB1 complex after addition of the anti-ZEB1-antibody. * denotes unbound labelled probe.

ZEB1 led to a shift with all three labelled probes confirming binding to the lead SNP region whereas no shift was observable when no nuclear extract was added (Figure 30B). The most intense band was detectable for the ZEB1 consensus sequence E1. Competition assays by adding unlabelled probes in a 100-fold excess confirmed the specificity of ZEB1 binding (Figure 30C). Additional supplementation with a ZEB1 antibody supershifted the protein-DNA complexes (Figure 30B).

4.2.4 Impact of ZEB1 on endogenous gene expression

4.2.4.1 Influence of *ZEB1* knockdown on *GUCY1A3* mRNA levels

To further confirm the observations on decreased gene expression upon knockdown of *ZEB1*, we investigated endogenous *GUCY1A3* mRNA levels in HEK 293 cells and VSMC

24, 48 and 74 h after transfection of *ZEB1* siRNA. Results of genotype analysis revealed HEK 293 cells being homozygous for the non-risk variant (AA genotype) and VSMC heterozygous for rs7692387 (AG genotype) (Figure 31). In HEK 293 cells silencing of *ZEB1* led to a significant decrease of *GUCY1A3* mRNA levels at all three time points tested with the strongest decrease of 25 % after 72 h ($p<0.01$; Figure 32A). In VSMC knockdown of *ZEB1* led to a significant reduction in *GUCY1A3* expression after 72 h (16 %; $p<0.01$; Figure 32B).

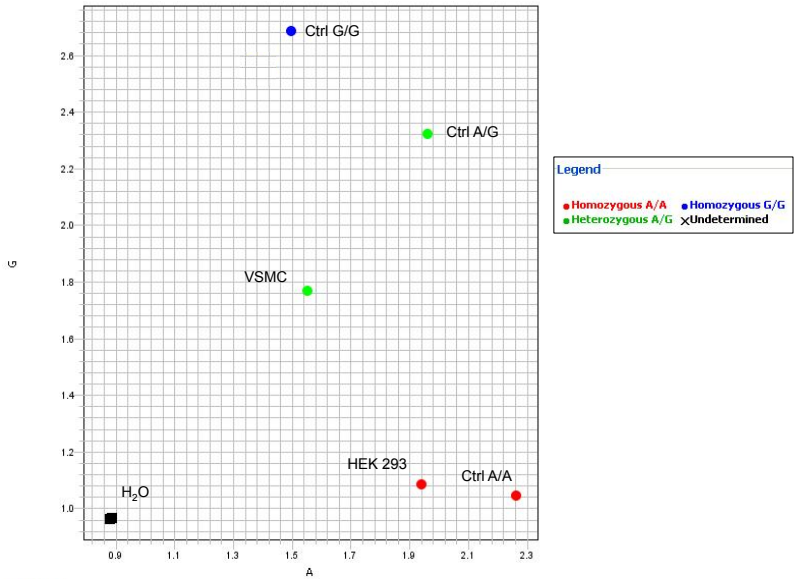

Figure 31 Allelic discrimination plot for SNP rs7692387. The genotyping revealed our investigated HEK 293 cells being homozygous for the non-risk allele A at rs7692387 whereas our used VSMC are heterozygous at that locus. *H_2O:* water control; *Ctrl:* DNA control of known genotype.

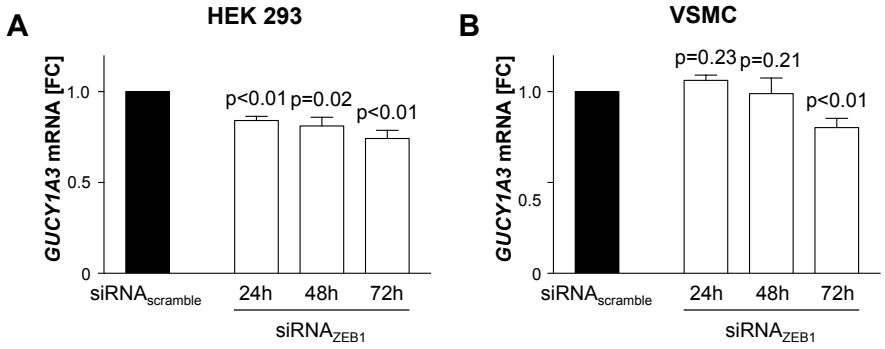

Figure 32 Changes of endogenous *GUCY1A3* mRNA levels in HEK 293 cells and VSMC after knockdown of *ZEB1*. Endogenous *GUCY1A3* mRNA levels were significantly decreased in HEK 293 cells after *ZEB1* knockdown at all three time points tested (A). In VSMC endogenous *GUCY1A3* mRNA levels were significantly reduced 72 h after transfection with *ZEB1* siRNA (B). Data are mean ± SEM of five (A) and four (B) independent experiments, respectively. Statistical significance was calculated by use of One-sample t test. Part of Figure 2 from Kessler/Wobst *et al.* Functional Characterization of the *GUCY1A3* Coronary Artery Disease Risk Locus. *Circulation* 2017. 136(5):476-489 (Kessler *et al.* 2017).

4.2.4.2 Influence of *ZEB1* knockdown on *GUCY1B3* mRNA levels

As sGC acts as a homodimer composed of α_1 and β_1 subunits we aimed to test if silencing of *ZEB1* – besides influencing *GUCY1A3* expression – also influences *GUCY1B3* expression. *GUCY1B3* mRNA levels were significantly decreased after 24 h of transfection ($p<0.01$; Figure 33).

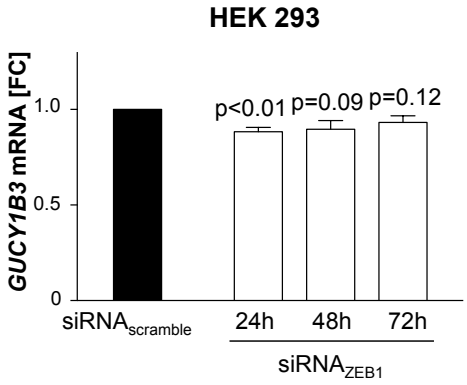

Figure 33 *GUCY1B3* mRNA levels in HEK 293 cells after knockdown of *ZEB1*. Endogenous *GUCY1B3* mRNA levels were significantly decreased in HEK 293 cells after *ZEB1* knockdown after 24 h only. Data are mean ± SEM of three independent experiments. Statistical significance was calculated by use of One-sample t test.

4.2.5 Cellular phenotype

4.2.5.1 *GUCY1A3* expression in VSMC and platelets

We investigated endogenous *GUCY1A3* mRNA levels in vascular smooth muscle cell lines which were part of the Systems Genetics Resource at the University of California, Los Angeles (van Nas *et al.* 2013) (*https://systems.genetics.ucla.edu/*). The cell line homozygous for the risk allele displayed significantly decreased *GUCY1A3* mRNA levels compared to cell line derived from the homozygous non-risk allele carrier ($p=0.03$; Figure 34).

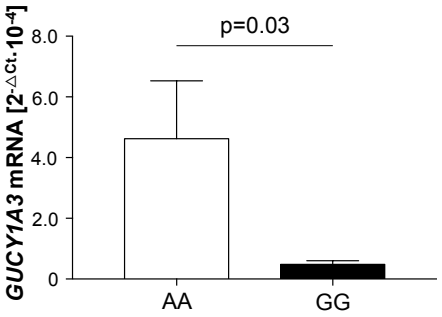

Figure 34 Endogenous *GUCY1A3* mRNA levels in VSMC homozygous for the non-risk and risk allele of rs7692387. Comparing AA and GG VSMC the cell line being homozygous for the non-risk allele A exhibited significantly higher *GUCY1A3* mRNA levels than the cell line being homozygous for the non-risk allele G. Data are mean ± SEM of four independent experiments (passage 4-8). Statistical significance was calculated from ΔC_t values by use of Student's unpaired t test. Part of Figure 3 from Kessler/Wobst *et al.* Functional Characterization of the *GUCY1A3* Coronary Artery Disease Risk Locus. *Circulation* 2017. 136(5):476-489 (Kessler *et al.* 2017).

We furthermore tried to investigate *GUCY1A3* mRNA levels in platelets. We were not able to detect *GUCY1A3* mRNA in platelets isolated from whole blood (data not shown). Nevertheless, we could show in leucocyte-depleted platelet concentrate that platelets contain *GUCY1A3* mRNA (Figure 35).

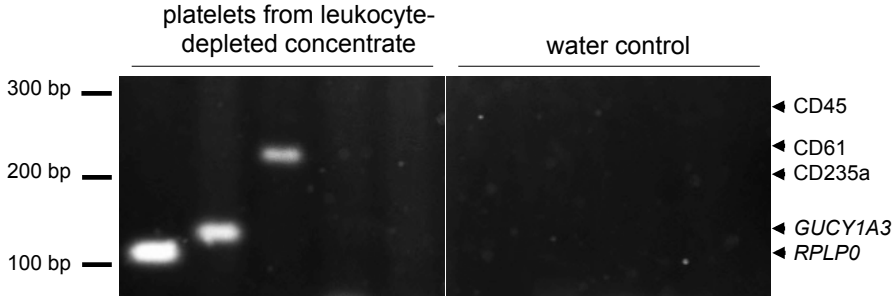

Figure 35 *GUCY1A3* mRNA was detectable in platelets from leukocyte-depleted concentrate. Whereas bands could be observed for *GUCY1A3*, the housekeeping gene *RPLP0* as well as the platelet marker CD61 (*ITGB3*), no bands were detected for the erythrocyte marker CD235a (*GYPA*) as well as the leukocyte marker CD45 (*PTPRC*). *RPLP0:* ribosomal protein lateral stalk subunit P0; *GYPA:* glycophorin A; *ITGB3:* integrin subunit beta 3; *PTPRC:* protein tyrosine receptor phosphatase C.

We then chose to investigate platelets for sGC α_1 protein levels. As part of a study conducted by Bernhard Wolf (Institute for Cardiovascular Diseases, German Heart Centre Munich, Germany), platelet rich plasma from a total of 22 probands (8=AA; 14=GG) was collected in order to test the effect of the NO donor sodium nitroprusside (SNP) with and without the addition of the PDE5 inhibitor sildenafil. Appendix Table 1 provides information on the baseline characteristics of the probands investigated. Except for a slight difference in platelet count AA and GG genotype carriers did not differ. For the present study these

platelets were investigated for sGC α_1 protein amount by Western blotting. Homozygous risk allele carriers thereby displayed significantly reduced sGC α_1 protein levels as compared to homozygous non-risk allele carriers ($p<0.001$; Figure 36). Plotting sGC α_1 protein levels against platelet aggregation revealed an inverse relationship: increased sGC α_1 expression was accompanied by reduced platelet aggregation ($p<0.01$; $R^2=0.29$).

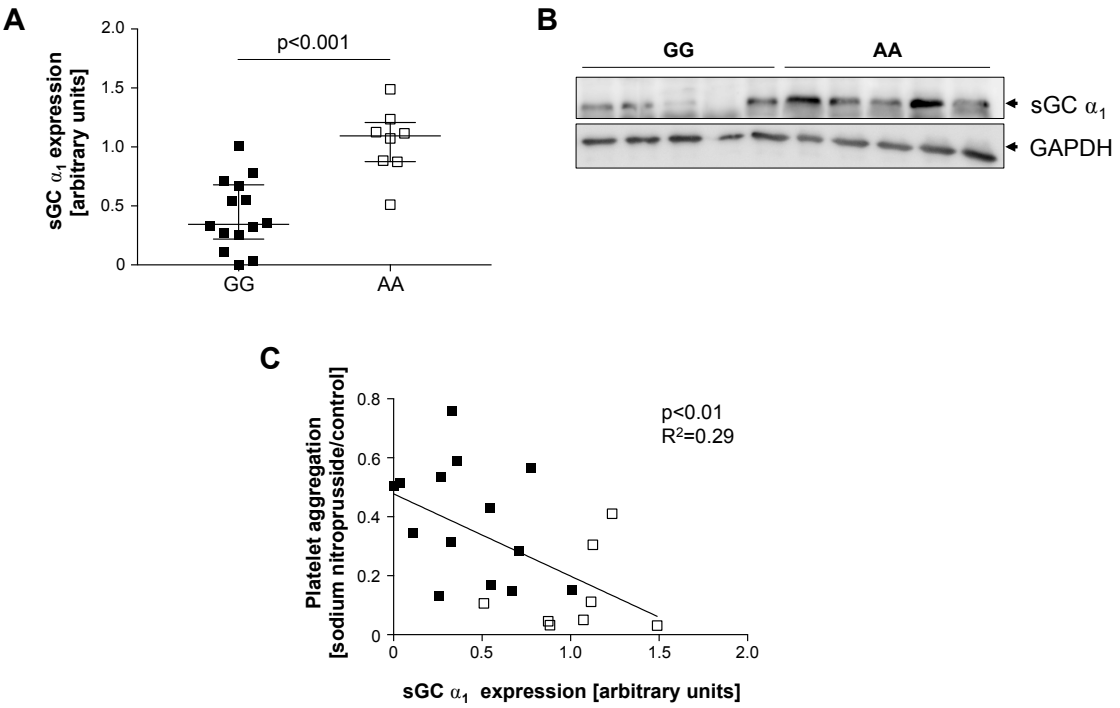

Figure 36 sGC α_1 expression in human platelets. *GUCY1A3* genotype influences expression of sGC α_1 subunit in platelets as the expression was significantly higher in homozygous non-risk allele carriers (n=8) compared to homozygous risk allele carriers (n=14; $p<0.001$) (A). Representative Western blot showing sGC α_1 levels and GAPDH as loading control (B). sGC α_1 expression and platelet aggregation displayed an inverse relationship, i.e., increased sGC α_1 expression was accompanied by reduced platelet aggregation (C). Data are median with interquartile range. Statistical significance was assessed by use of Mann-Whitney test (A), correlation by linear regression (C), respectively. (A) and (B) are from Figure 4 from Kessler/Wobst *et al.* Functional Characterization of the *GUCY1A3* Coronary Artery Disease Risk Locus. *Circulation* 2017. 136(5):476-489 (Kessler *et al.* 2017).

4.2.5.2 Migration of VSMC

To assess whether the rs7692387 genotype influences VSMC migration, we performed scratch wound assays in cell lines from the Systems Genetics Resource at the University of California, Los Angeles (van Nas *et al.* 2013) (*https://systems.genetics.ucla.edu/*), for which *GUCY1A3* mRNA levels had also been assessed (Figure 34). We measured reclosure areas of the scratch wounds under vehicle treatment and compared them to reclosure areas after treatment with the specific sGC

stimulator BAY 41-2272. In the homozygous non-risk allele (AA) donor cell line migration was reduced by 17 % after BAY 41-2272 treatment (p<0.01; Figure 37A, B). In comparison, BAY 41-2272 did not exhibit an effect on the cell line homozygous for the risk allele (GG) (p=0.89; Figure 37C, D).

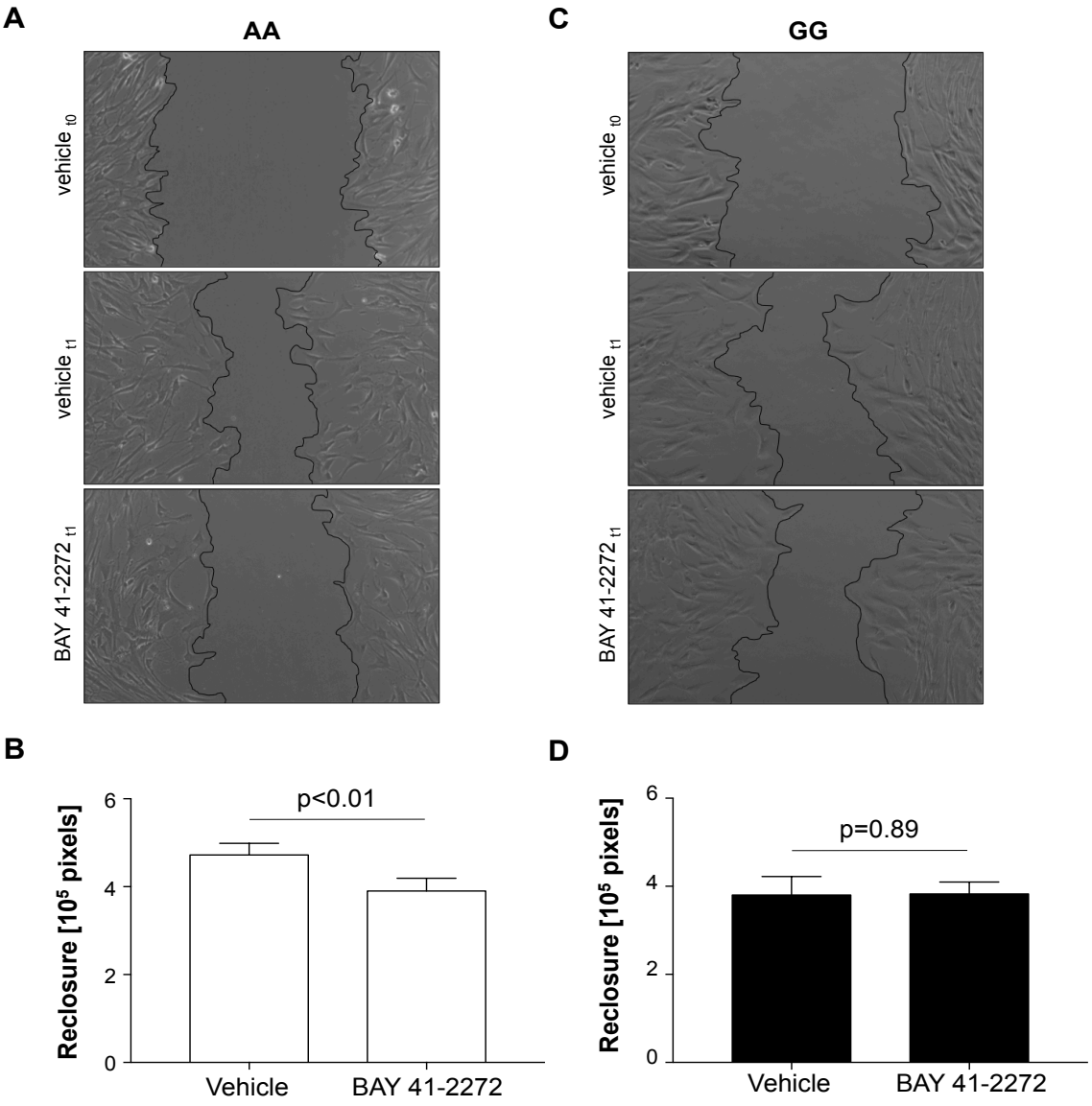

Figure 37 Migration assessment of VSMC after treatment with the sGC stimulator BAY 41-2272. Whereas the sGC stimulator BAY 41-2272 in comparison to treatment with vehicle led to a 17 % decrease in wound reclosure in the cell line homozygous for the non-risk allele A (A-B) no effect of BAY 41-2272 could be observed on the cell line homozygous for the risk allele G (C-D). Data are mean ± SEM from five independent experiments each (passage 4-8) with every sample transfected in triplicates. Statistical significance was assessed by Student's paired t test. Part of Figure 3 from Kessler/Wobst *et al.* Functional Characterization of the *GUCY1A3* Coronary Artery Disease Risk Locus. *Circulation* 2017. 136(5):476-489 (Kessler *et al.* 2017).

Heterozygous cells displayed a phenotype rangeing between homozygous risk allele carriers and homozygous non-risk allele carriers (Figure 38).

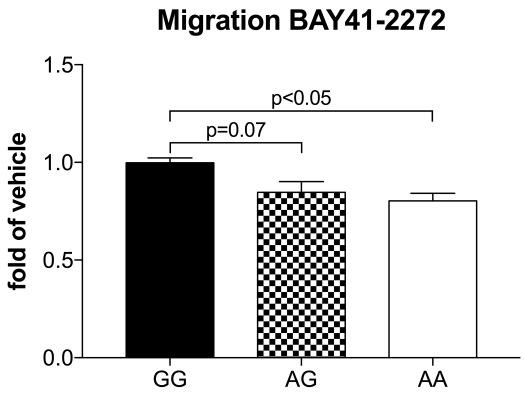

Figure 38 *GUCY1A3* genotype influences response to sGC stimulation by BAY 41-2272 regarding VSMC migration. Inhibition of VSMC migration by BAY 41-2272-mediated sGC stimulation was significantly stronger in VSMC from a homozygous non-risk allele carrier (AA, 19%) compared to VSMC from a homozygous risk allele carrier (GG, <1%). Heterozygous VSMC displayed a trend towards same direction (AG, 15%). Data are mean ± SEM of up to five independent experiments (passage 3-8). Statistic calculations were performed with Ordinary one-way ANOVA ($p<0.05$) followed by Dunnett's multiple comparisons test (vs. GG). Supplement Figure 8 from Kessler/Wobst *et al.* Functional Characterization of the *GUCY1A3* Coronary Artery Disease Risk Locus. *Circulation* 2017. 136(5):476-489 (Kessler *et al.* 2017).

4.2.5.3 VASP phosphorylation in VSMC

As a further readout of cellular phenotype, we analysed cGMP-dependent phosphorylation of vasodilator-stimulated pophosphoprotein (VASP) by Western blotting which is established as an indirect detection of sGC activity. We investigated VASP phosphorylation in VSMC being heterozygous (AG genotype) and homozygous (GG genotype) for the risk allele of rs7692387. For that, we treated the cells either with the sGC stimulator BAY 41-2272 (10 µM), with the NO-donor GSNO (100 µM) or with a combination of both and compared the band intensities to those resulting from treatment with vehicle.

Whereas bands in the cells with AG genotype for BAY 41-2272 and GSNO alone were relatively weak, the addition of BAY 41-2272 to the NO donor GSNO led to significantly enhanced VASP phosphorylation over the control samples ($p<0.05$; Figure 36A, C). In comparison, GG genotype cells did not elicit any phosphorylation of VASP at all independent of the agents used (Figure 36B).

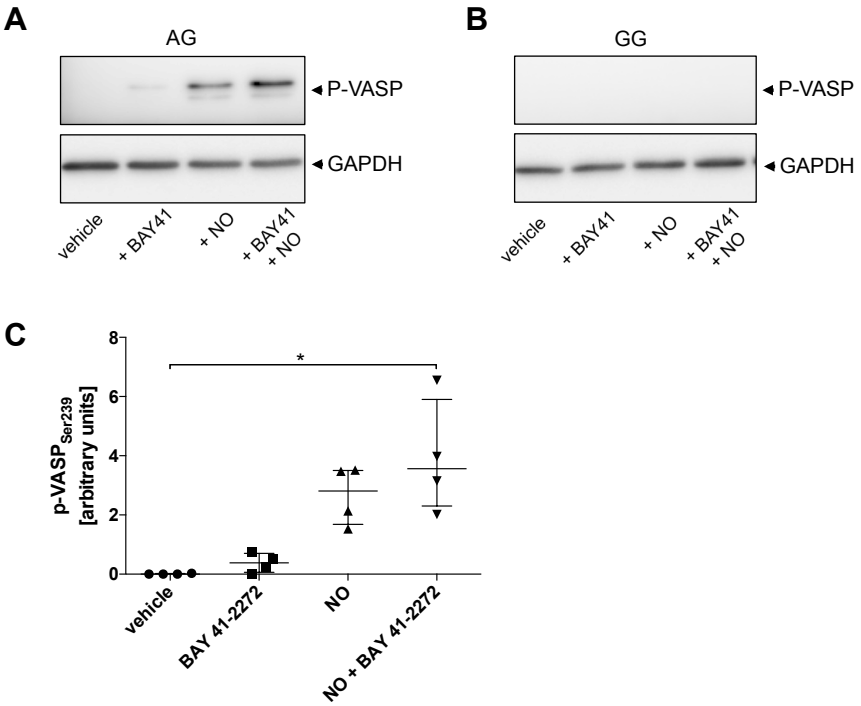

Figure 39 VASP phosphorylation in VSMC upon stimulation with BAY 41-2272 and/or NO. (A) Representative Western blot showing the extent of VASP phosphorylation in lysates from a cell line heterozygous for the risk allele (AG) after stimulation with the sGC stimulator BAY 41-2272 (10 µM) and/or the NO donor GSNO (100 µM). Phosphorylation of VASP increases from left to right with the most intense band for stimulation with the combination of the NO donor and BAY 41-2272. (B) Lysates of a cell line homozygous for the risk allele (GG) do not exhibit any bands for phosphorylated VASP at all. (C) The combination of the NO donor and the sGC stimulator BAY 41-2272 resulted in significantly stronger phosphorylation compared to control in the cell line heterozygous for the risk allele (AG). Data are median with interquartile range of four independent experiments. Statistical analysis was done with Friedman test followed by Dunn's multiple comparisons test. *: $p<0.05$.

5 Discussion

The nitric oxide (NO)/cyclic guanosine-3',5'-monophosphate (cGMP) signalling pathway has been long known to play a key role in the development of cardiovascular disorders. Especially the *GUCY1A3* gene coding for the α_1 subunit of soluble guanylyl cyclase (sGC), which together with the β_1 subunit forms the catalytically active holoenzyme, has been shown to be involved in coronary artery disease (CAD) and myocardial infarction (MI) risk.

Recently, genome-wide association studies identified 56 loci significantly associated with CAD with one of them tagging the *GUCY1A3* gene (Nikpay *et al.* 2015). The *GUCY1A3-GUCY1B3* locus had already previously been shown to be genome-wide significantly associated with blood pressure (International Consortium for Blood Pressure Genome-Wide Association Studies *et al.* 2011), representing a major risk factor for CAD. Furthermore, an extended family was identified suffering from premature CAD and MI (Erdmann *et al.* 2013). Members of this family in which a digenic loss-of-function mutation affecting *GUCY1A3* and *CCT7*, coding for the chaperonin CCTη known to interact with *GUCY1A3*, was found, were affected in 100 % of cases. The genetic situation in this family is, however, unique as this particular coding mutation has not been found in any other patient outside the family. However, several coding *GUCY1A3* mutations have been shown to be enriched in patients suffering from premature CAD and MI (Erdmann *et al.* 2013). Also other diseases like Moyamoya, a rare progressive cerebrovascular disorder, or Achalasia, a disease where the lower esophagus sphincter is not able to close properly, have been linked to dysfunctional sGC due to mutations in the coding sequence of *GUCY1A3* (Hervé *et al.* 2014, Wallace *et al.* 2016).

Todays goal of treating complex diseases including cardiovascular diseases lies in individualised medicine which is driven by new diagnostics and therapeutics (Jameson and Longo 2015). For achieving such a targeted precison medicine the identification of causal variants and their functional effects is indispensable. In this study we sought to functionally investigate the impact of rare and common variants in *GUCY1A3* on CAD. Our results provide fundamental functional evidence for the involvement of sGC in CAD and MI and in case of the rare *GUCY1A3* variants offer first therapeutic treatment approaches for the recovery of cGMP formation.

5.1 Rare coding variants in *GUCY1A3*

A comprehensive search in exome sequencing data from extended families with high prevalence of premature CAD/MI, young MI cases with a positive family history as well as the ESP-EOMI study opened into the identification of a total of nine rare heterozygous missense variants in the coding sequence of *GUCY1A3*: eight newly identified variants in addition to the already investigated and published loss-of-function mutation p.Leu163Phefs*24, leading to a shortened protein by 505 amino acids thereby lacking the catalytic domain (Erdmann *et al.* 2013).

We showed that five out of the eight newly identified rare missense variants in the coding region of *GUCY1A3* led to diminished cGMP levels upon stimulation of the enzyme with an NO donor. Except for the variant p.Gly537Arg which led to a reduced amount of the sGC protein, decreased cGMP amounts could be explained by diminished enzymatic activity itself. Of note, the eight variants investigated are distributed over the entire *GUCY1A3* transcript with five variants, i.e., p.Ser478Gly, p.Gly537Arg, p.Ile571Val, p.Val587Ile, and p.Cys610Tyr being located in the catalytic domain and three variants, i.e., p.Lys53Glu, p.Thr64Ala, and p.Thr229Met, residing within intermediate regions (Figure 10). One could have expected that variants within the catalyitc domain might have a stronger impact on protein function than variants located within other regions. However, variant p.Ser478Gly, for example, located in the catalytic domain did not show any influence at all on the enzyme activity as measured cGMP amounts did not differ from amounts synthesised by wildtype sGC. Also the PolyPhen-2 predicition on damaging impact of the variants on protein function (Table 50) did not completely overlap with our results as variant p.Val587Ile, for example, was denoted as benign whereas this variant showed one of the most prominent effects on sGC activity in our cGMP measurements.

We further showed that diminished sGC activity could be rescued by the specific sGC stimulator BAY 41-2272. sGC stimulators are increasingly recognised as a treatment option for cardiovascular diseases. The stimulator Riociguat, for example, is approved for the treatment of pulmonary arterial hypertension (Ghofrani *et al.* 2016) and chronic thromboembolic pulmonary hypertension (Ghofrani *et al.* 2013a). With this study on rare coding *GUCY1A3* variants we provide first evidence that also patients suffering from athersoclerosis secondary to genetic alterations in *GUCY1A3* could benefit from treatment with sGC stimulators.

sGC function can be affected on several levels. One possible mechanism for decreased cGMP formation could be a reduced expression of the enzyme. In a first experiment we therefore focused on immunoblotting of lysates from HEK 293 cells overexpressing the rare *GUCY1A3* variants for assessing protein expression levels of sGC

α_1 and β_1 subunits. In addition to the loss-of-function p.Leu163Phefs*24 mutation which could not be detected due to a lack of the C-terminal tag, one variant, namely p.Gly537Arg, exhibited significantly decreased protein levels. Interestingly, of the nine investigated *GUCY1A3* variants only those two identified in extended families had an influence on protein expression levels.

As it is known that sGC is degraded via the proteasome (Xia *et al.* 2007) we treated cells overexpressing wildtype and p.Gly537Arg sGC α_1 subunits together with β_1 with the 26S proteasome inhibitor bortezomib. Indeed, we could reproduce that wildtype sGC is significantly enriched after inhibition of the proteasome. However, for the p.Gly537Arg variant no difference of sGC protein amounts could be detected after inhibition of the proteasome leading to the conduction of a second experiment investigating *GUCY1A3* mRNA levels. With that we could show, that this variants somehow influences RNA stability as mRNA levels were reduced by almost 50 % compared to wiltype *GUCY1A3* mRNA.

As the sGC is only functional when present as a heterodimer we also investigated the impact of the sGC α_1 variants on dimerisation with the β_1 subunit. As first two approaches we did this by bimolecular fluorescence complementation as well as with time-resolved fluorescence resonance energy transfer (TR-FRET), with both attempts revealing no results. A possible explanation for the lacking signals could be at least for the TR-FRET experiment a conformational problem. The HA and Flag tags used for detection by antibody-fluorophor complexes were cloned directly adjacent to the coding sequences of *GUCY1A3* and *GUCY1B3* without a linker sequence. This missing linker might explain a spatial inaccessibility for the antibody-fluorophor complexes to the tags.

We therefore investigated protein-protein interaction of the respective sGC α_1 variants with β_1 subunit by co-immunoprecipitation followed by immunobloting. As expected we did not detect the truncated loss-of-function mutation as explained by the missing tag at the C-terminus. One variant, p.Gly537Arg, exhibited very weak bands for both subunits which can probably be explained by reduced α_1 protein levels for this variant. All other variants evidently showed similar intensities as compared to wildtype sGC subunit bands. We could show for every variant, except for the truncating loss-of-function mutation, that dimerisation was not restricted.

In a third experiment we investigated the influence of the mutations on NO-mediated cGMP formation. Indeed, we found five of the investigated variants, in addition to the truncated one, to exhibit significantly decreased activity.

Our aim was then to test if this diminished cGMP formation secondary to genetic alteration could be rescued by the administration of the specific sGC stimulator BAY 41-2272. We deliberately chose to use a stimulator instead of an activator as by using the stimulator a direct comparison to the cGMP amount achieved by stimulation with NO only is

possible. As a reminder, stimulators mainly exhibit their effect by acting synergistically with NO as they both target the reduced state of sGC. sGC activators, however, exhibit additive effects to NO as they target the oxidised/haem free form of the sGC. Out of sGC stimulators we decided on BAY 41-2272 because of the following: BAY 41-2272 is more potent and specific compared to YC-1; BAY 41-2272 alone only leads to sGC stimulation by 20-fold, whereas BAY 41-8543 and BAY 63-2521 (Riociguat) alone lead to sGC stimulation by 92-fold and 73-fold, respectively (Stasch *et al.* 2011). As we were mostly interested in studying the synergistic effect of a sGC stimulator with NO and not the sole effect of the stimulator, we chose BAY 41-2272 for our experiments.

Before administrating the sGC stimulator BAY 41-2272 to HEK 293 cells overexpressing the variants its effect was tested in a preliminary experiment on wildtype mouse platelets in order to determine suitable concentrations of the stimulator for subsequent experiments. As platelet aggregation in humans depends on various factors, including pharmacological treatment, which can be easily taken into regard, but also genetic variants and environmental factors the C57Bl/6NCrl mouse as an inbread strain provides the unique possibility to rule out genetic and environmental factors and focus on pharmacologic effects only.

Results revealed a dose-dependent effect of BAY 41-2272 on inhibition of ADP-induced platelet aggregation in the presence of the NO donor sodium nitroprusside (SNP). Of note, BAY 41-2272 alone did not influence platelet aggregation. Aggregation was significantly decreased after addition of the NO donor SNP alone. The administration of a combination of SNP and BAY 41-2272 led to a further reduction of platelet aggregation compared to the NO donor SNP alone, emphasising the synergistic effect together with NO. Same effect was confered to phosphorylation of vasodilator-stimulated phosphoprotein (VASP) which serves as an indirect measure for the amount of cGMP present in the cell.

Indeed, the NO donors used for platelet aggregation experiments (SNP) and cGMP measurement experiments (GSNO) are chemically different and the effects on platelet aggregation were therefore not one-to-one transferable to the cGMP data. The preliminary platelet aggregation experiment was rather used, as above-mentioned, to determine an effective BAY 41-2272 concentration for later cGMP measurement in overexpressing HEK 293 cells. The reason for choosing SNP for platelet aggregation analyses and GSNO for cGMP formation, respectively, is that these had been used in comparable published studies (Mullershausen *et al.* 2004, Roger *et al.* 2010).

Based on the aggregation experiment and literature search we chose two different BAY 41-2272 concentrations for the stimulation of those variants which exhibited reduced cGMP formation upon NO addition and yet measurable sGC α_1 subunit amounts. The empirically determined concentrations were comparable with previous published studies on

BAY 41-2272 (Stasch *et al.* 2001, Roger *et al.* 2010). The administration of the combination of NO and BAY 41-2272 led to a rescue of cGMP formation in all investigated variants with unchanged protein amounts. Also the variant p.Gly537Arg leading to decreased protein amounts significantly improved through treatment with 100 µM NO plus 1 µM BAY 41-2272. Increase of the BAY 41-2272 concentration to 10 µM, however, did not entail a further increase in cGMP formation, which can probably be explained by limited enzymatic capacity due to decreased protein amounts. In all other variants a dose-dependent increase in cGMP formation could be noticed, they even reached same cGMP amounts as wildtype sGC stimulated with the NO donor only. As we only tested the effect of the sGC stimulator BAY 41-2272 we can not conclude that other sGC stimulators would have rescued impaired cGMP formation to the same extent.

Although we determined a molecular phenotype in HEK 293 cells overexpressing *GUCY1A3* and *GUCY1B3,* we still do not know the relevant cell type mediating risk *in vivo*. As impaired inhibition of platelet aggregation could be the causing mechanism (Freedman 2014), it would have been desirable to directly study the effect of BAY 41-2272 on the variants in platelets of mutation carriers. However, due to the very low prevalence of these variants which were initially identified in large exome sequencing datasets (Erdmann *et al.* 2013) it would have been almost impossible to collect a meaningful amount of samples. Besides ethical obstacles regarding recontacting of individuals, which is further complicated by the international composition of the providing consortia, a huge sequencing effort would be needed to identify a suitable number of individuals also available for platelet aggregation testing. We also want to allude to the fact that the variants have mainly been detected in CAD cases. These individuals are often treated with antiplatelet drugs that influence platelet aggregation but cannot be easily paused from an ethical point of view.

It was an interesting finding that most of the tested variants resulted in decreased cGMP formation. The fact that the addition of the sGC stimulator BAY 41-2272 was able to rescue this phenotype is maybe not surprising, but it provides a translational perspective. There is evidence from several *in vitro* and *in vivo* studies from other groups that sGC dysfunction seems to be causal for CAD/MI. Melichar *et al.* demonstrated hypercholesterolemic rabbits exhibiting reduced sGC expression and function in the aorta (Melichar *et al.* 2004). Ahrens *et al.* showed platelets of CAD patients displaying an elevated oxidative status due to reactive oxygen species and consequently impaired sGC function to benefit from pharmacological treatment with the sGC activator Cinaciguat (BAY 58-2667) (Ahrens *et al.* 2011). Erdmann *et al.* demonstrated that impaired sGC activity leading to reduced cGMP levels likely promotes atherothrombotic events (Erdmann *et al.* 2013). Conversely, enhanced cGMP formation reduces the expression of adhesion molecules and leukocyte recruitment which seems to be rather atheroprotective (Ahluwalia *et al.* 2004). It

has also been reported that the activation of the sGC prevents from formation of foam cells and reduces atherosclerotic lesions in *ApoE* knockout mice (Tsou *et al.* 2014). Furthermore, it had been shown that treatment with BAY 41-2272 and BAY 58-2667 (Cinaciguat) reduces the expression of tissue factor, which is linked to the initiation of coagulation, inflammation and atherosclerosis (Sovershaev *et al.* 2009).

Despite the limitations discussed above we think that our data together with previous published data on sGC function in the context of atherosclerosis provide a starting point for the discovery of strategies to recover impaired sGC function in carriers of rare mutations in *GUCY1A3* affecting the risk of atherosclerosis by the use of sGC modulators.

5.2 Common *GUCY1A3* lead SNP rs7692387

A comprehensive 1000 Genomes-based genome-wide association meta-analysis identified the *GUCY1A3* locus as one out of 56 loci significantly associated with MI and CAD (Nikpay *et al.* 2015). The *GUCY1A3* lead SNP rs7692387 is located withinin the ninth intron of the gene (NC_000004.12 Reference GRCh38.p7 Primary Assembly) on chromosome 4. The two allele variants of the lead SNP occur as the non-risk allele A and the risk allele G, with the latter one having an allele frequency of 0.795. In other words, 63 % of the European population are homozygous for the risk variant G whereas only 4 % carry the protective non-risk allele A homozygously (1000 genomes Project Phase 3; *http://www.ensembl.org/Homo_sapiens/Variation/Population?db=core;r=4:155713657-155714657;v=rs7692387;vdb=variation;vf=4491101*). Loci known so far to be genome-wide significantly associated with CAD explain approximately 10 % of CAD heritability (Schunkert *et al.* 2011). Bearing in mind the frequent occurence of the *GUCY1A3* lead SNP risk variant within the population, it is very important not only to identify causal loci but also to get deeper insights about their functional implications. Its nature as a common and non-coding variant already implies a mechanism that is more complicated than just altered protein function. Indeed, most of the variants identified by genome-wide association studies are supposed to act through regulatory mechanisms (CARDIoGRAMplusC4D Consortium *et al.* 2013).

With a number of experiments in human cell lines and human samples, we could show that the intronic region flanking the lead SNP rs7692387 at the *GUCY1A3* locus exhibits regulatory properties. It has to be taken into account that the lead SNP is not necessarily the causal SNP, it may rather be in linkage disequilibrium (LD) with a functionally relevant allele that is located in close proximity at this locus (Kessler *et al.* 2016). Nevertheless, we could show that no other SNP being in high LD with the lead SNP seems to have regulatory properties, as only the lead SNP is located within a DNase I

hypersensitivity site. Furthermore, the lead SNP region was predicted to interfere with the zinc finger E box-binding homeobox 1 transcription factor (ZEB1) – previously known as TCF8 – in a genotype-specific manner: ZEB1 was predicted to differentially interact with the non-risk allele A. We therefore hypothesised the nucleotide exchange to lead to a modulation of the binding site for the transcription factor ZEB1 as it had already been shown for the interaction of C/EBP transcription factor with a variant at the *SORT1* locus (Musunuru *et al.* 2010).

Publicly available ChIP sequencing data generated on hepatocellular carcinoma (HepG) cells located ZEB1 binding adjacent to the lead SNP. As part of a collaborational study with Frank Kaiser (Institute of Human Genetics, UKSH Lübeck, Germany) we also conducted ChIP experiments using formaldehyde-crosslinked chromatin of primary fibroblasts to confirm specific binding of ZEB1 to this genomic region. For that, a ChIP-grade ZEB1 antibody was used for precipitation followed by PCR amplification of a 407 bp fragment including the SNP rs7692387. While the *GUCY1A3* intronic region was specifically precipitated by the use of the ZEB1 antibody, no signal was obtained using an IgG antibody as control (Figure 40).

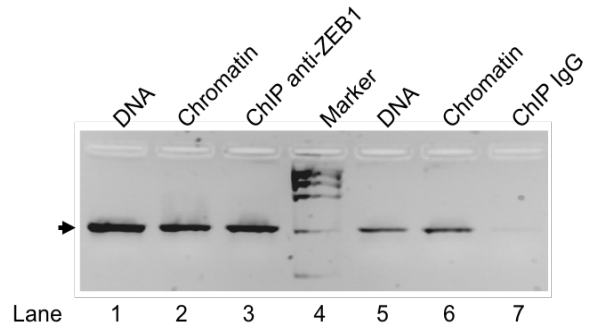

Figure 40 Binding of ZEB1 to the *GUCY1A3* lead SNP (rs7692387) region. Targeted ChIP in fibroblasts confirmed binding of ZEB1 directly to the rs7692387 region (arrow indicates PCR product specific for the intronic rs7692387 region). Specific amplification of the 407 bp fragment was shown on total DNA of the fibroblasts (lanes 1 and 5) and chromatin before precipitation (lanes 2 and 6) as controls. While the *GUCY1A3* intronic region was specifically precipitated by the use of a ZEB1 antibody (lane 3) no signal was obtained using an IgG antibody as control (lane 7). Part of Supplemental Figure 4 from Kessler/Wobst *et al.* Functional Characterization of the *GUCY1A3* Coronary Artery Disease Risk Locus. *Circulation* 2017. 136(5):476-489 (Kessler *et al.* 2017). ChIP experiment was conducted by Frank Kaiser (Institute of Human Genetics, UKSH Lübeck, Germany).

As we wanted to unravel the exact binding position we performed an electrophoretic mobility shift assays. We were indeed able to show that ZEB1 binds to the lead SNP region which was not known previously.

Using different luciferase constructs carrying the lead SNP region flanking the risk or the non-risk allele with or without *GUCY1A3* promoter we could show that the lead SNP region not only exhibits regulatory properties but that the non-risk allele mediates enhancing characteristics. By knocking down the transcription factor ZEB1 in an siRNA approach we

showed that luciferase activity rather decreased in case of the non-risk allele than in case of the risk allele. This was confirmed by testing varying concentrations of siRNA for the knockdown. We in collaboration with Frank Kaiser (Institute of Human Genetics, UKSH Lübeck, Germany) were also able to show the vice versa effect of overexpressed *ZEB1* leading to enhanced luciferase activity. In every case the effect was more pronounced for the non-risk allele construct.

In order to see if this observation could be translated to endogenous *GUCY1A3* levels we investigated *GUCY1A3* mRNA in HEK 293 cells and vascular smooth muscle cells (VSMC) after knockdown of *ZEB1*. Indeed, we could observe significant decreases of *GUCY1A3* mRNA. In HEK 293 cells the consequence of the knockdown was already detectable 24 h after transfection of *ZEB1* siRNA. In VSMC 72 h post transfection with siRNA *GUCY1A3* mRNA levels significantly went down. This can probably be explained by the fact, that HEK 293 cells were homozygous for the non-risk allele whereas VSMC were heterozygous at the lead SNP locus. An indirect effect of *ZEB1* knockdown could also be detected for *GUCY1B3* mRNA levels in HEK 293 cells.

Comparing *GUCY1A3* expression in AA- and GG-genotyped VSMC and platelets revealed that *GUCY1A3* is expressed in a genotype-specific manner: in VSMC as well as platelets *GUCY1A3* mRNA and sGC α_1 protein levels, respectively, were significantly lower in GG genotype carriers. As migration of VSMC represents an important step in the development and progression of atherosclerosis (Figure 1) we performed scratch wound assays. We were able to show inhibited migration of VSMC after pharmacologic stimulation with the specific sGC stimulator BAY 41-2272 only in cells homozygous for the non-risk allele but not in cells homozygous for the risk allele. Heterozygous VSMC displayed intermediate inhibition of migration. In other words, the extent of *GUCY1A3* expression seems to be decisive for the extent of migration.

Fitting to our results on VSMC phenotype, and considering that thrombus formation also represents an important step in atherosclerosis, likewise platelets exhibited a genotype-dependent phenotype. Results of platelet aggregation experiments conducted by Bernhard Wolf (Institute for Cardiovascular Diseases, German Heart Centre Munich, Germany) revealed that platelets homozygous for the non-risk allele display significantly stronger inhibition of ADP-induced platelet aggregation after treatment with an NO donor than platelets homozygous for the risk allele (Figure 41B). The effect could further be enhanced by the additional supplementation of the specific phosphodiesterase 5 (PDE5) inhibitor sildenafil (Figure 41C). Of note, there was no difference in platelet aggregation under baseline conditions (Figure 41A).

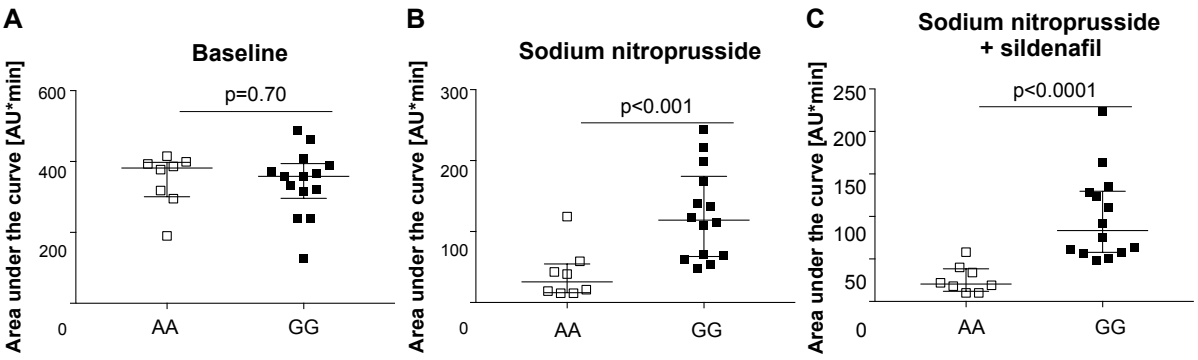

Figure 41 Genotype-dependent platelet response to NO *in vitro*. Baseline ADP-induced platelet aggregation did not differ between the genotypes (AA=8 and GG=14) (A). Supplementation of the NO donor SNP (10 µM) led to significantly stronger inhibition of ADP-induced platelet aggregation in homozygous non-risk allele carriers compared to homozygous risk allele carriers (p<0.001) (B). The effect was even enhanced after the additional inhibition of cGMP degradation by the PDE5 inhibitor sildenafil (10 µM; p<0.0001) (C). Data are median with interquartile range. Statistical significance was assessed by Mann-Whitney test. Supplemental Figure 10 from Kessler/Wobst *et al.* Functional Characterization of the *GUCY1A3* Coronary Artery Disease Risk Locus. *Circulation* 2017. 136(5):476-489 (Kessler *et al.* 2017) and was conducted by Bernhard Wolf (Institute for Cardiovascular Diseases, German Heart Centre Munich, Germany).

As a second readout, cGMP-dependent phosphorylation of VASP was investigated. In VSMC the addition of BAY 41-2272 to the NO donor GSNO led to increased levels of cGMP compared to treatment with GSNO only. However, as expected from expression and migration assays, phosphorylated VASP could only be observed in cells carrying at least one non-risk allele but not in cells being homozygous for the risk allele. In concordance with the fact that VSMC homozygous for the risk allele did not exhibit VASP phosphorylation at all also the platelets emanating from the aggregation experiment exhibited VASP phosphorylation in a genotype-dependent manner (Figure 42A). Phosphorylation was significantly higher in platelets homozygous for the non-risk allele as compared to those homozygous for the risk allele both after SNP treatment and also after additional sildenafil supplementation. Increased phosphorylation due to increased VASP expression in homozygous non-risk allele carriers could be excluded by investigating vehicle-treated platelets for total VASP by Western blotting which revealed no difference when comparing both genotypes (Figure 42B).

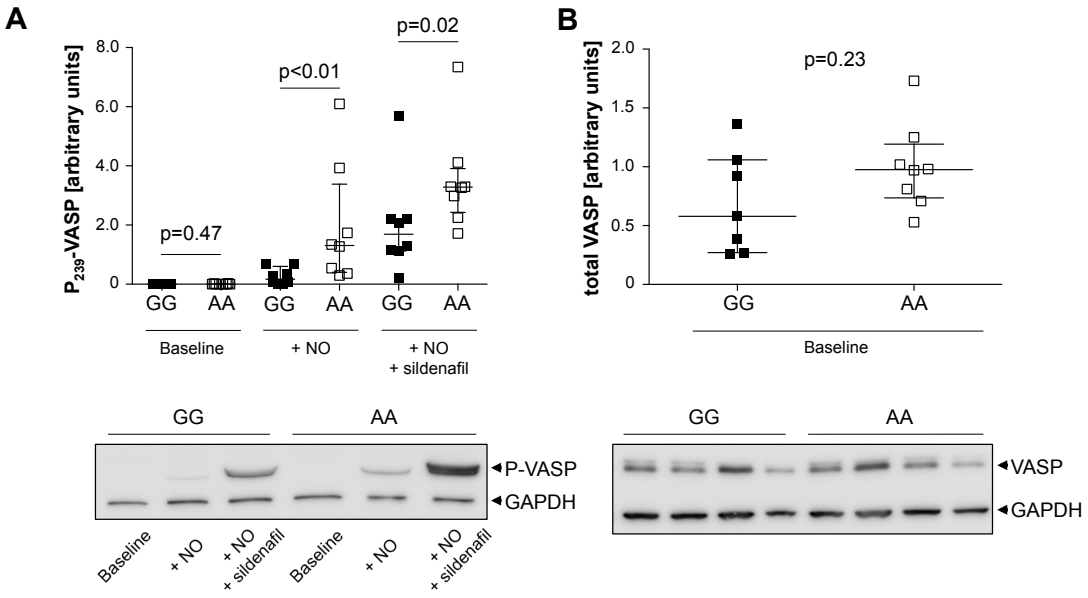

Figure 42 NO leads to stronger cGMP-dependent phosphorylation of VASP in homozygous non-risk allele platelets. Proteinkinase G-dependent phosphorylation of VASP was significantly stronger in homozygous non-risk allele carriers (n=8) than in homozygous risk allele carriers (n=8) after the addition of the NO donor SNP (p<0.01) (A). After additional supplementation with the phosphodiesterase 5 inhibitor sildenafil to SNP, phosphorylation was enhanced with homozygous non-risk allele carriers again displaying significantly stronger phosphorylation of VASP compared to homozygous risk allele carriers (p=0.02) (A). Both genotypes exhibited same amounts of VASP in baseline samples (GG=7, AA=8; p=0.23) (B). Data are median with interquartile range. Statistical significance was assessed by Mann-Whitney test. (A) is from Figure 6 from Kessler/Wobst *et al.* Functional Characterization of the *GUCY1A3* Coronary Artery Disease Risk Locus. *Circulation* 2017. 136(5):476-489 (Kessler *et al.* 2017) and conducted by Bernhard Wolf (Institute for Cardiovascular Diseases, German Heart Centre Munich, Germany).

We are aware that VSMC migration experiments as well as experiments on platelets presented here do not fully resemble the *in vivo* human situation. We also do not assume the transcription factor ZEB1 exclusively to bind to the non-risk allele as it is relatively unlikely that a single nucleotide exchange involves a complete disruption of a binding site. However, results indicate that ZEB1 at least preferably binds to the non-risk alle A. Sánchez-Tilló *et al.* stated that ZEB1 can act as both activator and repressor, achieved through differential recruitment of cofactors (Sanchez-Tillo *et al.* 2011). Yamada *et al.* found out that the depletion of ZEB1 in cultured HEK 293 cells results in significant changes in the expression of various atherosclerosis-related genes (Yamada *et al.* 2014). It had been reported that deregulation of ZEB1 is involved in smooth muscle cell (SMC) phenotype transformation, i.e., in the dedifferentiation of contractile and quiescent SMC to proliferative, migratory and synthetic ones (Karagiannis *et al.* 2013).

Missense mutations in *ZEB1* have been associated with posterior polymorphous corneal dystrophy (Krafchak *et al.* 2005) and late-onset fuchs corneal dystrophy (Riazuddin *et al.* 2010) in humans with the latter one being associated with cardiovascular diseases (Olsen 1984).

Lately, the *NOS3* gene has been identified to be also genome-wide significantly associated wit CAD (Nikpay *et al.* 2015). *NOS3* codes for endothelial nitric oxide synthase, another key enzyme within the NO/cGMP signalling pathway, responsible for the generation of NO. Furthermore a mutation in the *PDE5* gene, coding for phosphodiesterase 5 responsible for cGMP degradation, has been identified in a family suffering from premature CAD and MI (Dang *et al.* 2015, Wobst *et al.* 2015a). Taken together, this illustrates the impact of cGMP signalling in atherosclerosis and the importance of sGC as a therapeutic target as it had already been discussed in the context of the rare variants in the *GUCY1A3* gene.

Trials on organic and inorganic nitrates in cardiovascular diseases, e.g., the NITRITE-AMI and the NIAMI studies, revealed conflicting results (Jones *et al.* 2014, Siddiqi *et al.* 2014). Also for PDE5 inhibitors inconsistent results have been reported (Thadani *et al.* 2002, DeBusk *et al.* 2004). Direct targeting of sGC might therefore be a promising therapeutic strategy for CAD/MI patients. As already discussed in the section on rare *GUCY1A3* variants the stimulator Riociguat is approved for the treatment of pulmonary arterial hypertension (Ghofrani *et al.* 2016) and chronic thromboembolic pulmonary hypertension (Ghofrani *et al.* 2013a). Cinaciguat, an sGC activator, has been shown to improve ischemia-reperfusion-injury (Korkmaz *et al.* 2009).

It should be mentioned at this point that most of the GWAS have focused on samples of European origin. Therefore, the loci altogether only explain a small fraction of the risk for CAD, and moreover, might not be applicable to other ethnic groups. rs1842896, for example, is a frequent variant in the *GUCY1A3* locus that has been discovered to be genome-wide significantly associated with CAD only in Han Chinese (Lu *et al.* 2012). Consequently, larger studies in populations of non-European ancestry are needed in the future to reveal more susceptibility loci for the improvement of understanding of causal pathways to CAD.

Nevertheless, for the first time, our results provide evidence for the involvement of a common variant in the *GUCY1A3* gene coming along with reduced expression of the gene affecting atherosclerosis. Allele-specific expression thereby seems to be mediated via modulation of a binding site for the transcription factor ZEB1, which translates to differential responses of VSMC and platelets to NO suggesting alteration of sGC activity.

5.4 Conclusion

We could show that coding *GUCY1A3* variants found to be enriched in CAD/MI patients led to decreased capability of cGMP formation due to decreased enzymatic activity and in part due to decreased expression which could be rescued by the sGC stimulator BAY

41-2272. We could also show that the lead SNP rs7692387 is located within an *cis*-regulatory site that modulates *GUCY1A3* promoter activity. The transcription factor ZEB1 preferably interacts with the non-risk allele leading to an increase in *GUCY1A3* expression, higher sGC levels, and higher enzymatic activity after sGC stimulation translating into VSMC and platelet phenotypes.

Taken together, our comprehensive genetic and functional data on rare and common variants in *GUCY1A3* emphasise that sGC is critically involved in mediating risk of atherosclerosis. Targeting the NO/cGMP signalling pathway – and in particular sGC – might represent a promising novel therapeutic strategy for CAD and MI patients.

6 Bibliography

Adzhubei IA, Schmidt S, Peshkin L, Ramensky VE, Gerasimova A, Bork P, Kondrashov AS and Sunyaev SR. A method and server for predicting damaging missense mutations. *Nat Methods* 2010. 7(4):248-249.

Ahluwalia A, Foster P, Scotland RS, McLean PG, Mathur A, Perretti M, Moncada S and Hobbs AJ. Antiinflammatory activity of soluble guanylate cyclase: cGMP-dependent down-regulation of P-selectin expression and leukocyte recruitment. *Proc Natl Acad Sci U S A* 2004. 101(5):1386-1391.

Ahrens I, Habersberger J, Baumlin N, Qian H, Smith BK, Stasch JP, Bode C, Schmidt HH and Peter K. Measuring oxidative burden and predicting pharmacological response in coronary artery disease patients with a novel direct activator of haem-free/oxidised sGC. *Atherosclerosis* 2011. 218(2):431-434.

Allerston CK, von Delft F and Gileadi O. Crystal structures of the catalytic domain of human soluble guanylate cyclase. *PLoS ONE* 2013. 8(3):e57644.

Antl M, von Bruhl ML, Eiglsperger C, Werner M, Konrad I, Kocher T, Wilm M, Hofmann F, Massberg S and Schlossmann J. IRAG mediates NO/cGMP-dependent inhibition of platelet aggregation and thrombus formation. *Blood* 2007. 109(2):552-559.

Behrends S, Harteneck C, Schultz G and Koesling D. A variant of the alpha 2 subunit of soluble guanylyl cyclase contains an insert homologous to a region within adenylyl cyclases and functions as a dominant negative protein. *J Biol Chem* 1995. 270(36):21109-21113.

Behrends S, Kazmierczak B, Steenpaß A, Knauf B, Bullerdiek J, Scholz H and Eiberg H. Assignment of GUCY1B2, the Gene Coding for the β2 Subunit of Human Guanylyl Cyclase to Chromosomal Band 13q14.3 between Markers D13S168 and D13S155. *Genomics* 1999. 55(1):126-127.

Bender AT and Beavo JA. Cyclic nucleotide phosphodiesterases: molecular regulation to clinical use. *Pharmacol Rev* 2006. 58(3):488-520.

Biel M. Cyclic nucleotide-regulated cation channels. *J Biol Chem* 2009. 284(14):9017-9021.

Biel M, Zong X, Distler M, Bosse E, Klugbauer N, Murakami M, Flockerzi V and Hofmann F. Another member of the cyclic nucleotide-gated channel family, expressed in testis, kidney, and heart. *Proc Natl Acad Sci U S A* 1994. 91(9):3505-3509.

Bonderman D, Ghio S, Felix SB, Ghofrani HA, Michelakis E, Mitrovic V, Oudiz RJ, Boateng F, Scalise AV, Roessig L, Semigran MJ and Left Ventricular Systolic Dysfunction Associated With Pulmonary Hypertension Riociguat Trial Study G. Riociguat for patients with pulmonary hypertension caused by systolic left ventricular dysfunction: a phase IIb double-blind, randomized, placebo-controlled, dose-ranging hemodynamic study. *Circulation* 2013. 128(5):502-511.

Bonvini P, Zorzi E, Basso G and Rosolen A. Bortezomib-mediated 26S proteasome inhibition causes cell-cycle arrest and induces apoptosis in CD-30+ anaplastic large cell lymphoma. *Leukemia* 2007. 21(4):838-842.

Boyle AP, Davis S, Shulha HP, Meltzer P, Margulies EH, Weng Z, Furey TS and Crawford GE. High-resolution mapping and characterization of open chromatin across the genome. *Cell* 2008. 132(2):311-322.

Budworth J, Meillerais S, Charles I and Powell K. Tissue Distribution of the Human Soluble Guanylate Cyclases. *Biochem Biophys Res Commun* 1999. 263(3):696-701.

Busse R and Fleming I. Regulation and functional consequences of endothelial nitric oxide formation. *Ann Med* 1995. 27(3):331-340.

Campbell MG, Underbakke ES, Potter CS, Carragher B and Marletta MA. Single-particle EM reveals the higher-order domain architecture of soluble guanylate cyclase. *Proc Natl Acad Sci U S A* 2014. 111(8):2960-2965.

CARDIoGRAMplusC4D Consortium, Deloukas P, Kanoni S, Willenborg C, Farrall M, Assimes TL, Thompson JR, Ingelsson E, Saleheen D, Erdmann J, Goldstein BA, Stirrups K, Konig IR, Cazier JB, Johansson A, Hall AS, Lee JY, Willer CJ, Chambers JC, Esko T, Folkersen L, Goel A, Grundberg E, Havulinna AS, Ho WK, Hopewell JC, Eriksson N, Kleber ME, Kristiansson K, Lundmark P, Lyytikainen LP, Rafelt S, Shungin D, Strawbridge RJ, Thorleifsson G, Tikkanen E, Van Zuydam N, Voight BF, Waite LL, Zhang W, Ziegler A, Absher D, Altshuler D, Balmforth AJ, Barroso I, Braund PS, Burgdorf C, Claudi-Boehm S, Cox D, Dimitriou M, Do R, Diagram Consortium, Cardiogenics Consortium, Doney AS, El Mokhtari N, Eriksson P, Fischer K, Fontanillas P, Franco-Cereceda A, Gigante B, Groop L, Gustafsson S, Hager J, Hallmans G, Han BG, Hunt SE, Kang HM, Illig T, Kessler T, Knowles JW, Kolovou G, Kuusisto J, Langenberg C, Langford C, Leander K, Lokki ML, Lundmark A, McCarthy MI, Meisinger C, Melander O, Mihailov E, Maouche S, Morris AD, Muller-Nurasyid M, MuTHER Consortium, Nikus K, Peden JF, Rayner NW, Rasheed A, Rosinger S, Rubin D, Rumpf MP, Schafer A, Sivananthan M, Song C, Stewart AF, Tan ST, Thorgeirsson G, van der Schoot CE, Wagner PJ, Wellcome Trust Case Control Consortium, Wells GA, Wild PS, Yang TP, Amouyel P, Arveiler D, Basart H, Boehnke M, Boerwinkle E, Brambilla P, Cambien F, Cupples AL, de Faire U, Dehghan A, Diemert P, Epstein SE, Evans A, Ferrario MM, Ferrieres J, Gauguier D, Go AS, Goodall AH, Gudnason V, Hazen SL, Holm H, Iribarren C, Jang Y, Kahonen M, Kee F, Kim HS, Klopp N, Koenig W, Kratzer W, Kuulasmaa K, Laakso M, Laaksonen R, Lee JY, Lind L, Ouwehand WH, Parish S, Park JE, Pedersen NL, Peters A, Quertermous T, Rader DJ, Salomaa V, Schadt E, Shah SH, Sinisalo J, Stark K, Stefansson K, Tregouet DA, Virtamo J, Wallentin L, Wareham N, Zimmermann ME, Nieminen MS, Hengstenberg C, Sandhu MS, Pastinen T, Syvanen AC, Hovingh GK, Dedoussis G, Franks PW, Lehtimaki T, Metspalu A, Zalloua PA, Siegbahn A, Schreiber S, Ripatti S, Blankenberg SS, Perola M, Clarke R, Boehm BO, O'Donnell C, Reilly MP, Marz W, Collins R, Kathiresan S, Hamsten A, Kooner JS, Thorsteinsdottir U, Danesh J, Palmer CN, Roberts R, Watkins H, Schunkert H and Samani NJ. Large-scale association analysis identifies new risk loci for coronary artery disease. *Nat Genet* 2013. 45(1):25-33.

Chen H and Kassab GS. Microstructure-based biomechanics of coronary arteries in health and disease. *J Biomech* 2016. 49(12):2548-2559.

Dang TA, Wobst J, Kessler T, Ameln SV, Lehm M, Prestel M, Braenne I, Aherrahrou R, Dichgans M, Hengstenberg C, Erdmannn J and Schunkert H. Investigating the impact of a mutation in PDE5A on myocardial infarction. *BMC Pharmacol Toxicol* 2015. 16(Suppl 1):A43.

Dangel O, Mergia E, Karlisch K, Groneberg D, Koesling D and Friebe A. Nitric oxide-sensitive guanylyl cyclase is the only nitric oxide receptor mediating platelet inhibition. *J Thromb Haemost* 2010. 8(6):1343-1352.

DeBusk RF, Pepine CJ, Glasser DB, Shpilsky A, DeRiesthal H and Sweeney M. Efficacy and safety of sildenafil citrate in men with erectile dysfunction and stable coronary artery disease. *Am J Cardiol* 2004. 93(2):147-153.

Derbyshire ER and Marletta MA. Structure and regulation of soluble guanylate cyclase. *Annu Rev Biochem* 2012. 81:533-559.

Desch M, Sigl K, Hieke B, Salb K, Kees F, Bernhard D, Jochim A, Spiessberger B, Hocherl K, Feil R, Feil S, Lukowski R, Wegener JW, Hofmann F and Schlossmann J. IRAG determines nitric oxide- and atrial natriuretic peptide-mediated smooth muscle relaxation. *Cardiovasc Res* 2010. 86(3):496-505.

Distler M, Biel M, Flockerzi V and Hofmann F. Expression of cyclic nucleotide-gated cation channels in non-sensory tissues and cells. *Neuropharmacology* 1994. 33(11):1275-1282.

Do R, Stitziel NO, Won HH, Jorgensen AB, Duga S, Angelica Merlini P, Kiezun A, Farrall M, Goel A, Zuk O, Guella I, Asselta R, Lange LA, Peloso GM, Auer PL, NHLBI Exome Sequencing Project, Girelli D, Martinelli N, Farlow DN, DePristo MA, Roberts R, Stewart AF, Saleheen D, Danesh J, Epstein SE, Sivapalaratnam S, Hovingh GK, Kastelein JJ, Samani NJ, Schunkert H, Erdmann J, Shah SH, Kraus WE, Davies R, Nikpay M, Johansen CT, Wang J, Hegele RA, Hechter E, Marz W, Kleber ME, Huang J, Johnson AD, Li M, Burke GL, Gross M, Liu Y, Assimes TL, Heiss G, Lange EM, Folsom AR, Taylor HA, Olivieri O, Hamsten A, Clarke R, Reilly DF, Yin W, Rivas MA, Donnelly P, Rossouw JE, Psaty BM, Herrington DM, Wilson JG, Rich SS, Bamshad MJ, Tracy RP, Cupples LA, Rader DJ, Reilly MP, Spertus JA, Cresci S, Hartiala J, Tang WH, Hazen SL, Allayee H, Reiner AP, Carlson CS, Kooperberg C, Jackson RD, Boerwinkle E, Lander ES, Schwartz SM, Siscovick DS, McPherson R, Tybjaerg-Hansen A, Abecasis GR, Watkins H, Nickerson DA, Ardissino D, Sunyaev SR, O'Donnell CJ, Altshuler D, Gabriel S and Kathiresan S. Exome sequencing identifies rare LDLR and APOA5 alleles conferring risk for myocardial infarction. *Nature* 2015. 518(7537):102-106.

Elfering SL, Sarkela TM and Giulivi C. Biochemistry of mitochondrial nitric-oxide synthase. *J Biol Chem* 2002. 277(41):38079-38086.

Erdmann J, Stark K, Esslinger UB, Rumpf PM, Koesling D, de Wit C, Kaiser FJ, Braunholz D, Medack A, Fischer M, Zimmermann ME, Tennstedt S, Graf E, Eck S, Aherrahrou Z, Nahrstaedt J, Willenborg C, Bruse P, Braenne I, Nothen MM, Hofmann P, Braund PS, Mergia E, Reinhard W, Burgdorf C, Schreiber S, Balmforth AJ, Hall AS, Bertram L, Steinhagen-Thiessen E, Li SC, Marz W, Reilly M, Kathiresan S, McPherson R, Walter U, CardioGram, Ott J, Samani NJ, Strom TM, Meitinger T, Hengstenberg C and Schunkert H. Dysfunctional nitric oxide signalling increases risk of myocardial infarction. *Nature* 2013. 504(7480):432-436.

Evgenov OV, Pacher P, Schmidt PM, Hasko G, Schmidt HH and Stasch JP. NO-independent stimulators and activators of soluble guanylate cyclase: discovery and therapeutic potential. *Nat Rev Drug Discov* 2006. 5(9):755-768.

Feil R and Kemp-Harper B. cGMP signalling: from bench to bedside. Conference on cGMP generators, effectors and therapeutic implications. *EMBO Rep* 2006. 7(2):149-153.

Fesenko EE, Kolesnikov SS and Lyubarsky AL. Induction by cyclic GMP of cationic conductance in plasma membrane of retinal rod outer segment. *Nature* 1985. 313(6000):310-313.

Finegold JA, Asaria P and Francis DP. Mortality from ischaemic heart disease by country, region, and age: statistics from World Health Organisation and United Nations. *Int J Cardiol* 2013. 168(2):934-945.

Finn AV, Nakano M, Narula J, Kolodgie FD and Virmani R. Concept of vulnerable/unstable plaque. *Arterioscler Thromb Vasc Biol* 2010. 30(7):1282-1292.

Francis SH, Corbun JD and Bischoff E. Cyclic GMP-hydrolyzing phosphodiesterases. *Handb Exp Pharmacol* 2009. (191):367-408.

Freedman JE. Inherited dysfunctional nitric oxide signaling and the pathobiology of atherothrombotic disease. *Circ Res* 2014. 114(9):1372-1373.

Friebe A, Mullershausen F, Smolenski A, Walter U, Schultz G and Koesling D. YC-1 potentiates nitric oxide- and carbon monoxide-induced cyclic GMP effects in human platelets. *Mol Pharmacol* 1998. 54(6):962-967.

Fritz BG, Hu X, Brailey JL, Berry RE, Walker FA and Montfort WR. Oxidation and loss of heme in soluble guanylyl cyclase from Manduca sexta. *Biochemistry* 2011. 50(26):5813-5815.

Furchgott RF and Zawadzki JV. The obligatory role of endothelial cells in the relaxation of arterial smooth muscle by acetylcholine. *Nature* 1980. 288(5789):373-376.

Galle J, Zabel U, Hubner U, Hatzelmann A, Wagner B, Wanner C and Schmidt HH. Effects of the soluble guanylyl cyclase activator, YC-1, on vascular tone, cyclic GMP levels and phosphodiesterase activity. *Br J Pharmacol* 1999. 127(1):195-203.

Ghofrani HA, D'Armini AM, Grimminger F, Hoeper MM, Jansa P, Kim NH, Mayer E, Simonneau G, Wilkins MR, Fritsch A, Neuser D, Weimann G, Wang C and Group C-S. Riociguat for the treatment of chronic thromboembolic pulmonary hypertension. *N Engl J Med* 2013a. 369(4):319-329.

Ghofrani HA, Galie N, Grimminger F, Grunig E, Humbert M, Jing ZC, Keogh AM, Langleben D, Kilama MO, Fritsch A, Neuser D, Rubin LJ and Group P-S. Riociguat for the treatment of pulmonary arterial hypertension. *N Engl J Med* 2013b. 369(4):330-340.

Ghofrani HA, Humbert M, Langleben D, Schermuly R, Stasch JP, Wilkins MR and Klinger JR. Riociguat: Mode of action and clinical development in pulmonary hypertension. *Chest* 2016. pii: S0012-3692(16):49111-49117.

Gileadi O. Structures of soluble guanylate cyclase: implications for regulatory mechanisms and drug development. *Biochem Soc Trans* 2014. 42(1):108-113.

Giuili G, Roechel N, Scholl U, Matei M-G and Guellaen G. Colocalization of the genes coding for the alpha 3 and beta 3 subunits of soluble guanylyl cyclase to human chromosome 4 at q31.3-q33. *Hum Genet* 1993. 91(3):257-260.

Gori T. Nitrate Tolerance: A Unifying Hypothesis. *Circulation* 2002. 106(19):2510-2513.

Grabe N. AliBaba2: context specific identification of transcription factor binding sites. *In Silico Biol* 2002. 2(1):S1-15.

Griffith F. The Significance of Pneumococcal Types. *J Hyg (Lond)* 1928. 27(2):113-159.

Hagg S, Skogsberg J, Lundstrom J, Noori P, Nilsson R, Zhong H, Maleki S, Shang MM, Brinne B, Bradshaw M, Bajic VB, Samnegard A, Silveira A, Kaplan LM, Gigante B, Leander K, de Faire U, Rosfors S, Lockowandt U, Liska J, Konrad P, Takolander R, Franco-Cereceda A, Schadt EE, Ivert T, Hamsten A, Tegner J and Bjorkegren J. Multi-organ expression profiling uncovers a gene module in coronary artery disease involving transendothelial migration of leukocytes and LIM domain binding 2: the Stockholm Atherosclerosis Gene Expression (STAGE) study. *PLoS Genet* 2009. 5(12):e1000754.

Hamalainen M, Lilja R, Kankaanranta H and Moilanen E. Inhibition of iNOS expression and NO production by anti-inflammatory steroids. Reversal by histone deacetylase inhibitors. *Pulm Pharmacol Ther* 2008. 21(2):331-339.

Hanafy KA, Martin E and Murad F. CCTeta, a novel soluble guanylyl cyclase-interacting protein. *J Biol Chem* 2004. 279(45):46946-46953.

Harteneck C, Koesling D, Söling A, Schultz G and Böhme E. Expression of soluble guanylyl cyclase. Catalytic activity requires two enzyme subunits. *FEBS Letters* 1990. 272(1):221-223.

Harteneck C, Wedel B, Koesling D, Malkewitz J, Böhme E and Schultz G. Molecular cloning and expression of a new alpha-subunit of soluble guanylyl cyclase. Interchangeability of the alpha-subunits of the enzyme. *FEBS Lett* 1991. 292(1-2):217-222.

Hathaway DR and Adelstein RS. Human platelet myosin light chain kinase requires the calcium-binding protein calmodulin for activity. *Proc Natl Acad Sci U S A* 1979. 76(4):1653-1657.

Hellman LM and Fried MG. Electrophoretic mobility shift assay (EMSA) for detecting protein–nucleic acid interactions. *Nature Protocols* 2007. 2(8):1849-1861.

Hervé D, Philippi A, Belbouab R, Zerah M, Chabrier S, Collardeau-Frachon S, Bergametti F, Essongue A, Berrou E, Krivosic V, Sainte-Rose C, Houdart E, Adam F, Billiemaz K, Lebret M, Roman S, Passemard S, Boulday G, Delaforge A, Guey S, Dray X, Chabriat H, Brouckaert P, Bryckaert M and Tournier-Lasserve E. Loss of alpha1beta1 soluble guanylate cyclase, the major nitric oxide receptor, leads to moyamoya and achalasia. *Am J Hum Genet* 2014. 94(3):385-394.

Hofmann F. The biology of cyclic GMP-dependent protein kinases. *J Biol Chem* 2005. 280(1):1-4.

Humbert P, Niroomand F, Fischer G, Mayer B, Koesling D, Hinsch K-D, Gausepohl H, Frank R, Schultz G and Böhme E. Purification of soluble guanylyl cyclase from bovine lung by a new immunoaffinity chromatographic method. *Eur J Biochem* 1990. 190:273-278.

Ignarro LJ. Signal transduction mechanisms involving nitric oxide. *Biochem Pharmacol* 1991. 41(4):485-490.

Ignarro LJ, Buga GM, Wood KS, Byrns RE and Chaudhuri G. Endothelium-derived relaxing factor produced and released from artery and vein is nitric oxide. *Proc Natl Acad Sci U S A* 1987. 84(24):9265-9269.

International Consortium for Blood Pressure Genome-Wide Association Studies, Ehret GB, Munroe PB, Rice KM, Bochud M, Johnson AD, Chasman DI, Smith AV, Tobin MD, Verwoert GC, Hwang SJ, Pihur V, Vollenweider P, O'Reilly PF, Amin N, Bragg-Gresham JL, Teumer A, Glazer NL, Launer L, Zhao JH, Aulchenko Y, Heath S, Sober S, Parsa A, Luan J, Arora P, Dehghan A, Zhang F, Lucas G, Hicks AA, Jackson AU, Peden JF, Tanaka T, Wild SH,

Rudan I, Igl W, Milaneschi Y, Parker AN, Fava C, Chambers JC, Fox ER, Kumari M, Go MJ, van der Harst P, Kao WH, Sjogren M, Vinay DG, Alexander M, Tabara Y, Shaw-Hawkins S, Whincup PH, Liu Y, Shi G, Kuusisto J, Tayo B, Seielstad M, Sim X, Nguyen KD, Lehtimaki T, Matullo G, Wu Y, Gaunt TR, Onland-Moret NC, Cooper MN, Platou CG, Org E, Hardy R, Dahgam S, Palmen J, Vitart V, Braund PS, Kuznetsova T, Uiterwaal CS, Adeyemo A, Palmas W, Campbell H, Ludwig B, Tomaszewski M, Tzoulaki I, Palmer ND, CARDIoGRAM Consortium, CKDGen Consortium, KidneyGen Consortium, EchoGen Consortium, Charge-Hf Consortium, Aspelund T, Garcia M, Chang YP, O'Connell JR, Steinle NI, Grobbee DE, Arking DE, Kardia SL, Morrison AC, Hernandez D, Najjar S, McArdle WL, Hadley D, Brown MJ, Connell JM, Hingorani AD, Day IN, Lawlor DA, Beilby JP, Lawrence RW, Clarke R, Hopewell JC, Ongen H, Dreisbach AW, Li Y, Young JH, Bis JC, Kahonen M, Viikari J, Adair LS, Lee NR, Chen MH, Olden M, Pattaro C, Bolton JA, Kottgen A, Bergmann S, Mooser V, Chaturvedi N, Frayling TM, Islam M, Jafar TH, Erdmann J, Kulkarni SR, Bornstein SR, Grassler J, Groop L, Voight BF, Kettunen J, Howard P, Taylor A, Guarrera S, Ricceri F, Emilsson V, Plump A, Barroso I, Khaw KT, Weder AB, Hunt SC, Sun YV, Bergman RN, Collins FS, Bonnycastle LL, Scott LJ, Stringham HM, Peltonen L, Perola M, Vartiainen E, Brand SM, Staessen JA, Wang TJ, Burton PR, Soler Artigas M, Dong Y, Snieder H, Wang X, Zhu H, Lohman KK, Rudock ME, Heckbert SR, Smith NL, Wiggins KL, Doumatey A, Shriner D, Veldre G, Viigimaa M, Kinra S, Prabhakaran D, Tripathy V, Langefeld CD, Rosengren A, Thelle DS, Corsi AM, Singleton A, Forrester T, Hilton G, McKenzie CA, Salako T, Iwai N, Kita Y, Ogihara T, Ohkubo T, Okamura T, Ueshima H, Umemura S, Eyheramendy S, Meitinger T, Wichmann HE, Cho YS, Kim HL, Lee JY, Scott J, Sehmi JS, Zhang W, Hedblad B, Nilsson P, Smith GD, Wong A, Narisu N, Stancakova A, Raffel LJ, Yao J, Kathiresan S, O'Donnell CJ, Schwartz SM, Ikram MA, Longstreth WT, Jr., Mosley TH, Seshadri S, Shrine NR, Wain LV, Morken MA, Swift AJ, Laitinen J, Prokopenko I, Zitting P, Cooper JA, Humphries SE, Danesh J, Rasheed A, Goel A, Hamsten A, Watkins H, Bakker SJ, van Gilst WH, Janipalli CS, Mani KR, Yajnik CS, Hofman A, Mattace-Raso FU, Oostra BA, Demirkan A, Isaacs A, Rivadeneira F, Lakatta EG, Orru M, Scuteri A, Ala-Korpela M, Kangas AJ, Lyytikainen LP, Soininen P, Tukiainen T, Wurtz P, Ong RT, Dorr M, Kroemer HK, Volker U, Volzke H, Galan P, Hercberg S, Lathrop M, Zelenika D, Deloukas P, Mangino M, Spector TD, Zhai G, Meschia JF, Nalls MA, Sharma P, Terzic J, Kumar MV, Denniff M, Zukowska-Szczechowska E, Wagenknecht LE, Fowkes FG, Charchar FJ, Schwarz PE, Hayward C, Guo X, Rotimi C, Bots ML, Brand E, Samani NJ, Polasek O, Talmud PJ, Nyberg F, Kuh D, Laan M, Hveem K, Palmer LJ, van der Schouw YT, Casas JP, Mohlke KL, Vineis P, Raitakari O, Ganesh SK, Wong TY, Tai ES, Cooper RS, Laakso M, Rao DC, Harris TB, Morris RW, Dominiczak AF, Kivimaki M, Marmot MG, Miki T, Saleheen D, Chandak GR, Coresh J, Navis G, Salomaa V, Han BG, Zhu X, Kooner JS, Melander O, Ridker PM, Bandinelli S, Gyllensten UB, Wright AF, Wilson JF, Ferrucci L, Farrall M, Tuomilehto J, Pramstaller PP, Elosua R, Soranzo N, Sijbrands EJ, Altshuler D, Loos RJ, Shuldiner AR, Gieger C, Meneton P, Uitterlinden AG, Wareham NJ, Gudnason V, Rotter JI, Rettig R, Uda M, Strachan DP, Witteman JC, Hartikainen AL, Beckmann JS, Boerwinkle E, Vasan RS, Boehnke M, Larson MG, Jarvelin MR, Psaty BM, Abecasis GR, Chakravarti A, Elliott P, van Duijn CM, Newton-Cheh C, Levy D, Caulfield MJ and Johnson T. Genetic variants in novel pathways influence blood pressure and cardiovascular disease risk. *Nature* 2011. 478(7367):103-109.

Jameson JL and Longo DL. Precision medicine–personalized, problematic, and promising. *N Engl J Med* 2015. 372(23):2229-2234.

Johnson AD, Handsaker RE, Pulit SL, Nizzari MM, O'Donnell CJ and de Bakker PI. SNAP: a web-based tool for identification and annotation of proxy SNPs using HapMap. *Bioinformatics* 2008. 24(24):2938-2939.

Jones DA, Pellaton C, Velmurugan S, Andiapen M, Antoniou S, van Eijl S, Webb AJ, Westwood M, Parmar M, Mathur A and Ahluwalia A. Randomized Phase 2 Trial of Intra-Coronary Nitrite During Acute Myocardial Infarction. *Circ Res* 2014. 116(3):437-447.

Kamisaki Y, Saheki S, Nakane M, Palmieri JA, Kuno T, Chang BY, Waldman SA and Murad F. Soluble guanylate cyclase from rat lung exists as a heterodimer. *J Biol Chem* 1986. 261(16):7236-7241.

Karagiannis GS, Weile J, Bader GD and Minta J. Integrative pathway dissection of molecular mechanisms of moxLDL-induced vascular smooth muscle phenotype transformation. *BMC Cardiovasc Disord* 2013. 13:4.

Kass DA, Champion HC and Beavo JA. Phosphodiesterase type 5: expanding roles in cardiovascular regulation. *Circ Res* 2007a. 101(11):1084-1095.

Kass DA, Takimoto E, Nagayama T and Champion HC. Phosphodiesterase regulation of nitric oxide signaling. *Cardiovasc Res* 2007b. 75(2):303-314.

Katzen F. Gateway((R)) recombinational cloning: a biological operating system. *Expert Opin Drug Discov* 2007. 2(4):571-589.

Kent WJ, Sugnet CW, Furey TS, Roskin KM, Pringle TH, Zahler AM and Haussler D. The human genome browser at UCSC. *Genome Res* 2002. 12(6):996-1006.

Kerppola TK. Design and implementation of bimolecular fluorescence complementation (BiFC) assays for the visualization of protein interactions in living cells. *Nat Protoc* 2006. 1(3):1278-1286.

Kerppola TK. Visualization of molecular interactions using bimolecular fluorescence complementation analysis: characteristics of protein fragment complementation. *Chem Soc Rev* 2009. 38(10):2876-2886.

Kessler T, Erdmann J and Schunkert H. Genetics of coronary artery disease and myocardial infarction. *Curr Cardiol Rep* 2013. 15(6):368.

Kessler T, Vilne B and Schunkert H. The impact of genome-wide association studies on the pathophysiology and therapy of cardiovascular disease. *EMBO Mol Med* 2016. 8(7):688-701.

Kessler T, Wobst J, Wolf B, Eckhold J, Vilne B, Hollstein R, von Ameln S, Dang TA, Sager HB, Moritz Rumpf P, Aherrahrou R, Kastrati A, Bjorkegren JLM, Erdmann J, Lusis AJ, Civelek M, Kaiser FJ and Schunkert H. Functional Characterization of the GUCY1A3 Coronary Artery Disease Risk Locus. *Circulation* 2017. 136(5):476-489.

Kim TK and Eberwine JH. Mammalian cell transfection: the present and the future. *Analytical and Bioanalytical Chemistry* 2010. 397(8):3173-3178.

Ko FN, Wu CC, Kuo SC, Lee FY and Teng CM. YC-1, a novel activator of platelet guanylate cyclase. *Blood* 1994. 84(12):4226-4233.

Koglin M, Vehse K, Budaeus L, Scholz H and Behrends S. Nitric oxide activates the beta 2 subunit of soluble guanylyl cyclase in the absence of a second subunit. *J Biol Chem* 2001. 276(33):30737-30743.

Korkmaz S, Radovits T, Barnucz E, Hirschberg K, Neugebauer P, Loganathan S, Veres G, Pali S, Seidel B, Zollner S, Karck M and Szabo G. Pharmacological activation of soluble guanylate cyclase protects the heart against ischemic injury. *Circulation* 2009. 120(8):677-686.

Krafchak CM, Pawar H, Moroi SE, Sugar A, Lichter PR, Mackey DA, Mian S, Nairus T, Elner V, Schteingart MT, Downs CA, Kijek TG, Johnson JM, Trager EH, Rozsa FW, Mandal MN,

Epstein MP, Vollrath D, Ayyagari R, Boehnke M and Richards JE. Mutations in TCF8 cause posterior polymorphous corneal dystrophy and ectopic expression of COL4A3 by corneal endothelial cells. *Am J Hum Genet* 2005. 77(5):694-708.

Lamas S, Marsden PA, Li GK, Tempst P and Michel T. Endothelial nitric oxide synthase: molecular cloning and characterization of a distinct constitutive enzyme isoform. *Proc Natl Acad Sci U S A* 1992. 89(14):6348-6352.

Lee DI and Kass DA. Phosphodiesterases and cyclic GMP regulation in heart muscle. *Physiology (Bethesda)* 2012. 27(4):248-258.

Libby P, Ridker PM and Hansson GK. Progress and challenges in translating the biology of atherosclerosis. *Nature* 2011. 473(7347):317-325.

Lincoln TM. Myosin phosphatase regulatory pathways: different functions or redundant functions? *Circ Res* 2007. 100(1):10-12.

Lu X, Wang L, Chen S, He L, Yang X, Shi Y, Cheng J, Zhang L, Gu CC, Huang J, Wu T, Ma Y, Li J, Cao J, Chen J, Ge D, Fan Z, Li Y, Zhao L, Li H, Zhou X, Chen L, Liu D, Chen J, Duan X, Hao Y, Wang L, Lu F, Liu Z, Yao C, Shen C, Pu X, Yu L, Fang X, Xu L, Mu J, Wu X, Zheng R, Wu N, Zhao Q, Li Y, Liu X, Wang M, Yu D, Hu D, Ji X, Guo D, Sun D, Wang Q, Yang Y, Liu F, Mao Q, Liang X, Ji J, Chen P, Mo X, Li D, Chai G, Tang Y, Li X, Du Z, Liu X, Dou C, Yang Z, Meng Q, Wang D, Wang R, Yang J, Schunkert H, Samani NJ, Kathiresan S, Reilly MP, Erdmann J, Coronary ARtery DIsease Genome-Wide Replication Meta-Analysis Consortium, Peng X, Wu X, Liu D, Yang Y, Chen R, Qiang B and Gu D. Genome-wide association study in Han Chinese identifies four new susceptibility loci for coronary artery disease. *Nat Genet* 2012. 44(8):890-894.

Ma X, Beuve A and van den Akker F. Crystal structure of the signaling helix coiled-coil domain of the beta1 subunit of the soluble guanylyl cyclase. *BMC Struct Biol* 2010. 10:2.

Martin E, Golunski E, Laing ST, Estrera AL and Sharina IG. Alternative splicing impairs soluble guanylyl cyclase function in aortic aneurysm. *Am J Physiol Heart Circ Physiol* 2014. 307(11):H1565-1575.

Mattila JT and Thomas AC. Nitric oxide synthase: non-canonical expression patterns. *Front Immunol* 2014. 5:478.

Melichar VO, Behr-Roussel D, Zabel U, Uttenthal LO, Rodrigo J, Rupin A, Verbeuren TJ, Kumar HSA and Schmidt HH. Reduced cGMP signaling associated with neointimal proliferation and vascular dysfunction in late-stage atherosclerosis. *Proc Natl Acad Sci U S A* 2004. 101(47):16671-16676.

Mergia E, Friebe A, Dangel O, Russwurm M and Koesling D. Spare guanylyl cyclase NO receptors ensure high NO sensitivity in the vascular system. *J Clin Invest* 2006. 116(6):1731-1737.

Methner C, Lukowski R, Grube K, Loga F, Smith RA, Murphy MP, Hofmann F and Krieg T. Protection through postconditioning or a mitochondria-targeted S-nitrosothiol is unaffected by cardiomyocyte-selective ablation of protein kinase G. *Basic Res Cardiol* 2013. 108(2):337.

Meurer S, Pioch S, Pabst T, Opitz N, Schmidt PM, Beckhaus T, Wagner K, Matt S, Gegenbauer K, Geschka S, Karas M, Stasch JP, Schmidt HH and Muller-Esterl W. Nitric oxide-independent vasodilator rescues heme-oxidized soluble guanylate cyclase from proteasomal degradation. *Circ Res* 2009. 105(1):33-41.

Mullershausen F, Russwurm M, Koesling D and Friebe A. In vivo reconstitution of the negative feedback in nitric oxide/cGMP signaling: role of phosphodiesterase type 5 phosphorylation. *Mol Biol Cell* 2004. 15(9):4023-4030.

Mullis K, Faloona F, Scharf S, Saiki R, Horn G and Erlich H. Specific enzymatic amplification of DNA in vitro: the polymerase chain reaction. *Cold Spring Harb Symp Quant Biol* 1986. 51(Pt 1):263-273.

Musunuru K, Strong A, Frank-Kamenetsky M, Lee NE, Ahfeldt T, Sachs KV, Li X, Li H, Kuperwasser N, Ruda VM, Pirruccello JP, Muchmore B, Prokunina-Olsson L, Hall JL, Schadt EE, Morales CR, Lund-Katz S, Phillips MC, Wong J, Cantley W, Racie T, Ejebe KG, Orho-Melander M, Melander O, Koteliansky V, Fitzgerald K, Krauss RM, Cowan CA, Kathiresan S and Rader DJ. From noncoding variant to phenotype via SORT1 at the 1p13 cholesterol locus. *Nature* 2010. 466(7307):714-719.

Nakagawa C, Inahata K, Nishimura S and Sugimoto K. Improvement of a Venus-Based Bimolecular Fluorescence Complementation Assay to Visualize bFos-bJun Interaction in Living Cells. *Bioscience, Biotechnology, and Biochemistry* 2014. 75(7):1399-1401.

Nikpay M, Goel A, Won HH, Hall LM, Willenborg C, Kanoni S, Saleheen D, Kyriakou T, Nelson CP, Hopewell JC, Webb TR, Zeng L, Dehghan A, Alver M, Armasu SM, Auro K, Bjonnes A, Chasman DI, Chen S, Ford I, Franceschini N, Gieger C, Grace C, Gustafsson S, Huang J, Hwang SJ, Kim YK, Kleber ME, Lau KW, Lu X, Lu Y, Lyytikainen LP, Mihailov E, Morrison AC, Pervjakova N, Qu L, Rose LM, Salfati E, Saxena R, Scholz M, Smith AV, Tikkanen E, Uitterlinden A, Yang X, Zhang W, Zhao W, de Andrade M, de Vries PS, van Zuydam NR, Anand SS, Bertram L, Beutner F, Dedoussis G, Frossard P, Gauguier D, Goodall AH, Gottesman O, Haber M, Han BG, Huang J, Jalilzadeh S, Kessler T, Konig IR, Lannfelt L, Lieb W, Lind L, Lindgren CM, Lokki ML, Magnusson PK, Mallick NH, Mehra N, Meitinger T, Memon FU, Morris AP, Nieminen MS, Pedersen NL, Peters A, Rallidis LS, Rasheed A, Samuel M, Shah SH, Sinisalo J, Stirrups KE, Trompet S, Wang L, Zaman KS, Ardissino D, Boerwinkle E, Borecki IB, Bottinger EP, Buring JE, Chambers JC, Collins R, Cupples LA, Danesh J, Demuth I, Elosua R, Epstein SE, Esko T, Feitosa MF, Franco OH, Franzosi MG, Granger CB, Gu D, Gudnason V, Hall AS, Hamsten A, Harris TB, Hazen SL, Hengstenberg C, Hofman A, Ingelsson E, Iribarren C, Jukema JW, Karhunen PJ, Kim BJ, Kooner JS, Kullo IJ, Lehtimaki T, Loos RJ, Melander O, Metspalu A, Marz W, Palmer CN, Perola M, Quertermous T, Rader DJ, Ridker PM, Ripatti S, Roberts R, Salomaa V, Sanghera DK, Schwartz SM, Seedorf U, Stewart AF, Stott DJ, Thiery J, Zalloua PA, O'Donnell CJ, Reilly MP, Assimes TL, Thompson JR, Erdmann J, Clarke R, Watkins H, Kathiresan S, McPherson R, Deloukas P, Schunkert H, Samani NJ and Farrall M. A comprehensive 1,000 Genomes-based genome-wide association meta-analysis of coronary artery disease. *Nat Genet* 2015. 47(10):1121-1130.

Nimmegeers S, Sips P, Buys E, Brouckaert P and Van de Voorde J. Functional role of the soluble guanylyl cyclase alpha(1) subunit in vascular smooth muscle relaxation. *Cardiovasc Res* 2007. 76(1):149-159.

O'Connell M, Murthy S, Phan S, Xu C, Buchanan J, Spilker R, Dalman R, Zarins C, Denk W and Taylor C. The three-dimensional micro- and nanostructure of the aortic medial lamellar unit measured using 3D confocal and electron microscopy imaging. *Matrix Biology* 2008. 27(3):171-181.

O'Donnell CJ and Nabel EG. Genomics of cardiovascular disease. *N Engl J Med* 2011. 365(22):2098-2109.

Olsen T. Is there an association between Fuchs' endothelial dystrophy and cardiovascular disease? *Graefes Arch Clin Exp Ophthalmol* 1984. 221(5):239-240.

Palmer RMJ, Ferrige AG and Moncada S. Nitric oxide release accounts for the biological activity of endothelium-derived relaxing factor. *Nature* 1987. 327(11):524-526.

Palmer RMJ, Rees DD, Ashton DS and Moncada S. L-arginine is the physiological precursor for the formation of nitric oxide in endothelium-dependent relaxation. *Biochem. Biophys. Res. Commun.* 1988. 153(3):1251-1256.

Paniagua OA, Bryant MB and Panza JA. Role of endothelial nitric oxide in shear stress-induced vasodilation of human microvasculature: diminished activity in hypertensive and hypercholesterolemic patients. *Circulation* 2001. 103(13):1752-1758.

Peden JF and Farrall M. Thirty-five common variants for coronary artery disease: the fruits of much collaborative labour. *Hum Mol Genet* 2011. 20(R2):R198-205.

Pellicena P, Karow DS, Boon EM, Marletta MA and Kuriyan J. Crystal structure of an oxygen-binding heme domain related to soluble guanylate cyclases. *Proc Natl Acad Sci U S A* 2004. 101(35):12854-12859.

Pulido T, Zayas N, de Mendieta MA, Plascencia K and Escobar J. Medical therapies for pulmonary arterial hypertension. *Heart Fail Rev* 2016. 21(3):273-283.

Purohit R, Weichsel A and Montfort WR. Crystal structure of the Alpha subunit PAS domain from soluble guanylyl cyclase. *Protein Sci* 2013. 22(10):1439-1444.

Ramji DP and Foka P. CCAAT/enhancer-binding proteins: structure, function and regulation. *Biochem J* 2002. 365(Pt 3):561-575.

Rhodin JA. Fine structure of vascular walls in mammals with special reference to smooth muscle component. *Physiol Rev Suppl* 1962. 5:48-87.

Riazuddin SA, Zaghloul NA, Al-Saif A, Davey L, Diplas BH, Meadows DN, Eghrari AO, Minear MA, Li YJ, Klintworth GK, Afshari N, Gregory SG, Gottsch JD and Katsanis N. Missense mutations in TCF8 cause late-onset Fuchs corneal dystrophy and interact with FCD4 on chromosome 9p. *Am J Hum Genet* 2010. 86(1):45-53.

Roger S, Badier-Commander C, Paysant J, Cordi A, Verbeuren TJ and Feletou M. The anti-aggregating effect of BAY 41-2272, a stimulator of soluble guanylyl cyclase, requires the presence of nitric oxide. *Br J Pharmacol* 2010. 161(5):1044-1058.

Rosenbloom KR, Armstrong J, Barber GP, Casper J, Clawson H, Diekhans M, Dreszer TR, Fujita PA, Guruvadoo L, Haeussler M, Harte RA, Heitner S, Hickey G, Hinrichs AS, Hubley R, Karolchik D, Learned K, Lee BT, Li CH, Miga KH, Nguyen N, Paten B, Raney BJ, Smit AF, Speir ML, Zweig AS, Haussler D, Kuhn RM and Kent WJ. The UCSC Genome Browser database: 2015 update. *Nucleic Acids Res* 2015. 43(Database issue):D670-681.

Rosenbloom KR, Sloan CA, Malladi VS, Dreszer TR, Learned K, Kirkup VM, Wong MC, Maddren M, Fang R, Heitner SG, Lee BT, Barber GP, Harte RA, Diekhans M, Long JC, Wilder SP, Zweig AS, Karolchik D, Kuhn RM, Haussler D and Kent WJ. ENCODE data in the UCSC Genome Browser: year 5 update. *Nucleic Acids Res* 2013. 41(Database issue):D56-63.

Rothkegel C, Schmidt PM, Atkins DJ, Hoffmann LS, Schmidt HH, Schröder H and Stasch JP. Dimerization region of soluble guanylate cyclase characterized by bimolecular fluorescence complementation in vivo. *Mol Pharmacol* 2007. 72(5):1181-1190.

Roy B, Mo E, Vernon J and Garthwaite J. Probing the presence of the ligand-binding haem in cellular nitric oxide receptors. *Br J Pharmacol* 2008. 153(7):1495-1504.

Russwurm M, Behrends S, Harteneck C and Koesling D. Functional properties of a naturally occurring isoform of soluble guanylyl cyclase. *Biochem J* 1998. 335(Pt 1):125-130.

Russwurm M, Wittau N and Koesling D. Guanylyl cyclase/PSD-95 interaction: targeting of the nitric oxide-sensitive alpha2beta1 guanylyl cyclase to synaptic membranes. *J Biol Chem* 2001. 276(48):44647-44652.

Ruth P, Pfeifer A, Kamm S, Klatt P, Dostmann WR and Hofmann F. Identification of the amino acid sequences responsible for high affinity activation of cGMP kinase Ialpha. *J Biol Chem* 1997. 272(16):10522-10528.

Rybalkin SD, Rybalkina IG, Shimizu-Albergine M, Tang X-B and Beavo JA. PDE5 is converted to an activated state upon cGMP binding to the GAF A domain. *EMBO Journal* 2003a. 23(3):469-478.

Rybalkin SD, Yan C, Bornfeldt KE and Beavo JA. Cyclic GMP phosphodiesterases and regulation of smooth muscle function. *Circ Res* 2003b. 93(4):280-291.

Sage PR, de la Lande IS, Stafford I, Bennett CL, Phillipov G, Stubberfield J and Horowitz JD. Nitroglycerin tolerance in human vessels: evidence for impaired nitroglycerin bioconversion. *Circulation* 2000. 102(23):2810-2815.

Salvi E, Kuznetsova T, Thijs L, Lupoli S, Stolarz-Skrzypek K, D'Avila F, Tikhonoff V, De Astis S, Barcella M, Seidlerova J, Benaglio P, Malyutina S, Frau F, Velayutham D, Benfante R, Zagato L, Title A, Braga D, Marek D, Kawecka-Jaszcz K, Casiglia E, Filipovsky J, Nikitin Y, Rivolta C, Manunta P, Beckmann JS, Barlassina C, Cusi D and Staessen JA. Target sequencing, cell experiments, and a population study establish endothelial nitric oxide synthase (eNOS) gene as hypertension susceptibility gene. *Hypertension* 2013. 62(5):844-852.

Sambrook J, Fritsch EF and Maniatis T. Molecular Cloning: A Laboratory Manual. *Cold Spring Harbor* 1989. 4th ed.

Sanchez-Tillo E, Siles L, de Barrios O, Cuatrecasas M, Vaquero EC, Castells A and Postigo A. Expanding roles of ZEB factors in tumorigenesis and tumor progression. *Am J Cancer Res* 2011. 1(7):897-912.

Schlossmann J, Ammendola A, Ashman K, Zong X, Huber A, Neubauer G, Wang GX, Allescher HD, Korth M, Wilm M, Hofmann F and Ruth P. Regulation of intracellular calcium by a signalling complex of IRAG, IP3 receptor and cGMP kinase Ibeta. *Nature* 2000. 404(6774):197-201.

Schmidt PM, Schramm M, Schröder H, Wunder F and Stasch JP. Identification of residues crucially involved in the binding of the heme moiety of soluble guanylate cyclase. *J Biol Chem* 2004. 279(4):3025-3032.

Schunkert H, Konig IR, Kathiresan S, Reilly MP, Assimes TL, Holm H, Preuss M, Stewart AF, Barbalic M, Gieger C, Absher D, Aherrahrou Z, Allayee H, Altshuler D, Anand SS, Andersen K, Anderson JL, Ardissino D, Ball SG, Balmforth AJ, Barnes TA, Becker DM, Becker LC, Berger K, Bis JC, Boekholdt SM, Boerwinkle E, Braund PS, Brown MJ, Burnett MS, Buysschaert I, Carlquist JF, Chen L, Cichon S, Codd V, Davies RW, Dedoussis G, Dehghan A, Demissie S, Devaney JM, Diemert P, Do R, Doering A, Eifert S, Mokhtari NE, Ellis SG, Elosua R, Engert JC, Epstein SE, de Faire U, Fischer M, Folsom AR, Freyer J, Gigante B,

Girelli D, Gretarsdottir S, Gudnason V, Gulcher JR, Halperin E, Hammond N, Hazen SL, Hofman A, Horne BD, Illig T, Iribarren C, Jones GT, Jukema JW, Kaiser MA, Kaplan LM, Kastelein JJ, Khaw KT, Knowles JW, Kolovou G, Kong A, Laaksonen R, Lambrechts D, Leander K, Lettre G, Li M, Lieb W, Loley C, Lotery AJ, Mannucci PM, Maouche S, Martinelli N, McKeown PP, Meisinger C, Meitinger T, Melander O, Merlini PA, Mooser V, Morgan T, Muhleisen TW, Muhlestein JB, Munzel T, Musunuru K, Nahrstaedt J, Nelson CP, Nothen MM, Olivieri O, Patel RS, Patterson CC, Peters A, Peyvandi F, Qu L, Quyyumi AA, Rader DJ, Rallidis LS, Rice C, Rosendaal FR, Rubin D, Salomaa V, Sampietro ML, Sandhu MS, Schadt E, Schafer A, Schillert A, Schreiber S, Schrezenmeir J, Schwartz SM, Siscovick DS, Sivananthan M, Sivapalaratnam S, Smith A, Smith TB, Snoep JD, Soranzo N, Spertus JA, Stark K, Stirrups K, Stoll M, Tang WH, Tennstedt S, Thorgeirsson G, Thorleifsson G, Tomaszewski M, Uitterlinden AG, van Rij AM, Voight BF, Wareham NJ, Wells GA, Wichmann HE, Wild PS, Willenborg C, Witteman JC, Wright BJ, Ye S, Zeller T, Ziegler A, Cambien F, Goodall AH, Cupples LA, Quertermous T, Marz W, Hengstenberg C, Blankenberg S, Ouwehand WH, Hall AS, Deloukas P, Thompson JR, Stefansson K, Roberts R, Thorsteinsdottir U, O'Donnell CJ, McPherson R, Erdmann J and Samani NJ. Large-scale association analysis identifies 13 new susceptibility loci for coronary artery disease. *Nat Genet* 2011. 43(4):333-338.

Seddon M, Melikian N, Dworakowski R, Shabeeh H, Jiang B, Byrne J, Casadei B, Chowienczyk P and Shah AM. Effects of neuronal nitric oxide synthase on human coronary artery diameter and blood flow in vivo. *Circulation* 2009. 119(20):2656-2662.

Sharina IG, Cote GJ, Martin E, Doursout MF and Murad F. RNA splicing in regulation of nitric oxide receptor soluble guanylyl cyclase. *Nitric Oxide* 2011. 25(3):265-274.

Sharina IG, Jelen F, Bogatenkova EP, Thomas A, Martin E and Murad F. Alpha1 soluble guanylyl cyclase (sGC) splice forms as potential regulators of human sGC activity. *J Biol Chem* 2008. 283(22):15104-15113.

Shrestha D, Jenei A, Nagy P, Vereb G and Szöllősi J. Understanding FRET as a Research Tool for Cellular Studies. *International Journal of Molecular Sciences* 2015. 16(4):6718-6756.

Siddiqi N, Neil C, Bruce M, MacLennan G, Cotton S, Papadopoulou S, Feelisch M, Bunce N, Lim PO, Hildick-Smith D, Horowitz J, Madhani M, Boon N, Dawson D, Kaski JC, Frenneaux M and investigators N. Intravenous sodium nitrite in acute ST-elevation myocardial infarction: a randomized controlled trial (NIAMI). *Eur Heart J* 2014. 35(19):1255-1262.

Smolenski A, Bachmann C, Reinhard K, Honig-Liedl P, Jarchau T, Hoschuetzky H and Walter U. Analysis and regulation of vasodilator-stimulated phosphoprotein serine 239 phosphorylation in vitro and in intact cells using a phosphospecific monoclonal antibody. *J Biol Chem* 1998. 273(32):20029-20035.

Sovershaev MA, Egorina EM, Hansen JB, Osterud B, Pacher P, Stasch JP and Evgenov OV. Soluble guanylate cyclase agonists inhibit expression and procoagulant activity of tissue factor. *Arterioscler Thromb Vasc Biol* 2009. 29(10):1578-1586.

Speir ML, Zweig AS, Rosenbloom KR, Raney BJ, Paten B, Nejad P, Lee BT, Learned K, Karolchik D, Hinrichs AS, Heitner S, Harte RA, Haeussler M, Guruvadoo L, Fujita PA, Eisenhart C, Diekhans M, Clawson H, Casper J, Barber GP, Haussler D, Kuhn RM and Kent WJ. The UCSC Genome Browser database: 2016 update. *Nucleic Acids Res* 2016. 44(D1):D717-725.

Stasch JP, Becker EM, Alonso-Alija C, Apeler H, Dembowsky K, Feurer A, Gerzer R, Minuth T, Perzborn E, Pleiss U, Schröder H, Schroeder W, Stahl E, Steinke W, Straub A and

Schramm M. NO-independent regulatory site on soluble guanylate cyclase. *Nature* 2001. 410(6825):212-215.

Stasch JP, Dembowsky K, Perzborn E, Stahl E and Schramm M. Cardiovascular actions of a novel NO-independent guanylyl cyclase stimulator, BAY 41-8543: in vivo studies. *Br J Pharmacol* 2002a. 135(2):344-355.

Stasch JP, Pacher P and Evgenov OV. Soluble guanylate cyclase as an emerging therapeutic target in cardiopulmonary disease. *Circulation* 2011. 123(20):2263-2273.

Stasch JP, Schmidt P, Alonso-Alija C, Apeler H, Dembowsky K, Haerter M, Heil M, Minuth T, Perzborn E, Pleiss U, Schramm M, Schroeder W, Schröder H, Stahl E, Steinke W and Wunder F. NO- and haem-independent activation of soluble guanylyl cyclase: molecular basis and cardiovascular implications of a new pharmacological principle. *Br J Pharmacol* 2002b. 136(5):773-783.

Stasch JP, Schmidt PM, Nedvetsky PI, Nedvetskaya TY, H SA, Meurer S, Deile M, Taye A, Knorr A, Lapp H, Muller H, Turgay Y, Rothkegel C, Tersteegen A, Kemp-Harper B, Muller-Esterl W and Schmidt HH. Targeting the heme-oxidized nitric oxide receptor for selective vasodilatation of diseased blood vessels. *J Clin Invest* 2006. 116(9):2552-2561.

Steiner AL, Pagliara AS, Chase LR and Kipnis DM. Radioimmunoassay for cyclic nucleotides. II. Adenosine 3',5'-monophosphate and guanosine 3',5'-monophosphate in mammalian tissues and body fluids. *J Biol Chem* 1972. 247(4):1114-1120.

Stone JR and Marletta MA. Soluble Guanylate Cyclase from Bovine Lung: Activation with Nitric Oxide and Carbon Monoxide and Spectral Characterization of the Ferrous and Ferric States. *Biochemistry* 1994. 33(18):5636-5640.

Stone JR and Marletta MA. Spectral and kinetic studies on the activation of soluble guanylate cyclase by nitric oxide. *Biochemistry* 1996. 35(4):1093-1099.

Stuehr DJ. Structure-function aspects in the nitric oxide synthases. *Annu. Rev. Pharmacol. Toxicol.* 1997. 37:339-359.

Thadani U, Smith W, Nash S, Bittar N, Glasser S, Narayan P, Stein RA, Larkin S, Mazzu A, tota R, Pomerantz K and Sundaresan P. The Effect of Vardenafil, a Potent and Highly Selective Phosphodiesterase-5 Inhibitor for the Treatment of Erectile Dysfunction, on the Cardiovascular Response to Exercise in Patients With Coronary Artery Disease. *J Am Coll Cardiol* 2002. 40(11):2006-2012i.

Thomas MK, Francis SH and Corbin JD. Characterization of a Purified Bovine Lung cGMP-binding cGMP Phosphodiesterase. *Journal of Biological Chemistry* 1990. 265(25):14964-14970.

Townsend N, Nichols M, Scarborough P and Rayner M. Cardiovascular disease in Europe--epidemiological update 2015. *Eur Heart J* 2015. 36(40):2696-2705.

Tsou CY, Chen CY, Zhao JF, Su KH, Lee HT, Lin SJ, Shyue SK, Hsiao SH and Lee TS. Activation of soluble guanylyl cyclase prevents foam cell formation and atherosclerosis. *Acta Physiol (Oxf)* 2014. 210(4):799-810.

Underbakke ES, Iavarone AT, Chalmers MJ, Pascal BD, Novick S, Griffin PR and Marletta MA. Nitric Oxide-Induced Conformational Changes in Soluble Guanylate Cyclase. *Structure* 2014. 22(4):602-611.

Ursell PC and Mayes M. The majority of nitric oxide synthase in pig heart is vascular and not neural. *Cardiovasc Res* 1993. 27(11):1920-1924.

van Nas A, Pan C, Ingram-Drake LA, Ghazalpour A, Drake TA, Sobel EM, Papp JC and Lusis AJ. The systems genetics resource: a web application to mine global data for complex disease traits. *Front Genet* 2013. 4:84.

Varga-Szabo D, Braun A and Nieswandt B. Calcium signaling in platelets. *J Thromb Haemost* 2009. 7(7):1057-1066.

Waldmann SA and Murad F. Cyclic GMP Synthesis and Function. *Pharmacological Reviews* 1987. 39(3):163-196.

Wallace S, Guo DC, Regalado E, Mellor-Crummey L, Banshad M, Nickerson DA, Dauser R, Hanchard N, Marom R, Martin E, Berka V, Sharina I, Ganesan V, Saunders D, Morris S and Milewicz DM. Disrupted Nitric Oxide Signaling due to GUCY1A3 Mutations Increases Risk for Moyamoya Disease, Achalasia and Hypertension. *Clin Genet* 2016. 90(4):351-360.

Wang J, Zhuang J, Iyer S, Lin X, Whitfield TW, Greven MC, Pierce BG, Dong X, Kundaje A, Cheng Y, Rando OJ, Birney E, Myers RM, Noble WS, Snyder M and Weng Z. Sequence features and chromatin structure around the genomic regions bound by 119 human transcription factors. *Genome Res* 2012. 22(9):1798-1812.

Warner TD, Mitchell JA, Sheng H and Murad F. Effects of cyclic GMP on smooth muscle relaxation. *Adv Pharmacol* 1994. 26:171-194.

Wellner U, Schubert J, Burk UC, Schmalhofer O, Zhu F, Sonntag A, Waldvogel B, Vannier C, Darling D, zur Hausen A, Brunton VG, Morton J, Sansom O, Schuler J, Stemmler MP, Herzberger C, Hopt U, Keck T, Brabletz S and Brabletz T. The EMT-activator ZEB1 promotes tumorigenicity by repressing stemness-inhibiting microRNAs. *Nat Cell Biol* 2009. 11(12):1487-1495.

Wobst J, Kessler T, Dang TA, Erdmann J and Schunkert H. Role of sGC-dependent NO signalling and myocardial infarction risk. *J Mol Med (Berl)* 2015a. 93(4):383-394.

Wobst J, Rumpf PM, Dang TA, Segura-Puimedon M, Erdmann J and Schunkert H. Molecular Variants of Soluble Guanylyl Cyclase Affecting Cardiovascular Risk. *Circulation Journal* 2015b. 79(3):463-469.

Wobst J, von Ameln S, Wolf B, Wierer M, Dang TA, Sager HB, Tennstedt S, Hengstenberg C, Koesling D, Friebe A, Braun SL, Erdmann J, Schunkert H and Kessler T. Stimulators of the soluble guanylyl cyclase: promising functional insights from rare coding atherosclerosis-related GUCY1A3 variants. *Basic Res Cardiol* 2016. 111(4):51.

World Health Organisation. The top 10 causes of death. *Fact Sheet N°310* 2014.

Xia T, Dimitropoulou C, Zeng J, Antonova GN, Snead C, Venema RC, Fulton D, Qian S, Patterson C, Papapetropoulos A and Catravas JD. Chaperone-dependent E3 ligase CHIP ubiquitinates and mediates proteasomal degradation of soluble guanylyl cyclase. *Am J Physiol Heart Circ Physiol* 2007. 293(5):H3080-3087.

Yamada Y, Nishida T, Horibe H, Oguri M, Kato K and Sawabe M. Identification of hypo- and hypermethylated genes related to atherosclerosis by a genome-wide analysis of DNA methylation. *Int J Mol Med* 2014. 33(5):1355-1363.

Yu F, Warburton D, Wellington S and Danziger RS. Assignment of GUCIA2, the Gene Coding for the a2 Subunit of Soluble Guanylyl Cyclase, to Position 11q21–q22 on Human Chromosome 11. *Genomics* 1996. 33(2):334-336.

Yuan JS, Reed A, Chen F and Stewart CN, Jr. Statistical analysis of real-time PCR data. *BMC Bioinformatics* 2006. 7:85.

Yusuf S, Hawken S, Ôunpuu S, Dans T, Avezum A, Lanas F, McQueen M, Budaj A, Pais P, Varigos J and Lisheng L. Effect of potentially modifiable risk factors associated with myocardial infarction in 52 countries (the INTERHEART study): case-control study. *The Lancet* 2004. 364(9438):937-952.

Zabel U, Hausler C, Weeger M and Schmidt HHHW. Homodimerization of Soluble Guanylyl Cyclase Subunits: Dimerization analysis using a glutathiones-transferase affinity tag. *Journal of Biological Chemistry* 1999. 274(26):18149-18152.

Zhao Y, Brandish PE, Di Valentin M, Schelvis JP, Babcock GT and Marletta MA. Inhibition of soluble guanylate cyclase by ODQ. *Biochemistry* 2000. 39(35):10848-10854.

Zoumi A, Lu X, Kassab GS and Tromberg BJ. Imaging coronary artery microstructure using second-harmonic and two-photon fluorescence microscopy. *Biophys J* 2004. 87(4):2778-2786.

Appendices

A Appendix Tables

Appendix Table 1 Baseline characteristics of probands in patelet aggregation study. For age and platelet counts which are mean ± SEM, statistical analysis was done by unpaired Student's t test. In order to compare categorical data of the probands Fisher's exact test was used. *CAD:* coronary artery disease; *WB:* whole blood; *PRP:* platelet rich plasma; *ADP-RA:* ADP-receptor antagonist (i.e., clopidogrel, prasugrel, and ticagrelor). Supplemental Table 4 from Kessler/Wobst *et al.* Functional Characterization of the *GUCY1A3* Coronary Artery Disease Risk Locus. *Circulation* 2017. 136(5):476-489 (Kessler *et al.* 2017).

	AA n=8	**GG n=14**	**p**
Presence of CAD (%)	2 (25)	5 (36)	>0.99
Routine aspirin therapy, n (%)	2 (25)	7 (50)	0.38
Routine ADP-RA therapy, n (%)	0 (0)	0 (0)	>0.99
Male gender, n (%)	4 (50)	6 (43)	>0.99
Age, years	59 ± 4	67 ± 4	0.17
WB platelet count, 10^3/µl	267 ± 17	218 ± 15	0.06
PRP platelet count, 10^3/µl	476 ± 22	381 ± 22	0.01

Appendix Table 2 Primers used for endpoint PCR and qPCR

Gene	**Direction**	**Sequence (5'-3')**	**Size (bp)**
GUCY1A3	for	CAA CCG TGC CCA TCT GTC AAG	147
	rev	CAT TCA GCC GTT CAA ACT CTG G	
GUCY1B3	for	CAC GCG CGA TCT TGT TCT TT	104
	rev	GGG CTC TTA ACG TGA GCT GT	
ZEB1	for	CCA GTG GTC ATG ATG AAA ATG G	239
	rev	CTG CGT CAC ATG TCT TTG ATC	
IRF8	for	CGC GCA CCA TTC AGC ATT CTC	409
	rev	CTG CAG CTC TCG GAA GAA CTG	
RPLP0	for	GGC ACC ATT GAA ATC CTG AGT G	120
	rev	GAT GAC CAG CCC AAA GGA GAA G	

Appendix Table 3 Primers used for endpoint PCR in platelets

Marker	Gene	Direction	Sequence (5'-3')	Size (bp)
CD61	*ITGB3*	for	AAG AGC CAG AGT GTC CCA AG	238
		rev	GTG CCC CGG TAC GTG ATA TT	
CD235a	*GYPA*	for	GGG ACA CAT ATG CAG CCA CT	177/216*
		rev	GGC TTT TCT TTA TCA GTC GGC G	
CD45	*PTPRC*	for	CTC TAC GCA AAG CTA GGC CA	276
		rev	TGA CAG AAT GTT CTG GCC CC	

*depending on amplification of *GYPA* transcript variant 1 or 2
GYPA: glycophorin A
ITGB3: integrin subunit beta 3
PTPRC: protein tyrosine receptor phosphatase C

Appendix Table 4 Primers for Gateway® cloning including *attB* sites, Shine-Dalgarno and Kozak sequences

Gene	Direction	Specification	Sequence (5'-3')	Size (bp)
*GUCY1A3**	for		GGG GAC AAG TTT GTA CAA AAA AGC AGG CTT CGA AGG AGA TAG AAC C**AT GTT CTG CAC GAA GCT CAA G**	2149
	rev	w/ stop	GGG GAC CAC TTT GTA CAA GAA AGC TGG GTC **CTA ATC TAT TCC TGA TGC TTT GCC**	2146
	rev	w/o stop	GGG GAC CAC TTT GTA CAA GAA AGC TGG GTC **ATC TAT TCC TGA TGC TTT GCC T**	
GUCY1B3[#]	for		GGG GAC AAG TTT GTA CAA AAA AGC AGG CTT CGA AGG AGA TAG AAC C**AT GTA CGG ATT TGT GAA TCA CG**	1936
	rev	w/ stop	GGG GAC CAC TTT GTA CAA GAA AGC TGG GTC **TCA GTC ATC ATC CTG CTT TGT TTC**	1933
	rev	w/o stop	GGG GAC CAC TTT GTA CAA GAA AGC TGG GTC **GTC ATC ATC CTG CTT TGT TTC C**	

cDNA-specific binding marked in bold
**GUCY1A3* isoform A cDNA incl. stop codon: 2073 bp
[#]*GUCY1B3* cDNA incl. stop codon: 1860 bp

Appendix Table 5 Primers for the generation of BiFC plasmids coding for human *GUCY1A3* and *GUCY1B3*

Gene	Enzyme	Direction	Specification	Sequence (5'-3')	Size (bp)
GUCY1A3	BsiWI	for		TC GA**C GTA CG**T ATG TTC TGC ACG AAG CTC AAG	2091*
	XbaI	rev	w/o stop	TAG C**TC TAG A**AT CTA TTC CTG ATG CTT TGC CTA	
GUCY1B3	BsiWI	for		TC GA**C GTA CG**T ATG TAC GGA TTT GTG AAT C	1878[#]
	BmgBI	rev	w/o stop	TAG C**GA CGT G**AG TCA TCA TCC TGC TTT GTT TC	

restriction sites marked in bold
**GUCY1A3* coding sequence 2070 bp
[#]*GUCY1B3* coding sequence 1857 bp

Appendix Table 6 Primers for ligation of rs7692387 lead SNP region into pGL4.10[*luc2*] vector (for reporter gene expression assay approach 1)

SNP	Enzyme	Direction	Sequence (5'-3')	Size (bp)
rs7962387	NheI	for	AGC T**GC TAG C**GA TGG GGT GTA GGA CCT GTG	579*
	HindIII	rev	AGC T**AA GCT T**CA GGG ATG GTC ACT GCT GTA	

restriction sites marked in bold
*SNP region 559 bp

Appendix Table 7 Mutagenesis primers for insertion of rare variants into the CDS of *GUCY1A3* cloned to Gateway® pcDNA™-DEST40

Mutation	Direction	Sequence (5'-3')
p.Lys53Glu	for	ATC TGT CAA GAC ATT CCT GAG **G**AG AAC ATA CAA GAA AGT CTT C
	rev	GAA GAC TTT CTT GTA TGT TCT **C**CT CAG GAA TGT CTT GAC AGA T
p.Thr64Ala	for	AAG AAA GTC TTC CTC AAA GAA AA**G** CCA GTC GGA GCC
	rev	GGC TCC GAC TGG CTT TT**C** TTT GAG GAA GAC TTT CTT
p.Leu163Phefs*24	for	GGT TGG AGG CAC CCT TAA AGA TTT TTT **T**AA ACA GCT TCA GTA C
	rev	GTA CTG AAG CTG TTT **A**AA AAA ATC TTT AAG GGT GCC TCC AAC C
p.Thr229Met	for	GCA GCT GCT CAC GTA TTA TAT GAA A**T**G GAA GTG GAA GTG
	rev	CAC TTC CAC TTC C**A**T TTC ATA TAA TAC GTG AGC AGC TGC
p.Ser478Gly	for	TGC AAG CCA AGA AGT TC**G** GTA ATG TCA CCA TGC TC
	rev	GAG CAT GGT GAC ATT AC**C** CAA CTT CTT GGC TTG CA
p.Gly537Arg	for	CCT ATT GTG TAG CTG GG**C** GAT TAC ACA AAG AGA GT
	rev	ACT CTC TTT GTG TAA TC**G** CCC AGC TAC ACA ATA GG
p.Ile571Val	for	CCC CAT GGA GAA CCT **G**TC AAG ATG CGA A
	rev	TTC GCA TCT TGA **C**AG GTT CTC CAT GGG G
p.Val587Ile	for	CAG TTT TTG CTG GCG TC**A** TTG GAG TTA AAA TGC CC
	rev	GGG CAT TTT AAC TCC AA**T** GAC GCC AGC AAA AAC TG
p.Cys610Tyr	for	GGC TAA CAA ATT TGA GTC CT**A** CAG TGT ACC ACG AAA AAT CA
	rev	TGA TTT TTC GTG GTA CAC TG**T** AGG ACT CAA ATT TGT TAG CC

changed base marked in bold

Appendix Table 8 Mutagenesis primers for the insertion of HA tags into Gateway® pcDNA™-DEST40-*GUCY1A3 w/ stop*

Location	Direction	Sequence (5'-3')
N-terminus	for	GAA GGA GAT AGA ACC ATG **TAC CCA TAC GAT GTT CCA GAT TAC GCT** TTC TGC ACG AAG CTC AAG
	rev	CTT GAG CTT CGT GCA GAA **AGC GTA ATC TGG AAC ATC GTA TGG GTA** CAT GGT TCT ATC TCC TTC
C-terminus	for	AGG CAA AGC ATC AGG AAT AGA T**TA CCC ATA CGA TGT TCC AGA TTA CGC T**TA GGA CCC AGC TTT CTT GTA C
	rev	GTA CAA GAA AGC TGG GTC CTA **AGC GTA ATC TGG AAC ATC GTA TGG GTA** ATC TAT TCC TGA TGC TTT GCC T

HA tag marked in bold

Appendix Table 9 Mutagenesis primers for the insertion of Flag tags into Gateway® pcDNA™-DEST40-*GUCY1B3 w/ stop*

Location	Direction	Sequence (5'-3')
N-terminus	for	CGA AGG AGA TAG AAC CAT G**GA CTA CAA AGA CGA TGA CGA CAA G**TA CGG ATT TGT GAA TCA CG
	rev	CGT GAT TCA CAA ATC CGT A**CT TGT CGT CAT CGT CTT TGT AGT C**CA TGG TTC TAT CTC CTT CG
C-terminus	for	ACA AAG CAG GAT GAT GAC **GAC TAC AAA GAC GAT GAC GAC AAG** TGA GAC CCA GCT TTC TTG
	rev	CAA GAA AGC TGG GTC TCA **CTT GTC GTC ATC GTC TTT GTA GTC** GTC ATC ATC CTG CTT TGT

Flag tag marked in bold

Appendix Table 10 Sequencing primers located in vector backbones

Name	Vector	Direction	Sequence (5'-3')	Manufacturer
M13	Gateway®	for	GTA AAA CGA CGG CCA G	Thermo Fisher
	pDONR™221	rev	CAG GAA ACA GCT ATG AC	Scientific
T7	Gateway®	for	TAA TAC GAC TCA CTA TAG GG	
V5	pcDNA™-DEST40	rev	ACC GAG GAG AGG GTT AGG GAT	
RV3	pGL4.10[*luc2*]	for	CTA GCA AAA TAG GCT GTC CC	Promega Corporation

Appendix Table 11 Sequencing primers for sequencing inserts after Gateway® cloning into Gateway® pDONR™221 and pcDNA™-DEST40

Gene	Direction	Sequence (5'-3')
GUCY1A3	for	GAG CAA GCA GTT GCA GCA GG
	for	CAA CCA GAC GTT TAG CGG GAT C
	for	CTC ATG CTG TTC AGA TAG CGC T
GUCY1B3	for	GAA ATG AAG AAT GTG ATC ATA CTC
	for	CTC CGT CTG TTG CCA ATG AG

Appendix Table 12 Primers for sequencing rs7692387 lead SNP region after ligation to pGL4.10[*luc2*]. These primers were used in order to check for the correct genotype.

SNP	Direction	Sequence (5'-3')
rs7962387	for	GTG AGA TAA TTC AAA GTA TGG C
	rev	AGG GAT GGT CAC TGC TGT ATC

Appendix Table 13 Oligonucleotides used for EMSA

Binding site	Direction	Sequence (5'-3')
E1 (ZEB1 consensus sequence)	for	ACA CCT CCA GGT GAC TAA GTG G
	rev	CCA CTT AGT CAC CTG GAG GTG T
Sequence flanking *GUCY1A3* lead SNP allele A	for	AGA GAC ATT TAA AAA AGA AAG
	rev	CTT TCT TTT TTA AAT GTC TCT
Sequence flanking *GUCY1A3* lead SNP allele G	for	AGA GAC ATT TGA AAA AGA AAG
	rev	CTT TCT TTT TCA AAT GTC TCT

E1: E-box 1; the sequences for E1 were adopted from Wellner *et al.* 2009

B Appendix Figures

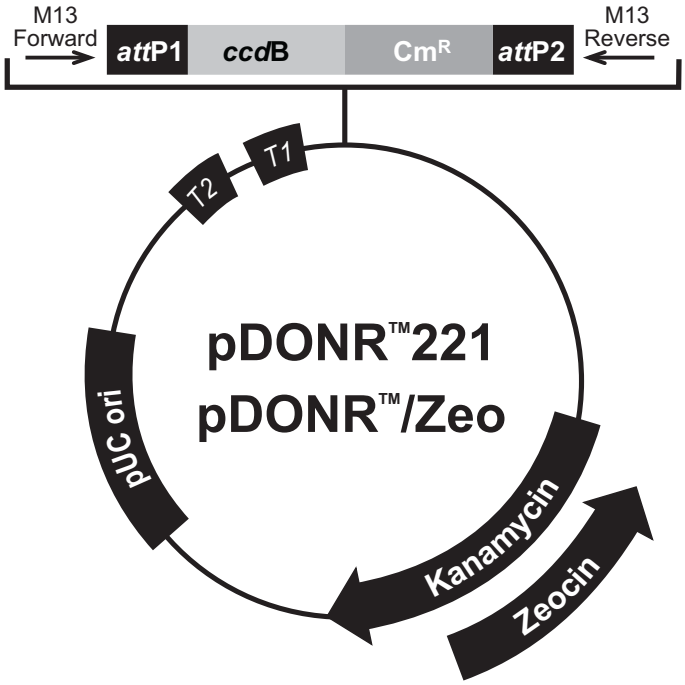

M13 Forward (-20) priming site

```
531  GACGTTGTAA AACGACGGCC AGTCTTAAGC TCGGGCCCCA AATAATGATT TTATTTTGAC
                                     AGCCCGGGGT TTATTACTAA AATAAAACTG

591  TGATAGTGAC CTGTTCGTTG CAACACATTG ATGAGCAATG CTTTTTTATA ATG CCA ACT
     ACTATCACTG GACAAGCAAC GTTGTGTAAC TACTCGTTAC GAAAAAATAT TAC GGT TGA
```

*att*L1

```
651                                                          2896
650  TTG TAC AAA AAA GCA GGC TNN --- --- --- NAC CCA GCT TTC TTG TAC AAA
     AAC ATG TTT TTT CGT CCG ANN ---  Gene  --- NTG GGT CGA AAG AAC ATG TTT
```

```
2906 GTT GGC ATT ATAAGAAAGC ATTGCTTATC AATTTGTTGC AACGAACAGG TCACTATCAG
     CAA CCG TAA TATTCTTTCG TAACGAATAG TTAAACAACG TTGCTTGTCC AGTGATAGTC
```

*att*L2

```
2965 TCAAAATAAA ATCATTATTT GCCATCCAGC TGATATCCCC TATAGTGAGT CGTATTACAT
     AGTTTTATTT TAGTAATAAA CGGTAGGTCG
```

M13 Reverse priming site

```
3025 GGTCATAGCT GTTTCCTGGC AGCTCTGGCC CGTGTCTCAA AATCTCTGAT GTTACATTGC
```

Appendix Figure 1 Gateway® pDONR™221 vector card. The 4761 bp Gateway® pDONR™221 entry vector is equipped with a kanamycin restistance for selection. Inserting coding sequences is achieved via homologous recombination of *attP* sites in the vector backbone with *attB* sites in PCR products thereby generating *attL* sites (Reprint from Gateway® pDONR™ vectors user guide MAN0000291, Thermo Fisher Scientific).

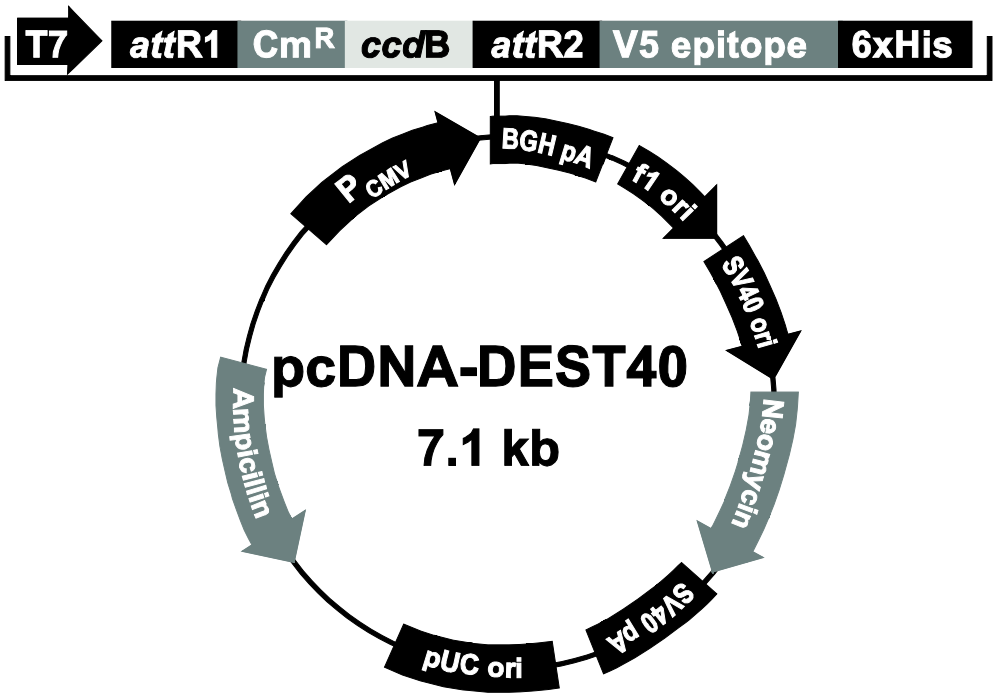


```
                    AATACGA CTCACTATAG GGAGACCCAA GCTGGCTAGT TAAGCTATCA
                    TTATGCT GAGTGATATC CCTCTGGGTT CGACCGATCA ATTCGATAGT
              918                                                2601
                                                  ... Pro Ala Phe Leu Tyr Lys Val Val
911 ACAAGTTTGT ACAAAAAAGC AGGCTN---- ---GENE-- NAC CCA GCT TTC TTG TAC AAA GTG GTT
    TGTTCAAACA TGTTTTTTCG TCCGAN--          -- NTG GGT CGA AAG AAC ATG TTT CAC CAA
                attB1                                          attB2

                                                                  V5 epitope
    Asp Leu Glu Gly Pro Arg Phe Glu Gly Lys Pro Ile Pro Asn Pro Leu Leu Gly
2617 GAT CTA GAG GGC CCG CGG TTC GAA GGT AAG CCT ATC CCT AAC CCT CTC CTC GGT
    CTA GAT CTC CCG GGC GCC AAG CTT CCA TTC GGA TAG GGA TTG GGA GAG GAG CCA

                                                  6xHis tag
    Leu Asp Ser Thr Arg Thr Gly His His His His His His ***
2671 CTC GAT TCT ACG CGT ACC GGT CAT CAT CAC CAT CAC CAT TGA GTTTAAAC
    GAG CTA AGA TGC GCA TGG CCA GTA GTA GTG GTA GTG GTA ACT CAAATTTG
```

Appendix Figure 2 Gateway® pcDNA™-DEST40 vector card. The 7143 bp Gateway® expression vector is equipped with an ampicillin as well as a neomycin restistance for selection. Inserting coding sequences is achieved by homologous recombination of *attP* sites in the vector backbone with attL sites from Gateway® pDONR™221 entry clones (Reprint from Gateway® pcDNA™-DEST40 vector user guide MAN0000223, Thermo Fisher Scientific).

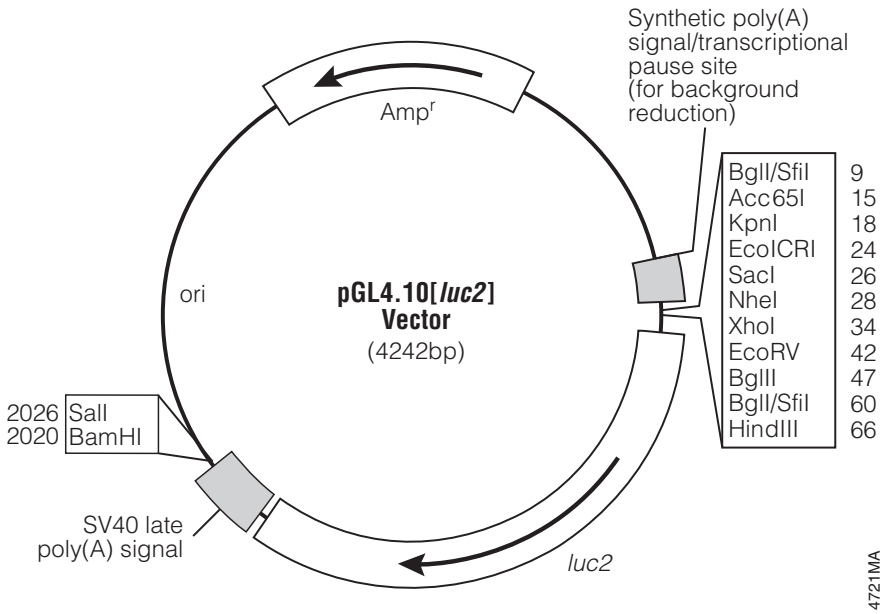

Appendix Figure 3 pGL4.10[*luc2*] vector card. The 4242 bp promoterless luciferase reporter vector pGL4.10[*luc2*] encodes firefly luciferase (*luc2*) and contains a multiple cloning site as well ampicillin resistance for selection (Reprint from pGL4.10[*luc2*] vector product Information #9PIE665, Promega Corporation).

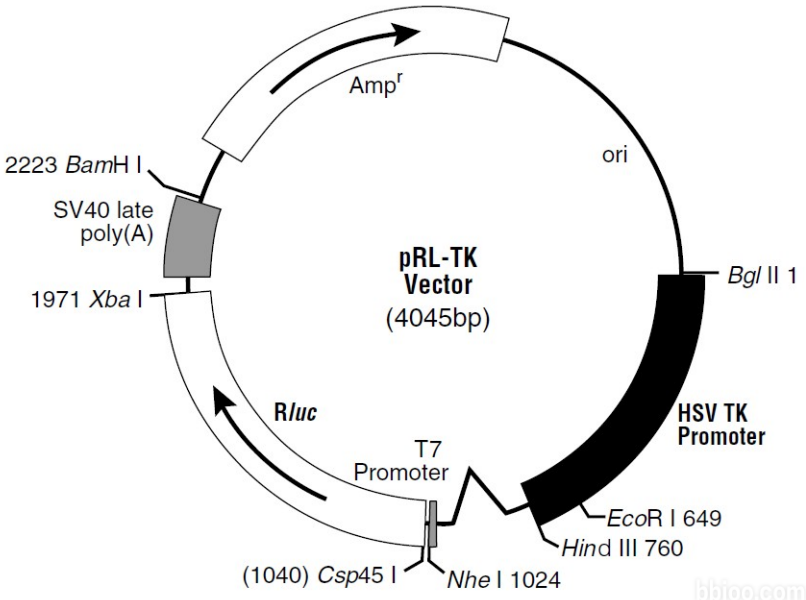

Appendix Figure 4 pRL-TK vector card. The 4045 bp internal control pRL-TK vector is equipped with ampicillin resistance for selection. The pRL-TK vector contains the herpes simplex virus thymidine kinase (HSV-TK) promoter to provide low to moderate levels of *Renilla (Rluc)* luciferase expression in cotransfected mammalian cells (Reprint from *https://www.promega.de/resources/vector-sequences/reporter-vectors/prl-renilla-luciferase-control-vectors/*).

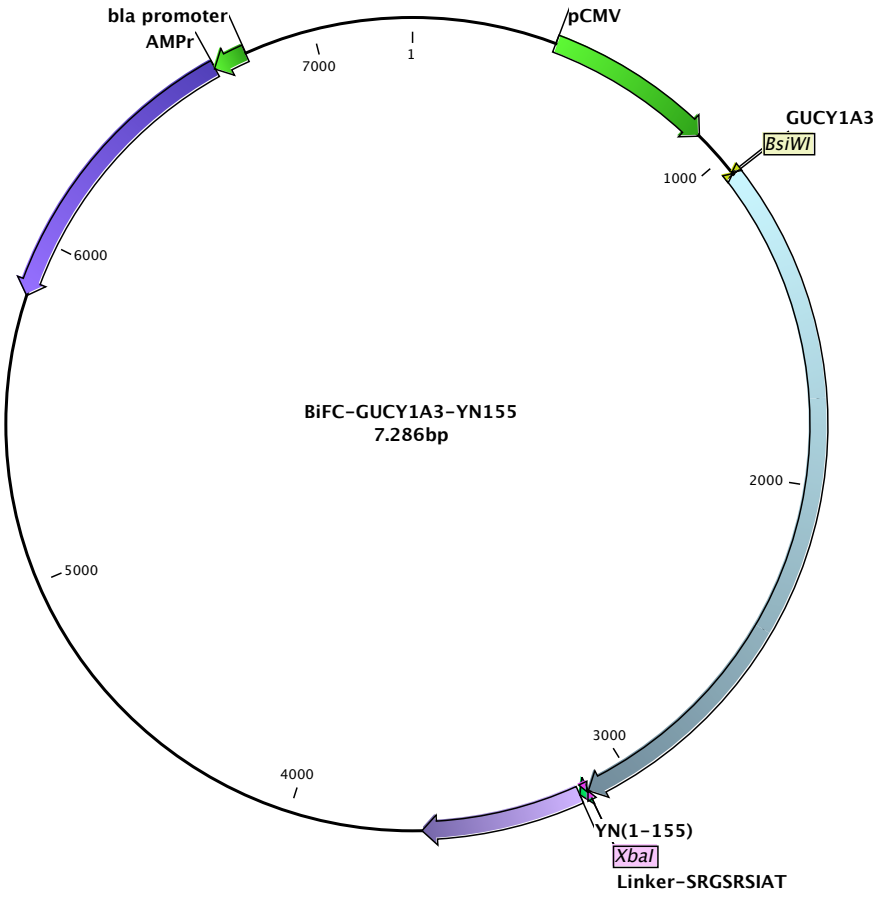

Appendix Figure 5 Plasmid encoding human *GUCY1A3* used for BiFC. To construct *GUCY1A3* fused to the N-terminal part of EYFP (YN), *GUCY1A3* was amplified from reverse transcribed human total heart RNA (BioChain) using primers containing BsiWI and XbaI restriction sites. The Plasmid BiFC-*Gucy1a3*-YN kindly provided by J.-P. Stasch (PharmaResearch Center, Bayer HealthCare, Wuppertal, Germany) (Rothkegel *et al.* 2007) as well as the *GUCY1A3* PCR product were double digested with both restriction enzymes and *GUCY1A3* was ligated into the BiFC vector backbone. *GUCY1A3* and the sequence encoding the amino acids 1 to 155 of EYFP (YN) were thereby connected by the linker sequence SRGSRSIAT.

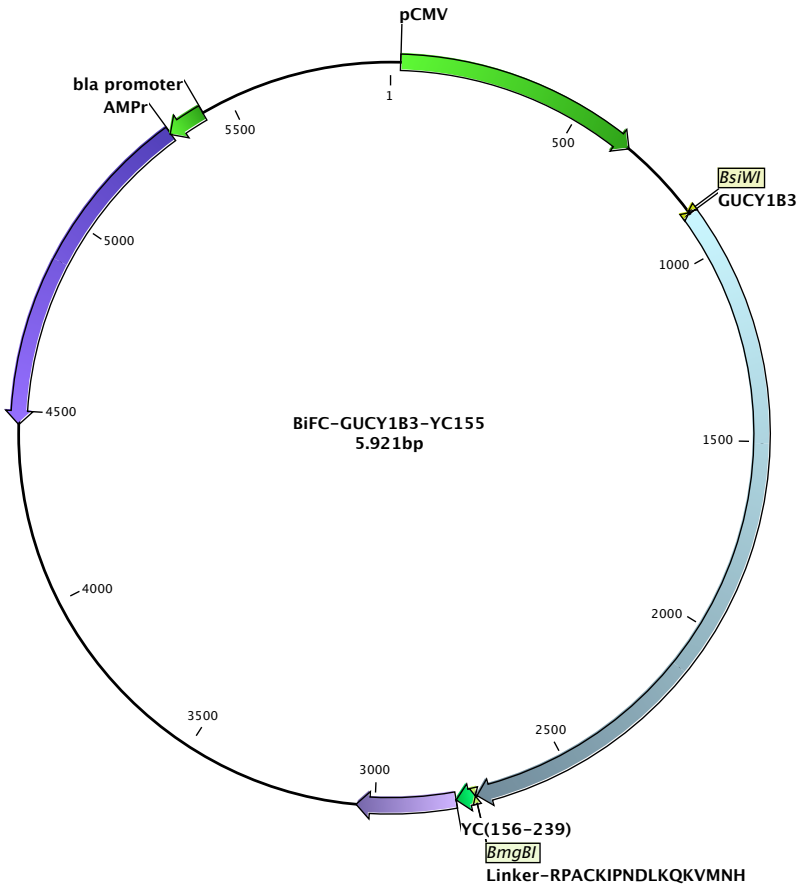

Appendix Figure 6 Plasmid encoding human *GUCY1B3* used for BiFC. To construct *GUCY1B3* fused to the C-terminal part of EYFP (YC), *GUCY1B3* was amplified from reverse transcribed human total heart RNA (BioChain) using primers containing BsiWI and BmgBI restriction sites. The Plasmid BiFC-*Gucy1b3*-YC kindly provided by J.-P. Stasch (PharmaResearch Center, Bayer HealthCare, Wuppertal, Germany) (Rothkegel *et al.* 2007) as well as the *GUCY1B3* PCR product were double digested with both restriction enzymes and *GUCY1B3* was ligated into the BiFC vector backbone. *GUCY1B3* and the sequence encoding the amino acids 156 to 239 of EYFP (YC) were thereby connected by the linker sequence SRPACKIPNDLKQKVMNH.

C Publications

Kessler T*, Wolf B*, Eriksson N, **Wobst J**, Åkerblom A, Sager HB, Kaess BM, Nordio F, Stroth M, Koch K, Mayer K, Bernlochner I, Solakov L, Bopp R, Sibbing D, O'Donoghue M, James S, Katus HA, Storey R, Becker RC, Laugwitz K-L, Koenig W, Wallentin L, Kastrati A, Schunkert H. Association of the coronary artery disease risk gene *GUCY1A3* with on-aspirin platelet reactivity and ischemic events after coronary intervention. *Submitted Manuscript* 2017.
*contributed equally

Kessler T*, **Wobst J***, Wolf B, Eckhold J, Vilne B, Hollstein R, von Ameln S, Dang TA, Sager HB, Rumpf PM, Aherrahrou R, Kastrati A, Bjoerkegren JLM, Erdmann J, Lusis AJ, Civelek M, Kaiser FJ, Schunkert H. Functional characterization of the *GUCY1A3* coronary artery disease risk locus. *Circulation* 2017. 136(5):476-489.
*contributed equally

Kemmner S, Burkhardt K, Lorenz G, **Wobst J**, Kessler T, Stock K, Wen M, Guenthner R, Heemann U, Baumann M, Schmaderer C. Dietary nitrate load lowers peripheral blood pressure and renal resistive index in patients with chronic kidney disease: a pilot study. *Nitric Oxide* 2017. 64:7-15.

Wobst J, von Ameln S, Wolf B, Wierer M, Dang TA, Sager HB, Tennstedt S, Hengstenberg C, Koesling D, Friebe A, Braun SL, Erdmann J, Schunkert H, Kessler T. Stimulators of the soluble guanylyl cyclase: promising functional insights from rare coding atherosclerosis-related *GUCY1A3* variants. *Basic Res Cardiol* 2016. 111(4):51.

Wobst J, Kessler T, Dang TA, Erdmann J, Schunkert H. Role of sGC-dependent NO signalling and myocardial infarction risk. *J Mol Med (Berl)* 2015. 93(4):383-394.

Wobst J, Rumpf PM, Dang TA, Segura-Puimedon M, Erdmann J, Schunkert H. Molecular Variants of Soluble Guanylyl Cyclase Affecting Cardiovascular Risk. *Circ J* 2015. 79:463-469.

D Talks

Interact 2016, Munich, Germany, 04.11.2016: Mechanistic link between the *GUCY1A3* locus and coronary artery disease risk.

DHM Basic Research Retreat, Munich, Germany, 14.10.2016: Causal link between *GUCY1A3* risk variants and CAD.

2nd Young DZHK Retreat, Bad Aibling, Germany, 14.-15.09.2016: Mechanistic link between the *GUCY1A3* locus and coronary artery disease risk.
Leducq Meeting, Lübeck, Germany, 27.-28.06.2016: Stimulators of the soluble guanylyl cyclase: promising functional insights from atherosclerosis-related rare coding *GUCY1A3* variants.

E Poster presentations

European Society of Cardiology 2017, Barcelona, Spain, 26.-30.08.2017: The 4q32.1 coronary artery disease locus influences disease risk via differential transcription factor binding.

SFB Retreat 2017, Grainau, Germany, 19.-21.07.2017: Functional assessment of the *GUCY1A3* gene, a novel causal factor for coronary artery disease.

MHA Summer Meeting 2017, Bernried, Germany, 03.07.2017: Functional Characterization of the *GUCY1A3* Coronary Artery Disease Risk Locus.

Deutsche Gesellschaft für Kardiologie, 83. Jahrestagung, Mannheim, Germany, 20.-22.04.2017: The 4q32.1 coronary artery disease risk locus influences soluble guanylyl cyclase activity in vascular smooth muscle cells and platelets.

European Society of Cardiology 2016, Rome, Italy, 27.-31.08.2016: Stimulators of the soluble guanylyl cyclase: promising functional insights from atherosclerosis-related rare coding *GUCY1A3* variants.

Cardiac Regeneration and Vascular Biology Conference 2016, San Servolo, Venice, Italy, 15.-17.06.2016: Mechanistic link between the *GUCY1A3* locus and coronary artery disease risk via differential transcription factor binding.

MHA Winter Meeting 2016, Munich, Germany, 18.01.2016: Mechanistic link between the *GUCY1A3* locus and coronary artery disease risk via differential transcription factor binding.

AHA Scientific Sessions 2015, Orlando, USA, 07.-11.11.2015: Functional relevance of rare *GUCY1A3* variants in patients affected by premature myocardial infarction.

E:Med Meeting 2015, Heidelberg, Germany, 26.-28.10.2015: Functional evaluation of rare *GUCY1A3* variants in patients affected by premature myocardial infarction.
MHA Summer Meeting 2015, Bernried, Germany, 23.07.2015: Influence of the Coronary Artery Disease Risk Allele *GUCY1A3* on Platelet Aggregation.

cGMP Congress 2015, Trier, Germany, 19.-21.06.2015: Functional Evaluation of *GUCY1A3* mutations affecting myocardial infarction risk.

MHA Winter Meeting 2015, Munich, Germany, 12.02.2015: Functional Evaluation of *GUCY1A3* mutations affecting myocardial infarction risk.